GL-TR-90-0014

EVALUATION OF MAGNETOSPHERIC INTERNAL MAGNETIC FIELD MODELS AND EXISTING SOFTWARE

C. E. Jordan
J. N. Bass

Radex., Inc.
Three Preston Court
Bedford, MA 01730

January 31, 1990

Scientific Report No. 3

GEOPHYSICS LABORATORY
AIR FORCE SYSTEMS COMMAND
UNITED STATES AIR FORCE
HANSCOM AIR FORCE BASE, MASSACHUSETTS 01731-5000

"This technical report has been reviewed and is approved for publication"

EDWARD C. ROBINSON
Contract Manager
Data Systems Branch
Aerospace Engineering Division

ROBERT E. McINERNEY, Chief
Data Systems Branch
Aerospace Engineering Division

FOR THE COMMANDER

C. NEALON STARK, Director
Aerospace Engineering Division

This report has been reviewed by the ESD Public Affairs Office (PA) and is releasable to the National Technical Information Service (NTIS).

Qualified requestors may obtain additional copies from the Defense Technical Information Center. All others should apply to the National Technical Information Service.

If your address has changed, or if you wish to be removed from the mailing list, or if the addressee is no longer employed by your organization, please notify GL/IMA, Hanscom AFB, MA 01731. This will assist us in maintaining a current mailing list.

Do not return copies of this report unless contractual obligations or notices on a specific document requires that it be returned.

REPORT DOCUMENTATION PAGE

1a. REPORT SECURITY CLASSIFICATION Unclassified	1b. RESTRICTIVE MARKINGS
2a. SECURITY CLASSIFICATION AUTHORITY	3. DISTRIBUTION / AVAILABILITY OF REPORT Approved for Public Release Distribution Unlimited
2b. DECLASSIFICATION / DOWNGRADING SCHEDULE	
4. PERFORMING ORGANIZATION REPORT NUMBER(S) RX-R-90012	5. MONITORING ORGANIZATION REPORT NUMBER(S) GL-TR-90-0014
6a. NAME OF PERFORMING ORGANIZATION RADEX, Inc. / 6b. OFFICE SYMBOL (If applicable)	7a. NAME OF MONITORING ORGANIZATION Geophysics Laboratory
6c. ADDRESS (City, State, and ZIP Code) Three Preston Court Bedford, MA 01730	7b. ADDRESS (City, State, and ZIP Code) Hanscom AFB Massachusetts 01731-5000
8a. NAME OF FUNDING / SPONSORING ORGANIZATION / 8b. OFFICE SYMBOL (If applicable)	9. PROCUREMENT INSTRUMENT IDENTIFICATION NUMBER Contract F19628-89-C-0068
8c. ADDRESS (City, State, and ZIP Code)	10. SOURCE OF FUNDING NUMBERS

PROGRAM ELEMENT NO.	PROJECT NO.	TASK NO.	WORK UNIT ACCESSION NO.
62101F	7659	05	AB

11. TITLE (Include Security Classification)

Evaluation of Magnetospheric Internal Magnetic Field Models and Existing Software

12. PERSONAL AUTHOR(S)

C. E. Jordan, J. N. Bass

13a. TYPE OF REPORT	13b. TIME COVERED	14. DATE OF REPORT (Year, Month, Day)	15. PAGE COUNT
Scientific Report #3	FROM 6/89 TO 1/90	1990, 01, 31	80

16. SUPPLEMENTARY NOTATION

COSATI CODES			18. SUBJECT TERMS (Continue on reverse if necessary and identify by block number)
FIELD	GROUP	SUB-GROUP	Magnetospheric internal magnetic field models, Spherical harmonic models, L-shell determination, Dipole moment

19. ABSTRACT (Continue on reverse if necessary and identify by block number)

Four magnetospheric internal magnetic field models have been reviewed: Barraclough 1975, MAGSAT 1980, IGRF 1985 and Cain 1990. Their derivations have been summarized. Each model was incorporated into software currently in use a AFGL. The results of these models were compared. IGRF 1985 was used as the standard and was found to be the bes suited for the current epoch. The software was also evaluated. Comparisons were made between the code used in hous and that which was sent by Dr. J. C. Cain. An interpolation technique compared favorably to the integration technique typically used.

20. DISTRIBUTION / AVAILABILITY OF ABSTRACT ☒ UNCLASSIFIED/UNLIMITED ☐ SAME AS RPT ☐ DTIC USERS	21. ABSTRACT SECURITY CLASSIFICATION Unclassified
22a. NAME OF RESPONSIBLE INDIVIDUAL E. C. Robinson	22b. TELEPHONE (Include Area Code) 22c. OFFICE SYMBOL (617)377-3840 GL/LCY

DD FORM 1473, 84 MAR 83 APR edition may be used until exhausted. All other editions are obsolete.

ACKNOWLEDGEMENTS

The authors would like to thank Dr. M. S. Gussenhoven, Dr. J. C. Cain, and Dr. D. Brautigam, for their help in preparing this report. They are also very grateful to S. Cline, Radex, for the preparation of the final manuscript.

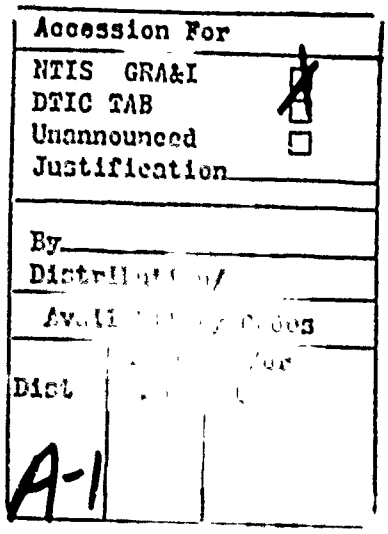

TABLE OF CONTENTS

Table of Contents (cont'd)

LIST OF FIGURES

LIST OF TABLES

1. INTRODUCTION

In preparation for analysis of the CRRES databases (to be taken from 1990 to 1995) and, in particular, for an updated static radiation belt model, a comparison has been made of four magnetospheric internal magnetic field models. Since there is interest in radiation belt models out to geosynchronous altitudes, it will be necessary to consider the external magnetic field models as well, but for now just the internal models will be discussed. The four models reviewed here are Barraclough, MAGSAT, IGRF 1985, and Cain. Each of these has an optimal time period associated with it: Barraclough 1975, MAGSAT 1980, IGRF 1985, and Cain 1990.

In the subsequent sections of this report, the derivations of these models will be summarized. They are all based on the spherical harmonic expansion of the magnetic field's scalar potential. The data used to determine each set of coefficients will be briefly discussed. Then the models will be evaluated by comparing the magnetic field and L-shell values obtained from each of the models. Finally, various computer codes which use these models to evaluate the field and L-shell, will be compared and evaluated in terms of their performance (i.e. accuracy and speed).

A primary concern for radiation belt models is reduction of the number of binning parameters by using B-L coordinates [*McIlwain*, 1961]. Thus, these four models were compared on the basis of the total magnetic field, its components, and L-shell values determined from each model's unique set of spherical harmonic coefficients. The comparisons were made to high latitudes (±75° in geographic coordinates), over all longitudes, and over a large altitude range (0 km - 40,000 km). This was done in the interest of completeness. However, the CRRES orbits will fall within a latitude range between ±20°. Also, beyond approximately 15,000 km the magnetic field due to external sources becomes significant. Thus, the focus of the analysis of these models will be within more limited latitude and altitude ranges.

In addition to the analysis of the models themselves, the software in which they are used has been reviewed as well. There are essentially four codes which have been considered, two of which are currently in use at the Geophysics Laboratory (GL) and two of which were sent by Dr. J. C. Cain. The two codes at GL are OPTRACE and HMIN. OPTRACE is a more extensive package than HMIN. Initially, OPTRACE was used in the model comparisons. However, when the codes themselves were to be evaluated, a modified version of HMIN was used to give a more accurate comparison of the CPU requirements of each of the codes. These codes trace along the field line in cartesian corrdinates. The two codes sent by Cain were reconstructed from work done by Kluge in the early 1970s. One of these integrates over the field line to find L using inverse coordinates centered on the dipole. This package will be referred to as Kluge/Cain Integration. The other package is a short routine which uses interpolation tables based on the Cain 1990 model as evaluated by Kluge/Cain Integration to find L for a given geographic point. This code will simply be referred to as Interpolation to avoid confusion with the other Kluge/Cain package.

The models were compared primarily to determine if there are experimentally significant differences which may affect how the data should be handled from CRRES. The primary model currently in use is the International Geomagnetic Reference Field Revision 1985 (IGRF 1985). However, a more recent paper by Cain reports a "jerk" (discontinuity) in the secular variation of the field in 1983. This is not accounted for in the secular variation coefficients of the IGRF 1985 model. Thus, Cain has derived a model for epoch 1990 which

does account for this jerk. In the magnetic field and L-shell comparisons, no significant effect was seen due to this jerk. Cain's model agrees quite well with IGRF 1985 extrapolated to 1990. The discrepancy arising from this jerk should become more apparent in future epochs. However, by the time this occurs, IGRF will have been revised with data extending beyond that which Cain used. Thus, this question will be resolved. For the time period considered here, the difference is not found to be significant.

The software was evaluated to determine the most efficient code. The GL codes use various numerical techniques to integrate over the field line in Cartesian coordinates to determine B and L. These techniques have been reviewed for accuracy and speed for both the SCATHA and CRRES satellite projects. The Kluge/Cain work uses inverse coordinates centered on the dipole so that the integration is performed over a straight line rather than a curve. This significantly reduces the computation time. Interpolation reduces it even further. However, the Interpolation routine as it now stands is only valid for the epoch for which the tables were generated. In order to obtain the same flexibility in epoch that one has with the integration techniques, tables for other epochs must be generated and a method of interpolation between the tables must be used.

The Interpolation routine was found to be the fastest. However, the tables were determined using Kluge/Cain Integration which incorporated a twenty year old value of the dipole moment. The dipole moment is decreasing over time. In the course of two decades, it has dropped enough to produce significant differences in the L-shell values. Thus for 1990, it would be useful to generate interpolation tables using the current dipole moment. Then one would be able to take advantage of this rapid technique to find L for a large set of data points.

The results from Kluge/Cain Integration agree well with those from OPTRACE and HMIN. It is a faster routine than those currently in use at GL. It is possible to use this technique with external model routines. So for cases where only a few points are required, or when one is interested in the magnetic field values, or until the revised interpolation tables are produced, this may be the code to use.

2. DESCRIPTIONS OF THE MODELS

2.1 OVERVIEW

The four models which are compared are IGRF 1985, Cain 1990, MAGSAT 1980, and Barraclough 1975. IGRF 1985 is used as the standard model to which the others are compared. This is because it is the model released by the International Association of Geomagnetism and Aeronomy and is the one which is most widely used for current epochs. Cain 1990 is considered here because of a possible discontinuity its authors found in the secular variation in 1983. This discontinuity was not incorporated in the IGRF 1985 model. Hence, as one approaches 1990, significant errors may arise from IGRF 1985 due to its handling of the secular variation. MAGSAT 1980 is presented because the basis of this model is satellite data. The MAGSAT satellite was specifically designed for the purpose of gathering high quality data with good global coverage to be used in determining the Earth's magnetic field. Previous models have all been developed using ground-based data. Note, the OGO series of satellites in the 1960's were used in modeling the field, but not to the same extent as MAGSAT. Barraclough 1975 is presented because it is a model which has been used at GL for years. Thus, it is of interest to those who have used it in the past and are familiar with it.

IGRF 1985, Cain 1990, MAGSAT 1980, and Barraclough 1975 are all models determined by fitting data (ground-based and satellite) to a mathematical model. Gauss [1839] found that the Earth's magnetic field could be expressed as the negative gradient of a harmonic scalar potential. This representation of the field will be discussed. Then the data used to obtain the four models will be briefly described.

Note, there are other ways to represent the field. Stern [1976] reviews five groups of field representations: a) those based on current density, b) those using a magnetic scalar potential (e.g. Gauss), c) poloidal and toroidal fields, d) Euler potentials, and e) local expansions of the field given a reference point. In a subsequent review paper by Backus [1986], a strong case is made for using poloidal and toroidal fields (the Mie representation) rather than the Gaussian representation. This is because Gauss assumes a current-free field. However, when using satellite data, this assumption is not valid. Iijima and Potemra [1976] observed field aligned currents at 800 km in the auroral zone. Even on quiet days, these led to magnetic perturbations of several hundred nanotesla. Backus presents in detail the Mie representation of the magnetic field in a spherical shell. This particular representation lends itself to combining satellite data with ground-based observations.

However, the Gaussian representation is still the most widely used for internal field models. For low latitudes and altitudes, the Gaussian representation of the internal fields is adequate. The four models considered in this report are all spherical harmonic expansions of the magnetic scalar potential. The alternate representations mentioned may be of interest, particularly when considering external field contributions as well as the internal ones, but are not the focus of this report.

2.1.1 Derivation of the Main Field and Its Components

Assume the main field can be expressed as the negative gradient of a scalar potential (V) which is a solution to Laplace's equation $\nabla^2 V = 0$. Then in spherical polar coordinates, this solution may be written as a series expansion in spherical harmonics:

$$V = a \sum_{n=1}^{N} (a/r)^{n+1} \sum_{m=0}^{n} (g_n^m \cos m\lambda + h_n^m \sin m\lambda) P_n^m(\cos \theta)$$

where

a	=	mean Earth radius
r	=	distance from Earth's center
θ	=	geocentric colatitude (measured from the geographic north pole)
λ	=	longitude (measured east from Greenwich)
P_n^m	=	Legendre polynomial of degree n and order m
g_n^m, h_n^m	=	spherical harmonic coefficients that constitute the desired models

Note, several different normalizations are used with the Legendre polynomials. The models presented here use Schmidt normalization. This correlates the magnitude of a term with its contribution to the field. Hence, the coefficients decrease with increasing n since the lower order terms contribute the most to the field (at least near the Earth's surface). There is no systematic variation with m for any given n. Other normalizations may be obtained by multiplying the Legendre polynomial by some factor, then dividing the corresponding coefficient by the same factor. Thus, V remains unchanged [*Stern*, 1976].

One may then get the geocentric components of the main field, $\mathbf{B} = -\nabla V$, by partial differentiation of V:

$$X = B_\theta = (1/r)(\delta V/\delta\theta)$$

$$Y = B_\phi = (-1/r \sin\theta)(\delta V/\delta\lambda)$$

$$Z = -B_r = \delta V/\delta r$$

where, X is the northward component, Y is the eastward component, and Z is the radially inward component of the field. The other geomagnetic components are related to X, Y, and Z by:

$$D = \text{declination} = \arctan(Y/X)$$
$$I = \text{inclination} = \arctan(Z/H)$$
$$H = \text{horizontal intensity} = (X^2 + Y^2)^{1/2}$$
$$F = \text{total intensity} = (X^2 + Y^2 + Z^2)^{1/2}$$

In addition to finding the main field at a given time (epoch), one is also interested in extrapolating any given model to other epochs. To do this, a secular variation (SV) model is required. This is found by assuming the coefficients have a linear dependence on time, eg. $a = a_o + at$, where a_o is the coefficient at some initial time and t is in years. In some cases, a quadratic term (secular acceleration) is also included [*Stern*, 1976].

2.1.2 Model Epochs and Degrees of Derivation

Variations between the models are due to two factors: a) the data used, and b) the number of coefficients determined. Each of these models is centered on a different epoch, Barraclough 1975, MAGSAT 1980, IGRF 1985, and Cain 1990. They have also been derived to different degrees, Barraclough N=12, MAGSAT N=66, IGRF N=10, and Cain N=15.

The distinguishing qualities of the data are when it was taken and how it was taken. The epochs given with each model reflect the date the model is best suited for. For MAGSAT, the data used was centered around 1980. For Barraclough, the data was centered around 1965 then the model was projected to 1975. Similarly, IGRF and Cain were based on data spanning the late 1970s to the early 1980s. These were then projected to 1985 and 1990. Each of the models uses a combination of data sources including, permanent observatories, repeat stations, ship-towed magnetometers, and satellite data. Satellite data has only been incorporated for the past two or three decades. The satellite "data" included in the Barraclough model was actually generated from another model which was based on data from the OGO series of satellites. The quality of the data varies due to the global coverage and the instrumentation used. For the ground-based data sets, the permanent observatory data is more accurate than the ship data. However, in order to adequately cover the globe, ship data is essential. Most of the models correct for the variation in quality by using weighting factors. The MAGSAT satellite data is of particularly high quality. This satellite was designed specifically to measure the magnetic field. The one drawback to this data is that it only covers a time span of about six months. Thus, one must be careful that temporal variations in the data don't appear to be spatial. These data are supplemented with ground-based data specifically to address this problem.

The other factor contributing to differences between the models is the degree and order to which the models are derived. The higher the degree of the model, the more complex the structure becomes. The core component of the field is seen primarily in the lower degree terms and is the dominant component to about n=13. The higher degree terms reflect the crustal component to the field. These become dominant around n=15. Thus, to most accurately model the internal field with all its local variations, a model which includes high degree terms is desirable. However, it may also be desirable to isolate the core component of the field and neglect smaller features due to the crust. In this case, one would truncate the coefficients at $n \leq 13$. IGRF 1985 is truncated at n=10 for this reason. Barraclough and Cain are limited to their respective degrees (12 and 15) due to the global coverage and accuracy of their data. MAGSAT has such a high degree due to the superior global coverage of the satellite, combined with highly accurate observatory data and less accurate scalar data available from remote regions.

2.1.3 High Latitude Limitations of the Models

Effort has been made to extend these models to high latitudes, but there are problems in doing so. The models are derived by fitting the data to the mathematical model. Thus, to obtain a reasonable model at high latitudes, one needs high latitude data. Clearly, data coverage in these regions is not as complete as in lower latitude regions. IGRF used vector data to $\pm 50^{\circ}$ and scalar data poleward of this. MAGSAT and Cain used data to within 7° of the poles, then interpolated over these regions. Barraclough used data to $\pm 85^{\circ}$. Thus, one must be careful when applying these models at high latitudes.

2.2 IGRF 1985

The International Geomagnetic Reference Field Revision 1985 (hereafter IGRF 1985) is the product of the International Association of Geomagnetism and Aeronomy (IAGA) Division I, Working Group 1. This 13 member group has produced a series of mathematical models of the Earth's main geomagnetic field and its secular variation. First adopted in 1968 and now with the fourth revision there are five IGRF models (1945, 1950, 1955, 1960 and 1965), four "definitive" models (DGRF 1965, 1970, 1975, and 1980), and a predictive model projecting the secular variation 1985 to 1990 [*IAGA*, 1986]. The models which will be discussed here are DGRF 1980, the predictive SV model 1985-1990, and IGRF 1985. Note that the IGRF 1985 model was produced by applying five years of secular variation (1980-1985) to DGRF 1980 [*Barraclough*, 1987].

In the fourth revision of IGRF, 23 models from five groups were submitted for models ranging from 1945 to 1990. For the models of interest here, the Working Group truncated the model GSFCMF80 (Goddard Space Flight Center Main Field 1980) by Langel and Estes [1985] to n=10 and kept it as the DGRF 1980. The secular variation model for 1980-1985 was the mean of models BGSSV82 (British Geological Survey Secular Variation 1982) by Quinn et al. [1987], IZMSV82 (Institute of Terrestrial Magnetism, Ionosphere and Radio Wave Propagation (IZMIRAN) Secular Variation 1982) by Golovkov and Kolomiitseva [1987], and USGSSV87 (United States Geological Survey Secular Variation 1987) by Peddie and Zunde [1987a]. The predictive model for 1985-1990 is the mean of BGSSV87 [*Barraclough and Kerridge*, 1987], IZMSV87 [*Golovkov and Kolomiitseva*, 1987], and USGSSV87. Since the IGRF 1985 coefficients were determined by taking DGRF 1980 and applying the secular variation for 1980-1985 to its coefficients, the derivation of the Langel and Estes model for 1980 will be described.

2.2.1 The Main Field Model

Langel and Estes used the data from MAGSAT (November 1979 to April 1980) plus data from 91 magnetic observatories (1978 to 1982) for their model of constant coefficients (degree and order 13) and secular variation coefficients (degree and order 10).

MAGSAT had an altitude range of 300-500 km with a sun-synchronous orbit at the terminator (i.e. day-night boundary). Thus, data was only taken at dawn and dusk in local time. This was the first global vector survey of the near-Earth geomagnetic field. However, in modeling the field using the gradient of the scalar potential, the field is assumed to be curl-free. This does not hold at satellite altitudes. MAGSAT passes through field-aligned currents which have an effect on the field magnitude. To compensate for this, component data was used only between ±50° geomagnetic latitude. Above this, only magnitude data was used.

Langel and Estes also investigated local time asymmetries by modeling the dawn and dusk data separately. They found significant differences between these two sets which they attributed to an eastward equatorial electrojet which lies below the satellite. The electrojet affected the dusk data at certain latitudes, but not the dawn data. Thus, the dusk data was corrected for B and X between ±20° geomagnetic latitude, Y between ±15°, and Z between ±50° using the difference between the dusk and dawn potentials. This removes some of the independence of the dusk and dawn data. A model of the electrojet itself would have been the best way to correct the data, but one was not available.

The data were put into three temporal groups: November-December 1979, January-February 1980, and March-April 1980. The dawn and dusk data were separated and put into 5° x 5° equiangular bins. Residuals were computed from a previous model and data which fell outside the acceptable range from these were rejected. Data were selected from each bin such that there were an equal number of points for equal areas all over the globe. Preference was given to dawn data and uncorrected dusk data where possible, with the corrected dusk data used as necessary. Data were also selected such that a good spread of Dst values between ±22.5 nT was obtained to improve the analysis of the external field. The data were estimated to be accurate to 6nT root-sum-square (rss) in each component and to 2nT rss in the field magnitude.

In addition, observatory data from 91 stations (1978-1982) was obtained from NOAA National Geophysical and Solar Terrestrial Data Center to supplement the MAGSAT data. The data were converted to X, Y, and Z in geodetic coordinates using an equatorial radius of 6378.165 km and flattening of 298.25.

For each coefficient the standard error was determined as was the error between dawn and corrected dusk models. As in any large statistical study, two sources of error are present, one in the data and the other in the averaging process. The errors derived only from the fit tend to underestimate inaccuracies due to model validity, improper estimates of data correlation, and systematic effects of non-core fields. Since the dawn set and dusk set have identical error characteristics except for the effects of the external fields, the difference in their errors reflect external influences while the coefficient standard errors reflect internal inconsistency.

2.2.2 The 1980-1985 Secular Variation Model

A secular variation model was then applied to DGRF to obtain IGRF 1985. Three candidate models were submitted to the IAGA committee. Rather than selecting one model over another, the committee decided to take the mean of all three and adopt that as the 1980-1985 secular variation model. The candidate models are BGSSV82, IZMSV82, and USGSSV87. Each of these will be briefly summarized below.

The BGSSV82 model [*Quinn et al.*, 1987] was based on magnetic observatory annual means primarily from the World Digital Data Centre C1 in Edinburgh, supplemented with data from World Data Centres A and B. Annual means from 172 observatories over the period 1969.5 to 1983.0 were used. The secular variation was estimated by finding the first differences of the component data. Linear fits to the data were computed using least squares with weights varying linearly from 1969.5 (given a weight of 0.5) to 1983.0 (given a weight of 1.0). They found that a single line was inadequate to fit the data. This is due to a discontinuity (or "jerk") in the secular variation in 1978. Thus, they used two line segments to fit the data. They obtained a model to degree n=8 with rms residuals of 5.8 nanoTesla/annum in X, 4.9 nT a^{-1} in Y, and 5.2 nT a^{-1} in Z.

The IZMSV82 model [*Golovkov and Kolomiitseva*, 1987] was based on data from 160 observatories. To this they added data at 34 locations (generally ocean areas) to fill gaps in the data due to the distribution of these observatories. The added data was generated from a previous model, IZMSV80. They graphically smoothed their X, Y, and Z data to obtain $\dot{X}$, $\dot{Y}$, and $\dot{Z}$. Using this technique, they tried to account for some of the non-linearities in the data. They found rms residuals of 4.0 nT a^{-1}, 3.5 nT a^{-1}, and 4.6 nT a^{-1} for $\dot{X}$, $\dot{Y}$, and $\dot{Z}$, respectively.

The USGSSV87 model [*Peddie and Zunde*, 1987a] was based on data from 148 observatories over the period 1980 to 1983. The data consisted primarily of annual all-day means (i.e. the mean of all the daily means for the year). When it was available for the complete series, quiet-day means were used. These are the annual means based on the five international quiet days per month. These are not available from most observatories. It is preferable to use the quiet-day means to reduce the external contributions to the secular variation models. A linear fit was made to the X, Y, and Z components using unweighted least squares. The slopes of these lines were taken as the estimates of $\dot{X}$, $\dot{Y}$, and $\dot{Z}$. The spherical harmonic analysis was then performed on these values. A model of degree n=8 was found to be a good compromise between model size and goodness of fit with 6.1 nT a^{-1} in $\dot{X}$, 5.3 nT a^{-1} in $\dot{Y}$, and 5.2 nT a^{-1} in $\dot{Z}$.

2.2.3 The 1985-1990 Secular Variation Model

The secular variation model adopted by the IAGA committee was also a mean of three models. These three were essentially by the same authors as the models described previously for the 1980-1985 SV model. These models are BGSSV87, IZMSV87, and USGSSV87. The USGSSV87 model was discussed in the previous section. The other two models will be briefly described below.

The BGSSV87 model [*Barraclough and Kerridge*, 1987] was obtained from data from 159 observatories taken from 1969.5 to 1983.0 . A linear fit to the data was made using weighted least squares. Two line segments were required to fit the data due to the jerk in 1978. This was the same procedure as that used to generate BGSSV82. Then they synthesized $\dot{X}$, $\dot{Y}$, and $\dot{Z}$ for 1987 by extrapolating the linear fit assuming a constant secular acceleration from 1969.5 to 1987.5. This extended data set was then used to get a model to degree n=8 with rms residuals of 10.4 nT a^{-1}, 10.1 nT a^{-1}, and 9.6 nT a^{-1} in $\dot{X}$, $\dot{Y}$, and $\dot{Z}$, respectively.

The IZMSV87 model [*Golovkov and Kolomiitseva*, 1987] used the IZMSV82 data set from 160 observatories. Then the predictive model was obtained by using a graphical extrapolation of $\dot{X}$, $\dot{Y}$, and $\dot{Z}$. They again filled the data gaps in the ocean regions, but this time they used their 1982 SV model to generate the data. This was to obtain a 1985 predictive model, this in turn was used to generate the data to fill in the gaps to obtain the 1987 predictive model.

2.2.4 Discussion

As pointed out by Golovkov and Kolomiitseva [1987], the SV models for 1985-1990 all have very similar background data. Thus, differences in the models arise due to how the non-uniform distribution of the observatories is handled and how the data is processed. These differences can be significant and can be indicative of the reliability of the model. These authors compared the three candidate models for 1985-1990 and found that IZMSV87 and USGSSV87 agreed quite well, whereas the BGSSV87 model was not in such good agreement.

Similarly, Peddie and Zunde [1987b] looked at the three candidate SV models for 1985-1990 and compared them to data from 148 magnetic observatories. They assume that the present rates of change will continue. Thus, their comparison was based on the most recent trend in SV (1980-1983 at these observatories). They also found IZMSV87 and USGSSV87 agreed fairly closely to the data whereas BGSSV87 did not agree as well.

Cain and Kluth [1987] also reviewed these models. They looked at the differences of the coefficients and the components $\dot{X}$, $\dot{Y}$, and $\dot{Z}$ between these models. Again, BGSSV87 was found to have poorer agreement with the other two models than they have with each other. BGSSV87 differed from the other two by up to 100 nT a^{-1}, whereas IZMSV87 and USGSSV87 agree to within 20 nT a^{-1} everywhere except in the eastern Pacific.

Rather than selecting one model over another for the SV model, the three candidate models were averaged together to comprise the SV 1985-1990 model. The three models were apparently combined equally without any statistical weights. It is not clear why this was done. No explanation was given by Barraclough [1987] in the report which describes what the IAGA committee selected (note, Barraclough was the chairperson of this committee).

2.3 CAIN

While conducting an analysis of candidate models for IGRF 1985, Cain and Kluth [1987] found what appeared to be a jerk in the secular change determined from the observatory data in mid-1983. If this jerk is real, a question arises as to how well the IGRF 1985 model might project to 1990. They concluded that the observatories gave inadequate coverage to ascertain whether this was a real phenomenon or not. In fact, they questioned whether the SV model based on these data alone give a reliable global estimate of SV at all. Thus, they decided to construct another secular variation model based on the observatory data plus, scalar data from ship-towed magnetometers and data from Project Magnet aircraft (from the U. S. Naval Oceanographic Office).

They investigated linear and parabolic secular change models. As a starting point, they truncated their n=66 MAGSAT model [*Cain et al.*, 1988] to n=15. This was done due to the limitations of the observatory, Project Magnet, and ship-towed magnetometer data sets. These do not have adequate global coverage to generate a reliable model of such high degree. These additional data sets were used to determine a secular change model to extrapolate MAGSAT to future epochs. Various secular variation models were derived with a linear model (M8386L) giving the best projection of the field to 1990 [*Cain*, 1987].

Note, in this section, only the derivation of the secular change model which is applied to the MAGSAT model to obtain the Cain 1990 model is discussed. The derivation of the MAGSAT model which is used here as the main field model will be presented in the subsequent section of this report (2.3 MAGSAT).

2.3.1 Description of the Secular Variation Data

The observatory data came from several sources, digital data at one and 2.5 minute intervals and tabular data of hourly and annual means with absolute scale offsets (most of the time). Most of the data was supplied by the National Oceanic and Atmospheric Administration (NOAA) in Boulder, Colorado. Additional data was obtained from the World Data Center B in Moscow. Plus, some data was sent directly from the magnetic observatories.

The observatory data needed to be put into a uniform format. Thus, they used hourly averages when it was possible and supplemented these with the annual all-day means. Cain [1987] points out that the quiet-day means are preferable to the all-day means (the former determine the annual mean using only the means from the five international quiet days, whereas the latter uses all of the daily means to evaluate the annual mean). However, these

are not as readily available as the annual means determined from the all-day means. Data was selected according to following criteria. To maximize the amount of data while minimizing Kp, Kp<2 was chosen as the cutoff for acceptable data. Similarly, to reduce the effects of diurnal variations, only data within four hours of local midnight was kept. To account for external contributions to the field, the Dst correction was calculated from near equatorial H values. There has not been a global determination of the zero-level Dst; thus they assumed it is constant over the data set and that its average may be derived. To simplify things somewhat, a ratio of internal to external effects equal to 0.28 was used. This may be too high for $\Sigma p<2$ and should be reconsidered. All of the data was expressed in terms of the X, Y, Z components, with the incomplete vector data dropped, and each component then corrected for Dst.

The Project Magnet data were provided by NOAA and by the Navy in five minute intervals. It was binned by year and by areas equivalent to an equatorial 10^{o} x 10^{o} square. Only data with $Kp \leq 2$ were retained. Data within two hours of local noon were deleted. Comparisons were made to a previous model, with data differing from the model by more than 400 nT rejected. Vector data was weighted and used along with the more accurate scalar data. Dst was corrected for in the same manner as the observatory data.

The ship-towed data is a vast database. Hence, one could be selective about which data to retain. Values were selected for $Kp<1^{+}$ and within four hours of local midnight. Again the Dst correction was the same as the rest and the binning was by year.

All the data was combined into a 40,000 record set. All the observatory data was used with the Project Magnet (vector and scalar) and ship towed (scalar) data filling in the rest.

2.3.2 Derivation of the Secular Variation Model

To obtain secular variation, the X, Y, and Z components are fit to a polynomial using least squares. Then the slope at a given time is determined to obtain $\dot{X}$, $\dot{Y}$, and $\dot{Z}$. To make the calculations easier, the hourly averages were grouped into 10 day means. The data set was put into several test models to optimize weighting factors and to check the stability of the solutions with the available data distributions. The test models led to a final parabolic model of degree n=7. To find the best projection of the field to 1990, it was decided to use this parabolic model to generate additional data to compensate for the lack of available data post-1983. Thus, the real data from 1980 to 1983 results in the best model for this epoch, while the calculated "data" influences the secular variation after 1983. It is assumed that a linear projection to future epochs is the best. Here, two linear models were obtained, one for 1980-1983 (M8083L) and the other for 1983 to the end of the data set (M8386L). These models were derived to degree n=7 (stable solutions did not exist beyond this). The latter model gives the best projection to 1990.

Cain [1987] states M8386L gives the best projection to 1990. IGRF 1985 does not account for the mid-1983 jerk, thus as one gets further away from 1983, it is anticipated that Cain 1990 will represent the field better than IGRF 1985. Project Magnet and ship towed data are consistent with the post-1983 model and confirm the jerk detected in 1983 as well.

2.4 MAGSAT

MAGSAT was a satellite which was placed in a sun-synchronous orbit in the dusk-dawn meridian for the specific purpose of measuring the Earth's magnetic field (See Section 2.1.1). Several people have used the MAGSAT database to derive magnetic field models. For this report, coefficients derived by Cain et al. [1989a] for an n=66 spherical harmonic expansion have been used. This high degree is obtained by using the Neumann method of Gauss-Legendre quadrature [*Schmitz et al.*, 1989]. Although the model goes to n=66, the set available at GL only contains the coefficients to n=50. For computational expediency, one may select a subset of this which has been truncated to n=15.

2.4.1 Description of the Data

Cain et al. [1989a] applied the Neumann method of Gauss-Legendre quadrature to the radial components (B_r) of the MAGSAT data. Starting with a previous MAGSAT model, new observatory data was added. To obtain better secular change (SV) data, hourly values were only selected within two hours of midnight and for a limited range beyond $Kp=1^+$. These were then corrected for Dst, averaged for each universal time day and converted to X, Y, Z. Using least squares, $\dot{X}$, $\dot{Y}$, $\dot{Z}$ were found. The fit was good except at the North Pole due to seasonal variations in the polar ionospheric currents, which lead to secular changes which are higher than one expects from the internal field.

In order to minimize annual variations which arise in data sets taken over a short period of time, data was added to expand the collection time of MAGSAT. However, it was not extended too far so as to avoid problems with the jerks in 1978 and 1983. Data from MAGSAT was selected every 128th observation (roughly 50 km along satellite orbit). Only values where $Kp \leq 2^+$ and which were within the 100 nT of the previous model were kept. Of the 1,330,285 observations, half were lost to the Kp requirement and 4478 were lost to the 100 nT requirement. Data were binned every 3° in longitude and into 64 latitudes (the roots of the n=64 Legendre polynomial). Using Sugiura's computation of Dst, the data near the equator were corrected. Note, this does not account for a zero-level in Dst; thus, there may be an offset to this correction. This computation was done only for near equator stations and is not easily extrapolated to higher latitudes. So beyond the range of Sugiura's correction, a constant ratio of .28 for the internal and external terms was used to correct the data for Dst contributions. This was checked via scatter plots of the correction versus observatory hourly values when $Kp \leq 2^+$, and was deemed reasonable.

In getting the residuals, the average external term was canceled in taking the differences since the average external term is calculated along with the internal terms. However, the average induced internal field is still unaccounted for. Five percent of the data was divided into dusk and dawn according to the local time of the observation and averaged by dip latitude. Analysis of these, points to a meridional current on the dusk meridian of the Y component [*Maeda et al.*, 1985] and to a weak westward electrojet flowing at dawn below MAGSAT altitudes in the E-region [*Cain et al.*, 1989a]. These were corrected for by using a simple function of dip colatitude to reduce the peak scatter (by as much as 15 nT at some latitudes).

2.4.2 Results from the Model

Ultimately, 100 to 400 data values were averaged per block with standard deviations of the means ranging from 3 nT to 40 nT with most under 10 nT. Using Neumann's method on a

data set with interpolated polar values, the same anomalies seen at n=29 were still present, but more sharply focussed in this case. Beyond n=35, some of the features may be of geologic significance [*Cain et al.*, 1983, *Cain et al.*, 1989b]. However, projections to the surface showed north-south striations which may be the result of inadequate noise reduction. The low degree terms in this model were also adjusted to look at the core components (n=11 to 14) which are cut-off in the n=10 models (i.e., IGRF and DGRF models). This technique makes it possible to obtain high degree models.

For the purposes of this report, small sample fields for 1980 were compared to see the differences in L-shell computed from the n=50 model, n=50 truncated to 20, and n=50 truncated to 15. The differences in the tested areas were very small, on the order of 10^{-4} - 10^{-5} for low altitude and no difference for higher altitude (>1000 km). One sample point showed a difference of .14 in L which is significant. However, the increase in computational time for the n=50 model did not seem justified for these comparisons. Thus, the model truncated to n=15 was used in the comparisons with Barraclough 1975, IGRF 1985, and Cain 1990.

2.5 BARRACLOUGH

Barraclough et al. [1975] derive three spherical harmonic models, the main field, the secular variation, and the secular acceleration. The main field model is composed of 168 spherical harmonic coefficients to degree and order 12. The secular variation model has 80 coefficients with degree and order 8. The secular acceleration model is comprised of the 26 most significant coefficients.

2.5.1 General Description of the Data

The main field coefficients are Schmidt quasi-normalized in nano-Tesla. They were derived from five data sets: survey, observatory, oceanographic, ships' compass, and satellite. The first four of these include all the 1955 to 1975 data from the World Digital Data Centre C1 at Herstmonceux. All the data were reduced to sea level and a common epoch, where the common epoch was chosen to be 1965. This was selected because it is the mean date of the observations and thus as many data are extrapolated forward as backward, thereby minimizing SV errors.

The survey data were obtained from land, sea and aircraft magnetic surveys of one or more of the following field components: Declination (D), inclination (I), horizontal intensity (H), vertical intensity (Z), and total intensity (F). The observatory data are the annual mean values from approximately 200 fixed stations with uneven global distribution. The observed components are generally D, H, and Z or I, but some of the high latitude stations also supplied north intensity (X) and east intensity (Y). The oceanographic data are comprised of a large number of total intensity observations made on surveys which covered most ocean areas. The ships' compass observations were used to fill in sparsely covered regions. They are generally D values of limited accuracy from compass record books of merchant vessels. Finally, the satellite data were obtained from a model (Cain 8/73) derived from the OGO series of satellites (numbers 2, 4, and 6, collectively referred to as POGO). The satellite data were handled differently and will be discussed later.

The data sets were binned into 1654 tesserae (regions defined by any two given latitude lines and any two given longitude lines) of approximately equal area (5° x 5° at the equator, 5° x

120° at the poles). Unlike the other models, the data for Barraclough 1975 are not centered on 1975, but rather on 1965. Thus, the data were evaluated using 1965.0 as the mean time of the data set, then the model was projected to 1975.0. The mean value of the data in each tessera was found with a separate series of means for each data set obtained. Post-1965 data were reduced to 1965.0 using a preliminary 1970 SV (secular variation) model by Malin and Clark [1974]. Updates from 1960 to 1965 were done using the 1960 SV model by Malin [1969] and the 1965 SV model by Malin and Clark [1974]. Error checking of the tesseral means using residuals between them and the corresponding IGRF 1965 values were performed.

The separate means for each data set were combined using a weighting system based on the number of observations, the date of the observation (1955-1965 was weighted by .5 due to their lesser importance), and the type of data (compass data was weighted by .01 since it is much less accurate). Then a differential method was used [*Cain et al.*, 1967] to obtain a spherical harmonic model of the main field from all of the elements of the geomagnetic field. With this technique, one solves for corrections to the coefficients of an approximate spherical harmonic model, IGRF 1965 in this case.

At this point, the satellite data set was incorporated into the model. Rather than re-evaluating the POGO data, Barraclough et al. used the POGO (8/73) model by Cain. This model includes the main field and secular variation to degree and order 14 for epoch 1970. With this, total intensity values were generated at 5° intervals of latitude and longitude between ±85° at 800 km (like real satellite data) for epoch 1965.0. These 2520 values were then used to obtain normal equations similar to the surface data equations. Then the satellite set and surface set were given equal weights to obtain the spherical harmonic model based on all the data.

2.5.2 Secular Variation

The secular variation model was derived from annual means from magnetic observatories, repeat stations (stations where observations are less frequent than once per day), survey data, and satellite data. The magnetic observatory data set came from 180 observatories and is comprised of D, H, and Z observations. The differences of each element were plotted versus time with the curves extrapolated to 1975. Each extrapolated value was given a range in which the actual value might fall based on the reliability of the data and on correlations with nearby observatories. This uncertainty range was then used to assign weights to the 532 values. Again, extensive error checking was performed on each data set using the average of the other four as the norm. The best linear fit of data from 656 stations (1877 data points) was used to determine $\dot{D}$, $\dot{H}$, $\dot{Z}$ at the mean epoch of observation.

$\dot{X}$, $\dot{Y}$, and $\dot{Z}$ values were generated from the difference between the 1960 and the 1970 eighth order main field spherical harmonic models. These were derived from 1955-1965 survey data and post-1965 survey and oceanographic data, respectively. These data points were generated at the center of each tessera and weighted according to the number of observations from 1960 or 1970 in that tessera (the lower of the two if they are not the same). Similarly, POGO (8/73) was used to get an interpolating function by synthesizing $\dot{F}$.

Of the four categories (observatory, repeat stations, survey and satellite data), only the first refers to 1975, the rest were updated with a secular acceleration model. A separate model was derived from each group and the models were compared to each other to double check the suitability of the observational equations used.

2.5.3 Secular Acceleration

The secular acceleration model used seven SV models. The five year means of X, Y, and Z from the same set of 80 observations (given equal weight) for four models (to 6th order and degree) 1942.5-1947.5, 1947.5-1952.5, 1952.5-1957.5, 1957.5-1962.5 were used. Similarly data from the 1962.5-1967.5 model was used, but this model was based on data from 118 observatories. The final two models, 1970 and 1975, were based on annual D, H, and Z means from 180 observatories weighted according to confidence limits on data. These last two models are complete to 5th order and degree, but they also have some coefficients out to 8th degree.

The linearity of the SA plots indicate higher order derivatives are negligible in comparison to SA. The coefficients were calculated using a least squares fit to the coefficients of the seven SV models of equal weight. Standard deviations were calculated from the scatter of points about the best straight line. The final model then, is composed of 26 coefficients exceeding the standard deviation by more than 2.5.

3. B FIELD COMPARISONS OF THE MODELS

Each of the models (IGRF 1985, Cain 1990, MAGSAT 1980, and Barraclough 1975) were used to obtain the total B field and its components at five altitudes (350 km, 850 km, 1500 km, 10,000 km, and 15,000 km) for 1990, 1985, and 1980. The differences between these models were then plotted for each altitude and year to get an overview of the model discrepancies. IGRF 1985 is used as the standard since it is the best known and most widely used of all the models. More detailed comparisons were made by looking at B values obtained from each model over a range of latitudes for a given longitude, epoch, and altitude. Initially, the whole latitude range was used (±75°). Then, the range CRRES will be in was examined more closely (±20°). Finally, contour plots of the field determined from IGRF 1985 for 1980 and 1990 at 350 km are presented to show the overall change in the field over this ten year span.

3.1 OVERALL MODEL DIFFERENCES

Figures 3.1a and 3.1b are examples of the contour plots produced initially to look for trends in the model differences over the full latitude and longitude ranges considered. Figure 3.1a shows the differences found for 1990 at an altitude of 350 km. The lower right panel of the plot shows the magnitude of B over the globe as calculated by IGRF 1985. The contours are drawn at increments of 5000 nT. The South Atlantic Anomaly (SAA) is clearly visible as are the poles. Note, the appearance of the two maxima in the northern hemisphere are a product of the projection. If this plot were mapped onto a sphere, there would only be one northern maximum indicative of the north magnetic pole. The magnetic field is strongest at the poles, decreasing towards the equator as is expected for a nearly dipole field. The other three panels show the absolute differences in nT between Cain, MAGSAT, and Barraclough versus IGRF, respectively.

The differences seen in Cain-IGRF and MAGSAT-IGRF are less than one percent of the total field. There does not appear to be any systematic difference in either of these plots. The scattered distribution of the difference contours is probably a reflection of the different degrees of these models. Both Cain and MAGSAT have higher order coefficients than IGRF. Thus, they represent some of the local crustal contributions to the field which IGRF does not. Still these are small differences. The differences seen in Barraclough-IGRF are somewhat larger than those observed in the other two plots. They are still only on the order of a percent or so. Here, the distribution of the contours is not scattered as it is with the others. This implies a more systematic variation from IGRF which is probably attributable to the projection of the model over 15 years to 1990.

Figure 3.1b is essentially the same as Figure 3.1a, however it shows the differences at an altitude of 10,000 km. This altitude is about as distant as one should go without including the external field calculations. Here, the field strength has dropped off by more than an order of magnitude. The polar maxima are still visible, but they are not as distinct. The SAA is still apparent, but again it is not as distinct as it is at perigee.

The differences seen in Cain-IGRF and MAGSAT-IGRF are less than one percent. The contours are not as scattered as previously. The crustal contributions to the field are not as pronounced as at lower altitudes. Cain-IGRF shows some differences centered around the SAA and some differences centered over the southern Indian and Pacific Oceans. This is to

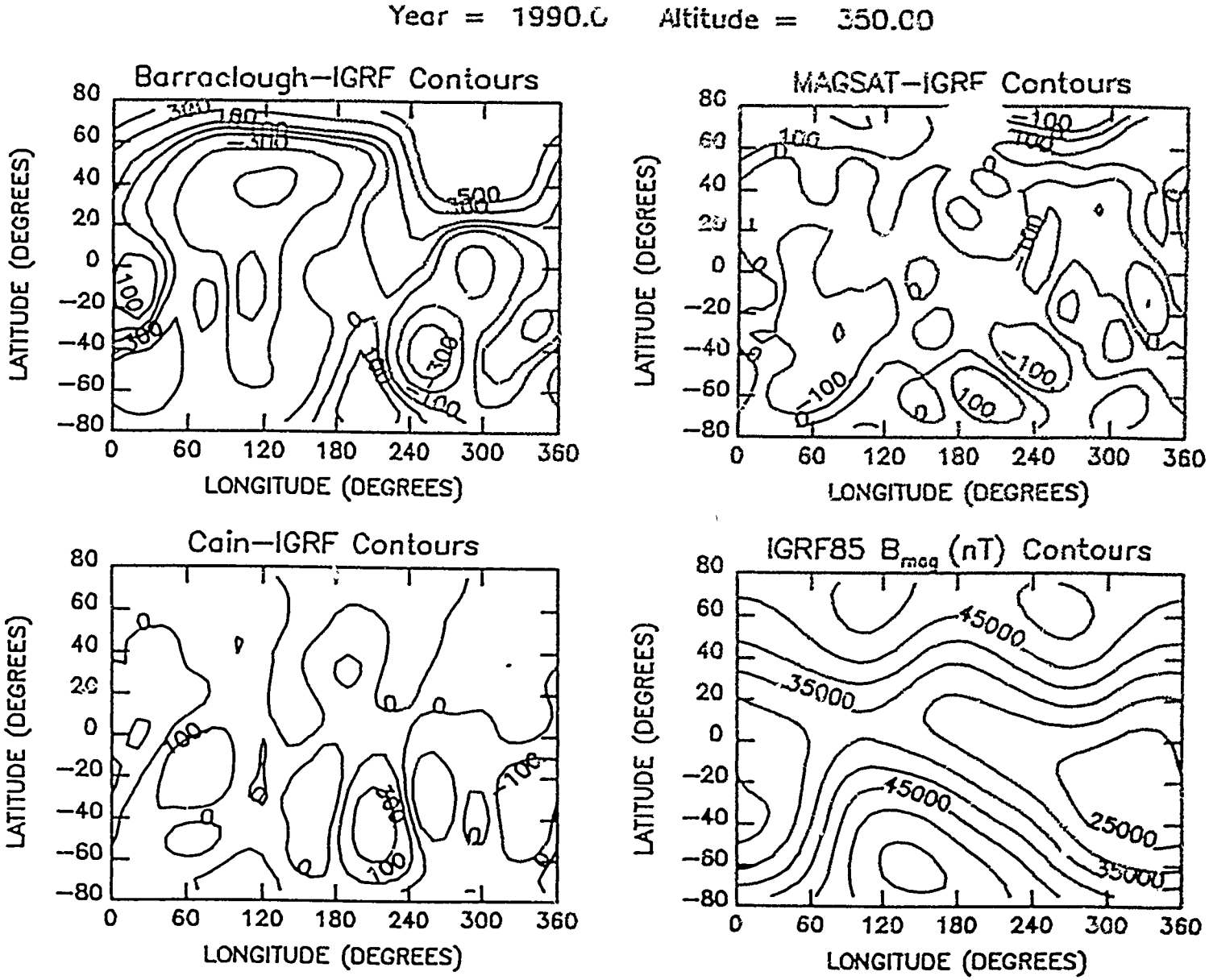

Figure 3.1a. Contour plots of model B_{mag} differences in nanoTesla covering the full latitude and longitude ranges. IGRF 1985 is used as the reference model. The comparisons are done for an altitude of 350 km (perigee) at 1990.0.

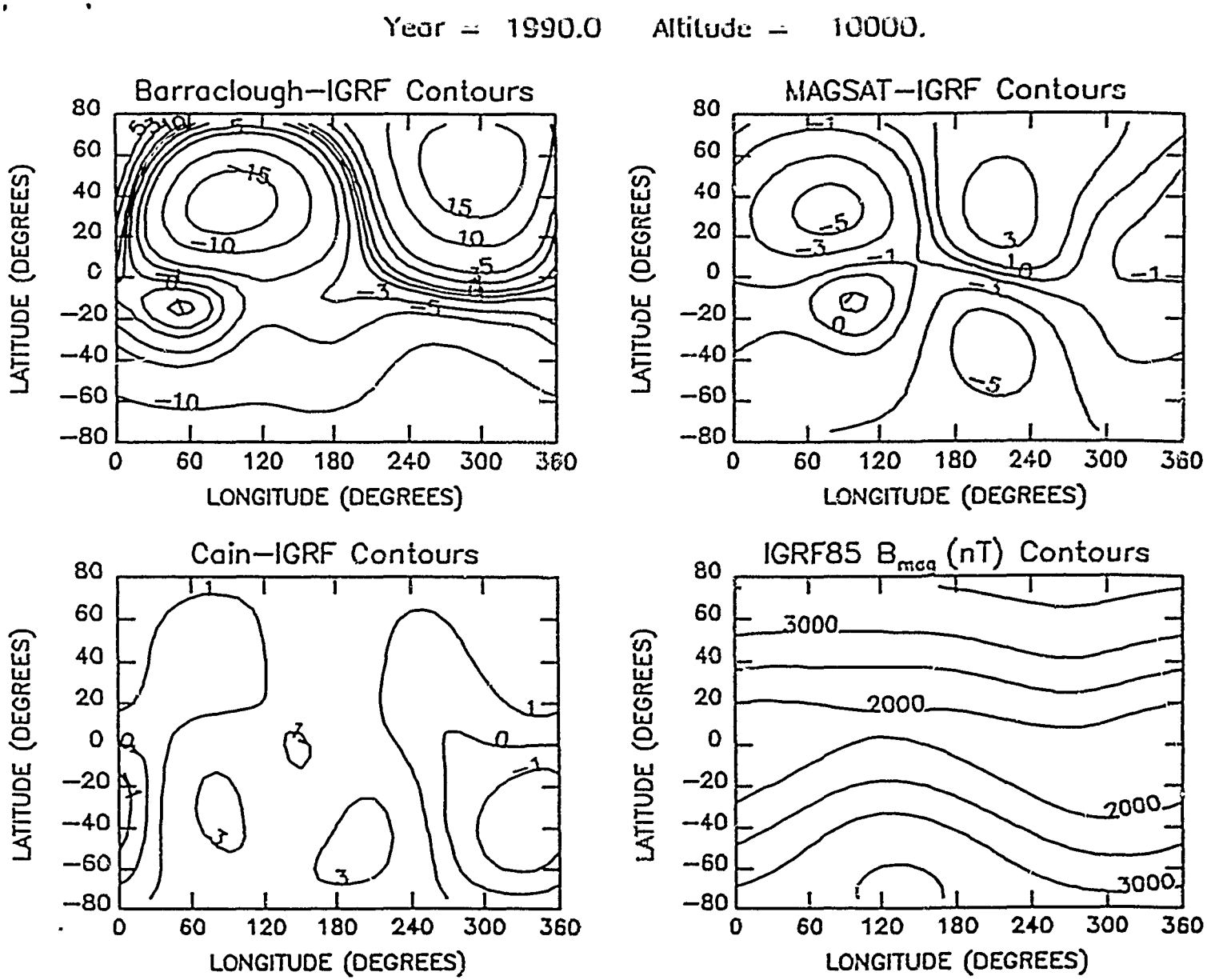

Figure 3.1b. Contour plots of model B_{mag} differences in nanoTesla covering the full latitude and longitude ranges. IGRF 1985 is used as the reference model. The comparisons are done for an altitude of 10,000 km at 1990.0.

be expected due to the poorer data coverage in the southern ocean regions. Similar features are seen in MAGSAT-IGRF. Here, there is no distinct difference centered on the SAA. However, there are a couple of distinct northern features. One set of contours is centered over the northern Pacific and another is centered over western China (a particularly mountainous region, presumably this area has not been covered well with ground-based observations). Again, the differences seen in both of these plots are quite small compared to the total field observed. The differences seen in Barraclough-IGRF are larger than the others, but still less than one percent of the magnitude of the field. The largest differences are centered around western China and the region around Baffin Bay (northeastern Canada). This latter area is surprising, since this region is reasonably well covered by magnetic observatories.

Table 3.1 presents the maximum differences between ±20° latitude for all of the years and altitudes calculated. Each model is compared to IGRF 1985 (model-IGRF). MAGSAT shows the closest agreement at 1980. By 1990, Cain agrees best with IGRF. For Barraclough and MAGSAT the differences steadily increase with time. For Cain, the differences are smallest for 1985 increasing as one extrapolates both forward and backward from this epoch. Note, that while the absolute differences drop with increasing altitude, so does the magnitude of the field. The percent differences also drop with increasing altitude slightly. These worst differences are all less than one percent of the magnitude of the field for 1980. MAGSAT and Barraclough are off by about 1.5% for 1990 at 350 km. For 10,000 km, these vary from IGRF by less than a percent.

3.2 COMPARISONS AT SPECIFIED LONGITUDES

Next, line plots of the magnitude of B were generated to high latitude at four longitudes over the globe (see Figure 3.2). All four models are plotted in each panel. The agreement is close, but there are clearly areas where the models do not coincide. As is expected, Barraclough varies the most, but careful examination (particularly of the lower left panel) shows that MAGSAT, Cain, and IGRF do not completely overlap each other either. These plots show polar maxima (the right two panels) and the SAA minimum (the lower right panel). Note, that the longitudes shown are not at the peaks of any of these features, but one can see how the field is changing over longitude. Taking a closer look at this sort of plot, Figure 3.3a focusses in on the ±20° range at 1990 (upper panel) and 1980 (lower panel) for 80° east longitude at perigee. The differences are apparent in 1980, but they have significantly increased by 1990. Figure 3.3b gives a similar comparison, but for an altitude of 10,000 km. The models are in much better agreement for both epochs at this altitude.

3.3 B DETERMINED BY IGRF 1985 FOR 1990

Figure 3.4a shows the difference between the constant B contours calculated using IGRF 1985 for epochs 1990 and 1980 at an altitude of 350 km. While the general shape and distribution of the field lines remains unchanged over the ten year span, the field strength is decreasing (this is most apparent at the edges of the plot). This is seen to be the case at all five altitudes which were compared. This is due to the fact that the dipole moment is decreasing (about 0.05% annually). The decreasing dipole has significant ramifications in computing the magnetic field (see section 4.3.3.1). Figures 3.4b and 3.4c are included for the benefit of the reader. These show the 1990 B magnitude contours determined from IGRF 1985 for the remaining four altitudes: 850 km, 1500 km, 10,000 km, and 15,000 km.

Table 3.1. MAXIMUM B_{mag} DIFFERENCES BETWEEN ±29° LATITUDE
All models Compared to IGRF 1985 (Model-IGRF)

Year	Alt. (km)	Cain (nT)	Magsat (nT)	Barraclough (nT)
1990	350	257.34	-306.22	-639.74
	850	162.7?	-175.11	-409.83
	1500	97.12	-98.37	-249.93
	10000	3.28	-5.58	-14.37
	15000	1.19	-2.36	-5.39
1985	350	95.57	-159.15	-442.93
	850	60.16	-90.13	-287.49
	1500	36.33	-51.14	-175.70
	10000	1.59	-2.65	-9.50
	15000	0.61	-1.13	-3.54
1980	350	163.59	66.05	-249.10
	850	105.47	40.45	-165.36
	1500	63.34	23.26	-106.03
	10000	1.95	-1.60	-4.97
	15000	0.72	-0.71	-1.73

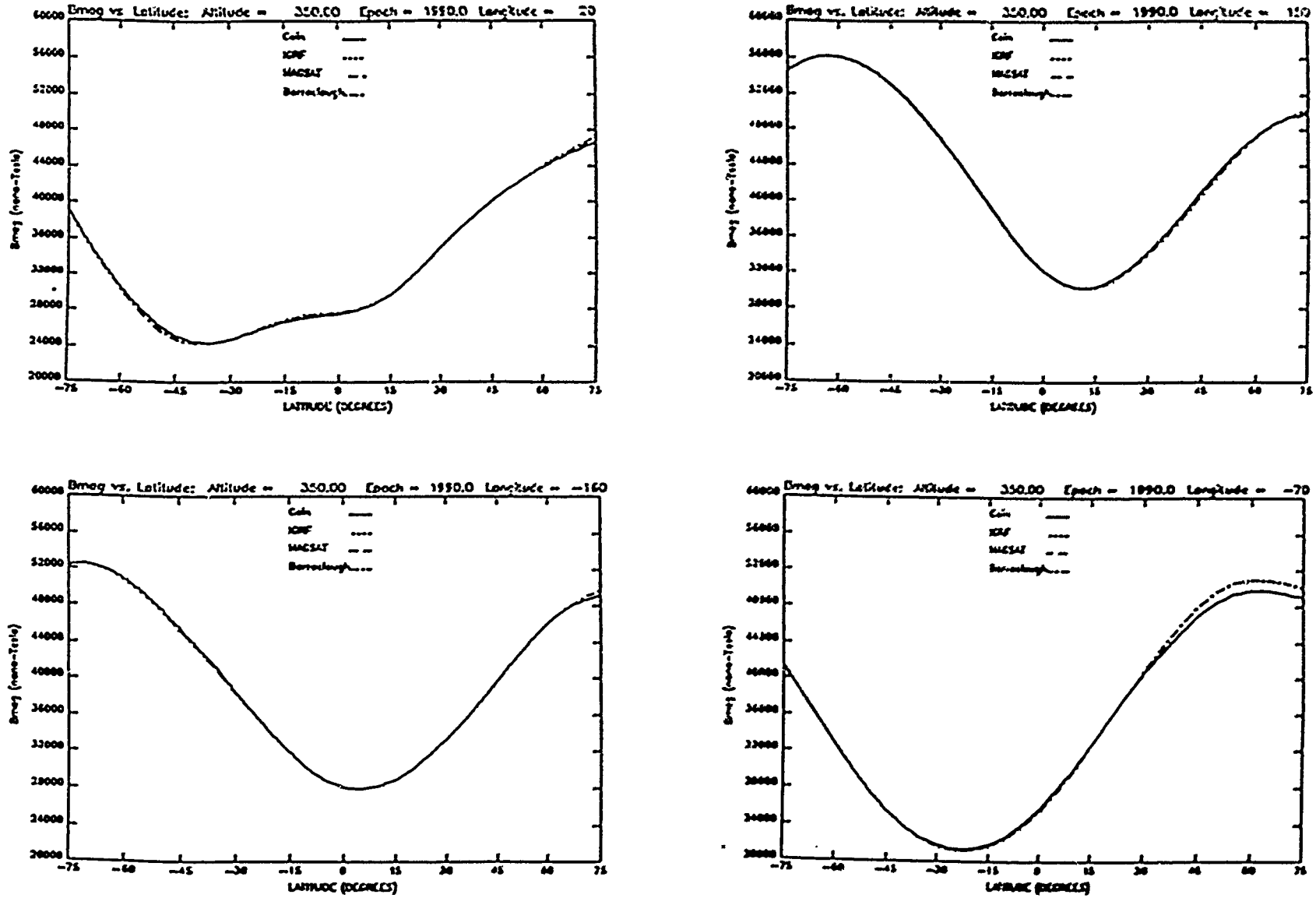

Figure 3.2. Line plots of the four models plotted together at four different longitudes over the globe for the full latitude range. For the most part the models agree at this resolution, although Barraclough is seen to vary somewhat in each of the plots.

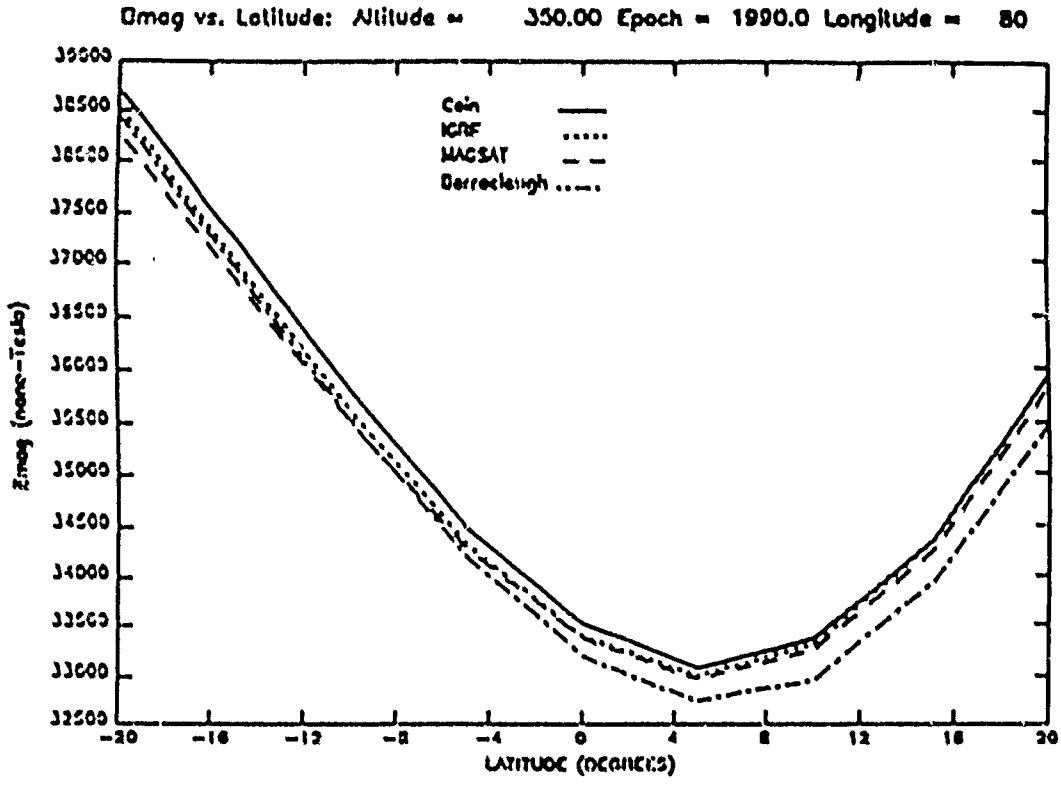

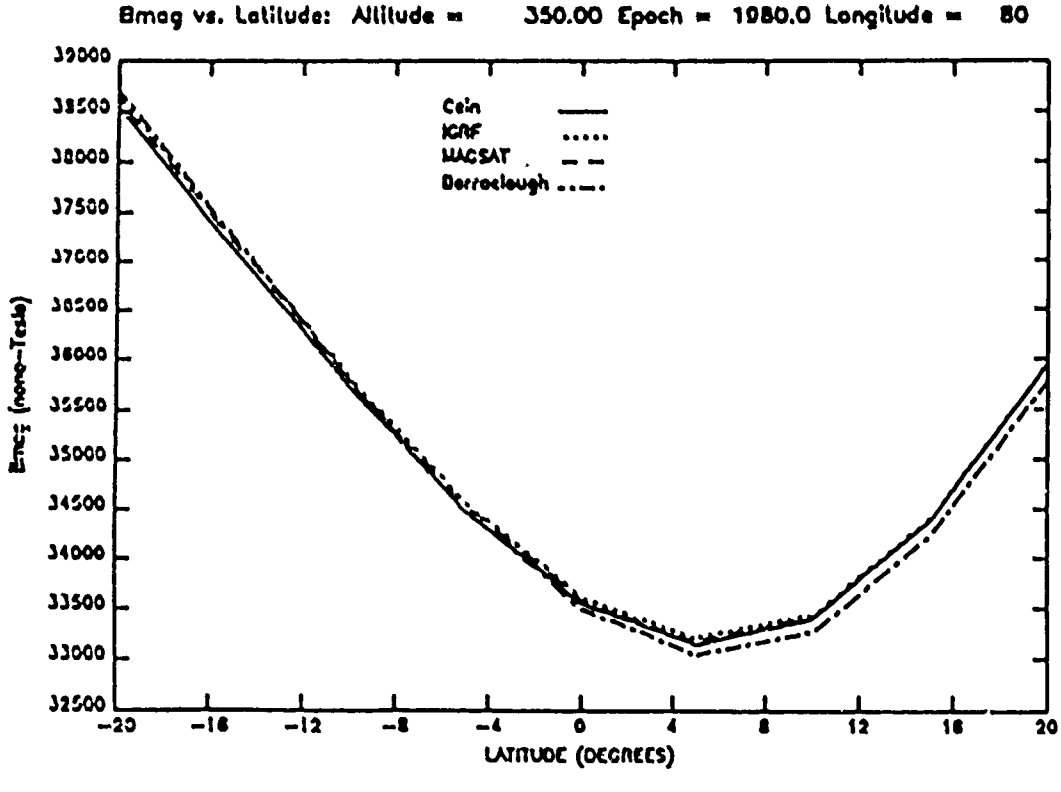

Figure 3.3a. Line plots similar to those in Figure 3.2, but over a smaller latitude range. At this resolution differences between the models are apparent. The top panel shows the differences at 350 km and 80° east longitude for 1990.0. The bottom panel is the same plot done for epoch 1980.0. Clearly discrepancies arise over time.

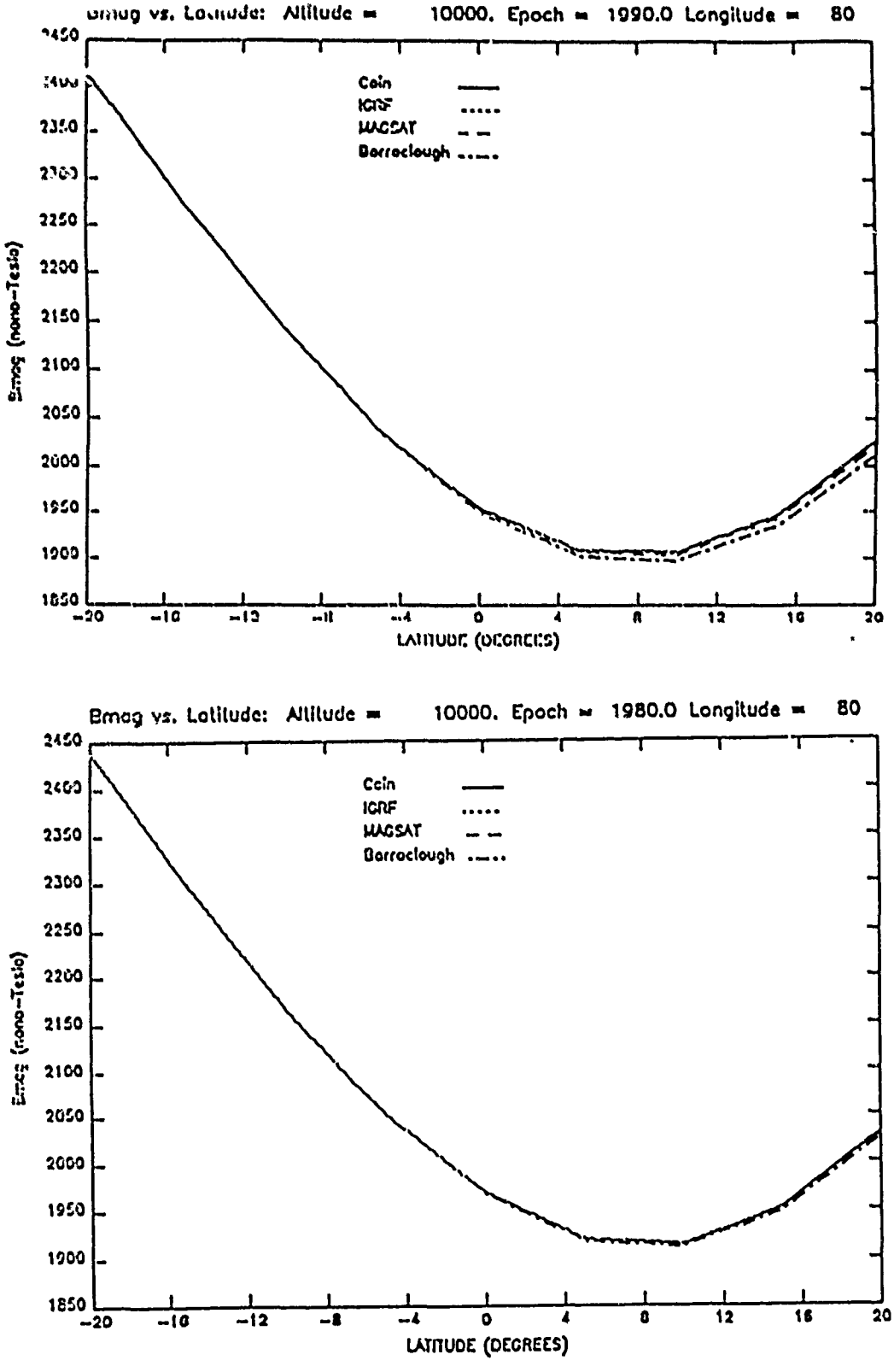

Figure 3.3b. Line plots very similar to those in Figure 3.3a, but for an altitude of 10,000 km rather than 350 km. The top panel shows differences seen at 1990 and the bottom panel shows differences at 1980 for 80° east longitude. The agreement for both these epochs is better at this altitude than at 350 km. As in Figure 3.3a, the models are in closer agreement at 1980 than 1990.

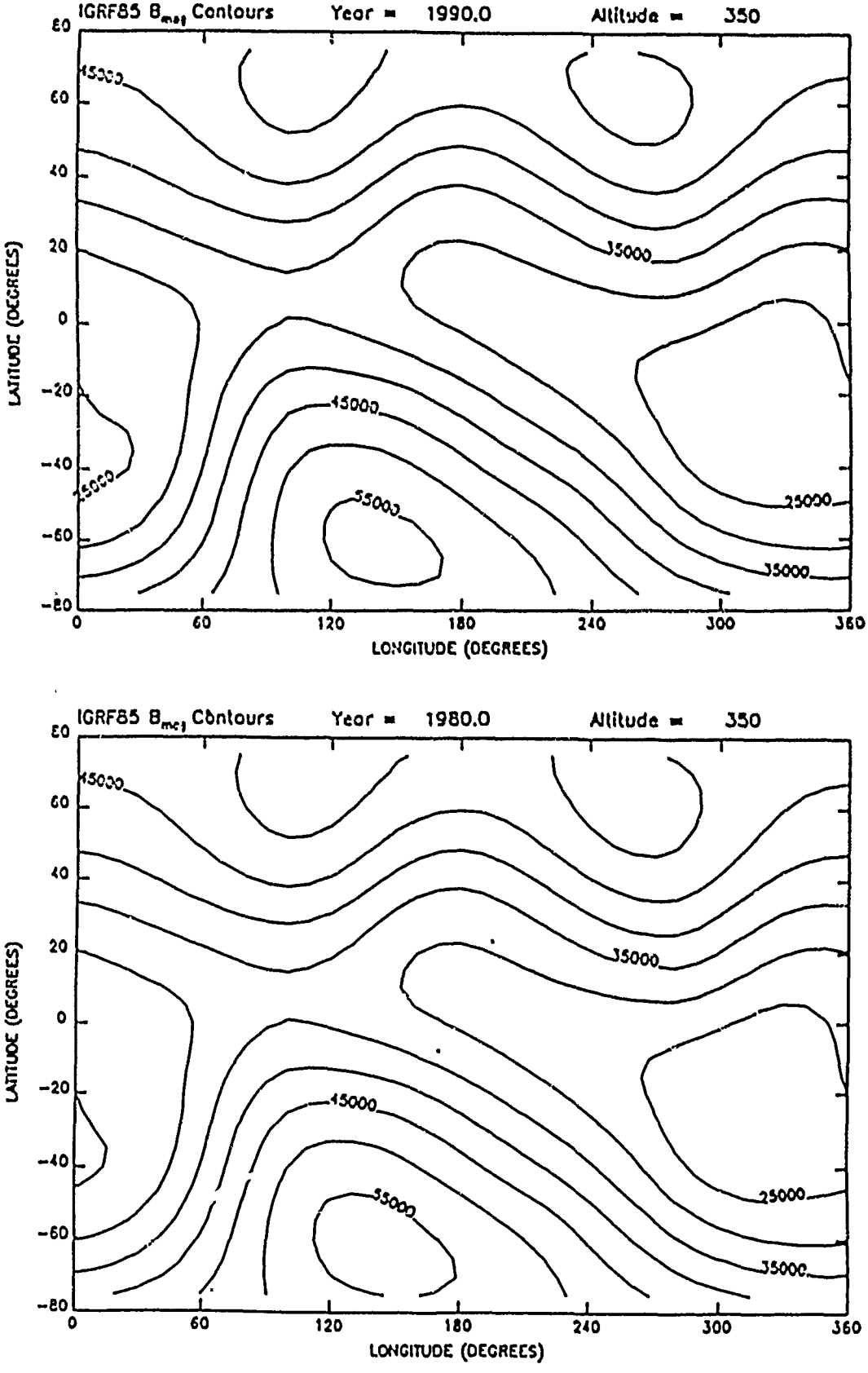

Figure 3.4a. Contours of B_{mag} as determined by IGRF 1985 over the full range of latitudes and longitudes at 350 km for 1990 (top) and 1980 (bottom). The field is decreasing slowly over time (this effect is most noticeable at the edges of the plots).

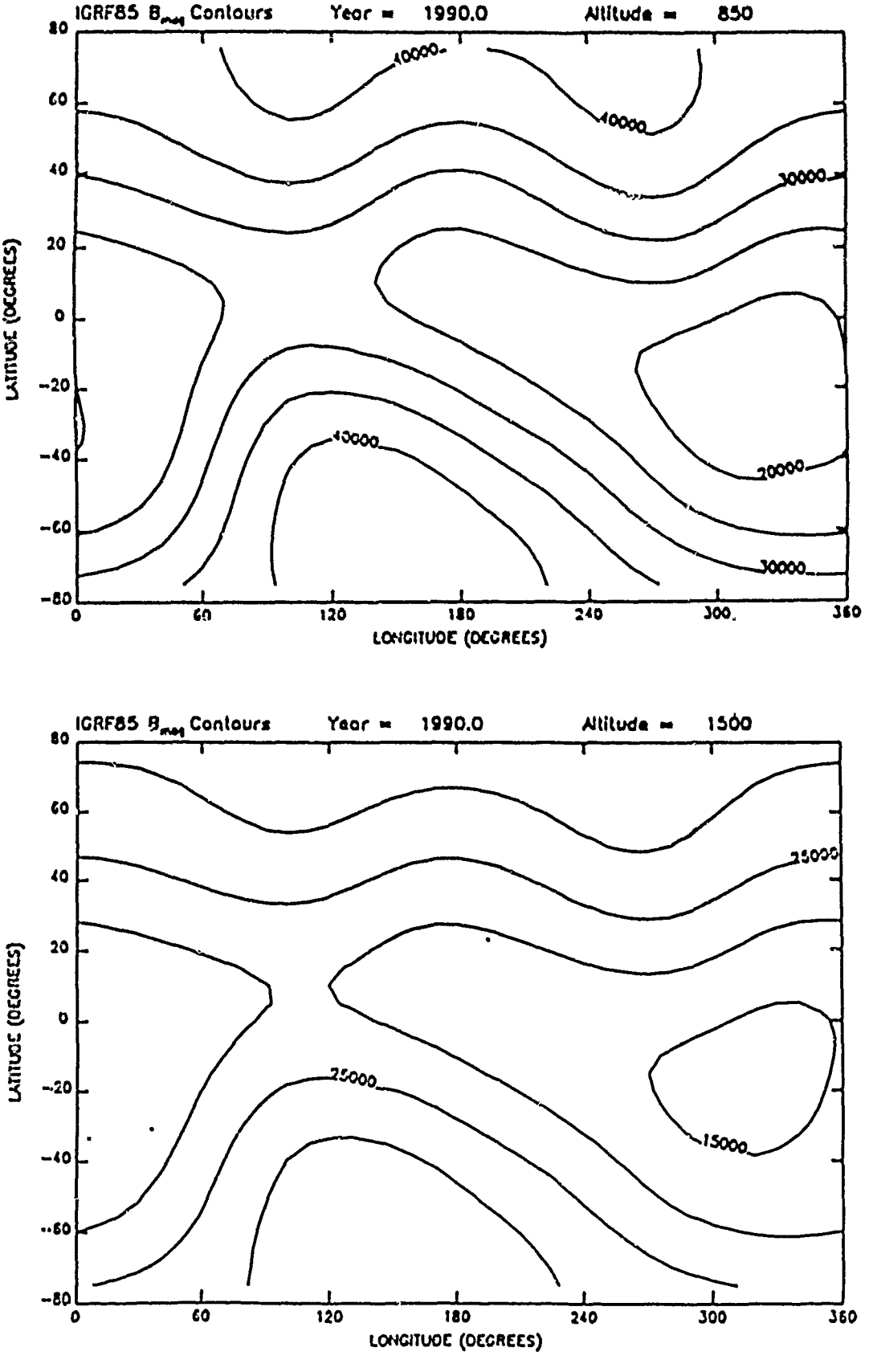

Figure 3.4b. Contours of B_{mag} as determined by IGRF 1985 for 1990 over the full range of latitudes and longitudes at 850 km (top) and 1500 km (bottom).

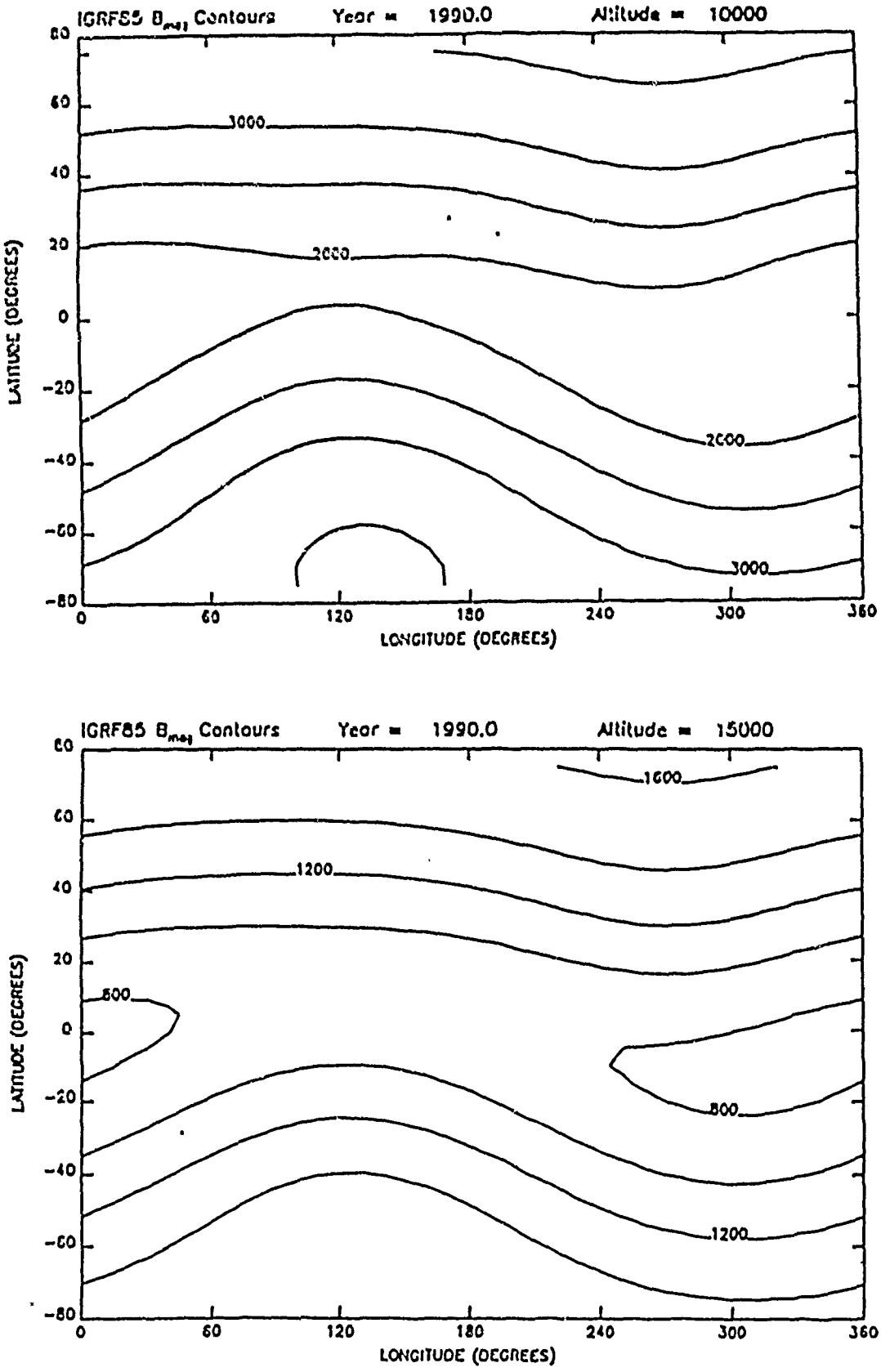

Figure 3.4c. Contours of B_{mag} as determined by IGRF 1985 for 1990 over the full range of latitudes and longitudes at 10,000 km (top) and 15,000 km (bottom).

4. DISCUSSION OF SOFTWARE

4.1 INTRODUCTION

Three basic software packages were used in this analysis. One has been derived from OPTRACE [*Radex, Inc.*, 1987], which was developed to compute the magnetic field quantities (model field vector, L parameter, 100 km field line intercepts, etc.) which will be stored in the CRRES ephemeris. This package incorporates the IGRF 1985 model, with the secular variation, for the internal portion of the magnetic field, and the Olson-Pfitzer tilt-dependent model [*Olson and Pfitzer*, 1977] for the external portion. This package was modified to include the other three models studied in this report (Barraclough 1975, Magsat 1980, and Cain 1990), and to exclude the external field. Finally, to save computation time, the computations of parameters other than the magnetic field vector and L were removed. This final package, called HMIN, was tested to assure exact reproduction of OPTRACE L values.

The other two packages, received from J. C. Cain, are resurrections of software developed by Kluge [1972], and Kluge and Lenhart [1972], respectively. The first package, SHELLC, uses a very fast algorithm [*Kluge*, 1970] for computation of the L parameter. The second package, INTEL, interpolates L from a prestored table, and is therefore even faster. However, the table is valid only for one epoch, i.e., no secular variation is included. The table was generated by Cain for his model at the 1990 epoch. However we do not at present possess the full software needed for generating tables for other models and epochs. The resurrected software was tested [*Cain*, 1987] with old cases run by Kluge to assure reproduction of results.

4.2 DEFINITION OF THE L PARAMETER

The L parameter maps points in a given magnetic field to points in a reference dipole field. The L parameter of a point [*McIlwain*, 1961] in a given magnetic field is the distance from the dipole, in earth radii, of the equatorial intersection of a dipole field line passing through a point with the same invariant integral I and field strength B in the reference dipole field as the point of interest in the given field. The invariant integral at a point A is the familiar field line integral

$$I = \int_A^C [1-B_s/B]^{1/2}\, ds$$

where C is the conjugate point to A, ds is the differential path length along the field line connecting A to C, B_s is the field strength along the magnetic field line, and B is the field strength at A and C. McIlwain showed that, for a dipole field of magnetic moment M, the required equatorial intersection distance r is given by a relation of the form:

$$r^3B/M = f(I^3B/M)$$

Although the function f cannot not be expressed exactly in analytic form, excellent approximations are available [*McIlwain*, 1961, 1966; *Hilton*, 1971]. By McIlwain's definition, the functional relationship between L, B, and I in the given field is the same as that between r, B, and I in the dipole: Thus, for a specified magnetic moment M, L is a function of the point values B and I.

In the definition of L presented here, we have deliberately omitted a specification of the reference dipole moment M to emphasize the present ambiguity in this regard. McIlwain initially selected a value that was valid in 1960. This fixed value was imbedded in software that he provided to other users. Meanwhile other software has been distributed which uses the updated dipole moment, derived from the dipole terms of the model used to compute the field. The consequences of ambiguity on the computed value of L will be discussed in detail in a later sub-section.

4.2.1 Elaboration

Contrary to what we have just said, let us assume that we have a universally accepted definition if M. Then let us clarify the rest of the definition of L by considering two magnetic field models: the model actually specifying the magnetic field vector at the point in question, and a reference dipole model with magnetic moment M. For either model, we can compute the field intensity at any point, except at the origin where it becomes infinite.

We can also compute the invariant integral at any point lying on a closed field line. In the dipole field all lines are closed except the one passing through the poles. On each closed dipole line the field strength minimizes at one point, on the equator, about which the original point and its conjugate are symmetrically located. In a more general, non-dipole field, there may be many open lines. For these we cannot define either I or L, so we will not concern ourselves with them. Open lines cannot occur in the radiation belt, for particles would escape along them. Most field lines in the radiation belts contain only one point of minimum field strength, not necessarily on the dipole equator; in exceptional cases, near the surface of the earth, there may be more. In any event, we may trace the field line from our original point, in the direction of decreasing field strength, past one or more points of minimum strength, and on to the conjugate point, the first point encountered where the field strength matches that at the original point. Then we compute the invariant integral, a line integral, in accordance with the definition, between our original point and its conjugate.

McIlwain showed that the locus of points of common B and I in a dipole field has a very simple geometric property: it lies on a shell of field lines intersecting the equator on a circle of radius

$$r = [(M/B)f(I^3B/M)]^{1/3}$$

The value of L of our point of interest, in the actual field, is set equal to this radius, in R_E, of the shell occupied by the points of the same B and I in the reference dipole field. Our point does not actually lie on this shell, unless the actual field coincides with the reference dipole field. However, in many instances, the radial distance of the actual equator crossing of the field line is close to L.

For self-conjugate points, I=0, L is easily obtained from B. In a dipole field, the self-conjugate points are on the equator, where

$$B = M/r^3$$

Therefore, the equatorial radius of the dipole shell containing the I=0 points of specified B is

$$r = (M/B)^{1/3}$$

We therefore must have for I=0 points in our actual field:

$$L = (M/B)^{1/3}$$

Incidentally it follows from these considerations that

$$f(0) = 1$$

4.2.2 Physical Significance

The L parameter is related to the properties of the adiabatic motion of trapped particles in a sufficiently slowly varying (both spatially and temporally) magnetic field. Under these conditions the motion of the particle can be decomposed into three components: the gyromotion around the magnetic field lines, the bounce motion between the conjugate mirror points, and the longitudinal drift motion around the earth. Associated with each of these components of the motion is an adiabatic invariant which is approximately a constant. The first two invariants, associated, respectively, with the gyromotion and the bounce motion, are:

$$\mu = p^2 \sin^2\alpha/(2mB)$$

$$J = 2pI_m$$

Here p is the particle's momentum, α is the pitch angle (angle between the velocity and the magnetic field vector), m is the mass, B is the magnetic field strength, and I_m is the invariant integral at the particle's mirror points, where the particle's pitch angle is 90° and the magnetic field strength B_m is given by conservation of the first adiabatic invariant μ:

$$B_m = B/\sin^2\alpha.$$

In the absence of an electric field, the magnetic field is static and the momentum p is a constant of the motion. Then the particle's mirror point magnetic field and invariant integral, B_m and I_m, are also constants of the motion, from which it follows that its mirror point L value, L_m is also a constant. Therefore the particle's motion is confined to a "shell" of magnetic field lines which contain the locus of points of the specified B_m and L_m.

In a pure dipole field of magnetic moment M, L_m is the equatorial radius of this shell, in earth radii, since the field lines intersect the equator at this distance. This simple geometric interpretation is the reason that L_m has long been favored over I_m as a parameter for modeling the radiation belts. In this dipole field, all particles found at a point possess the same L_m, since L is constant along the field line. In a non-dipole field, however, the L parameter is not in general equal to the equatorial intersection distance of the field line through the point, nor is L a constant along the field line, although both of these properties

are often approximately satisfied. *Therefore the L parameter at a point is the conserved L_m only for the particles mirroring at that point, that is, those particles with 90° pitch angles at that point. The appropriate L_m parameter value for particles with smaller pitch angles must be computed at their particular mirror points, and in general will therefore be different from the L parameter value at the point of observation.*

4.3 COMPUTATIONAL METHODS

From the definition of L given here, it is evident that four steps are required, in the following order:

1. Compute the model field vector and magnitude B at the point in question.

2. Trace the field line through the point to its conjugate point, storing the magnetic field magnitude B_s at points along this path.

3. Compute the line integral along the field line to obtain I.

4. Compute L from I, B, and M.

Step 1 is reasonably straightforward, given the mathematical specification of the field model, and will not be discussed further here. Step 2, the field line tracing, is the most time consuming computationally, since it requires solution of a vector system of nonlinear ordinary differential equations expressing the local tangency of the magnetic field vector. Step 3 requires only a quadrature integration along the field line, having determined from step 2 the field strength as a function of the distance along the field line from starting point. Finally, in step 4, we must compute L, given I, B, and M. The shortest of the four steps of our procedure, this final step requires selection of a algorithm for computing L with sufficient accuracy, *and specification of the magnetic moment M of the reference dipole field.*

The expense of the computation of L directly from its definition may be avoided by interpolation of prestored tables, if the same model will be employed many times more than the number of tabular entries required to interpolate L to sufficient accuracy.

4.3.1 Step 2 - Field Line Tracing

The desired field line is the solution of the ordinary differential equations

$$dx/ds = B_x/B$$

$$dy/ds = B_y/B$$

$$dz/ds = B_z/B$$

satisfying the initial conditions that x, y, z at s=0 are the coordinates of the point at which we wish to compute L. Here x, y, and z are the cartesian coordinates of a point on the field line, and s is the distance of the point, measured along the field line, from our original given point, with a positive sign if the tracing is parallel to the magnetic field vector, a negative

sign if the tracing is antiparallel. Thus, the field line is defined as a series of points, specified by their Cartesian coordinates, as functions of the independent variable s.

4.3.1.1 Kluge's method

Programs OPTRACE and HMIN solve these equations as indicated. The principal difference between the two programs arises because OPTRACE must obtain the 100 km intercepts of the field line as part of the CRRES requirements. Therefore it must trace the field all the way to these intercepts, in both hemispheres. HMIN, concerned only with computing L, traces only to the conjugate point.

SHELLC, using Kluge's method, invokes a change of coordinates to the inverse variables.

$$\xi = x/r^2$$

$$\eta = y/r^2$$

$$\zeta = z/r^2$$

Here x, y, and z are in a dipole-oriented system, the z axis parallel to the dipole. From the inverse coordinates we can readily recover the direct coordinates:

$$x = \xi/\rho^2$$

$$y = \eta/\rho^2$$

$$z = \zeta/\rho^2$$

where

$$\rho^2 = \xi^2 + \eta^2 + \zeta^2 = 1/r^2$$

There is also a change in the independent variable from s to the variable t, such that

$$dt = \rho^5 dt' = \rho^5 ds/B$$

The differential equation for ξ becomes

$$d\xi/dt = \partial W/\partial\xi + \xi W/\rho^2$$

where

$$W = -rV$$

and V is the scalar potential from which the field is derived:

$$B = -\nabla V$$

Fully analogous equations follow for η and ζ. If the field is not derivable from a scalar potential, as when the external portion (due to ring currents, etc.) is included, we instead would obtain

$$d\xi/dt = \rho^{-5}[(\partial\xi/\partial x)B_x + (\partial\xi/\partial y)B_y + (\partial\xi/\partial z)B_z]$$

$$= \rho^{-5}[\rho^2 B_x - 2\xi(\xi B_x + \eta B_y + \zeta B_z)]$$

At this point the final change of coordinates is made, replacing ξ and η by

$$u = \xi/\rho^{1/2}$$

$$v = \eta/\rho^{1/2}$$

In a pure dipole field, u and v are constants along the field line:

$$u = \cos\phi/L^{1/2}$$

$$v = \sin\phi/L^{1/2}$$

Also, $d\zeta/dt$ is shown to be positive everywhere (at least for the pure dipole case). Since ζ and t are therefore single-valued functions of each other, ζ can serve as the independent variable instead of t. Then from the definitions of u and v, equations are obtained for $du/d\zeta$ and $dv/d\zeta$:

$$du/d\zeta = [\rho^{-1/2}d\xi/dt - (1/2)\rho^{-3/2}\xi d\rho/dt]/(d\zeta/dt)$$

$$dv/d\zeta = [\rho^{-1/2}d\eta/dt - (1/2)\rho^{-3/2}\eta d\rho/dt]/(d\zeta/dt)$$

The right-hand sides of these equations can be expressed completely in terms of u, v, and ζ. First note that

$$d\rho/dt = (\xi d\xi/dt + \eta d\eta/dt + \zeta d\zeta/dt)/\rho$$

The derivatives $d\xi/dt$, $d\eta/dt$, and $d\zeta/dt$ are given above in terms of ρ, ξ,η, and ζ. Thus $du/d\zeta$ and $dv/d\zeta$ are expressible entirely in terms of these variables. To eliminate ρ, ξ, and η, make the substitutions:

$$\xi = u\rho^{1/2}$$

$$\tau_i = v\rho^{1/2}$$

$$\rho = (1/2)(u^2 + v^2 + [(u^2 + v^2)^2 + 4\zeta^2]^{1/2})$$

The expressions for ξ and η come from inversion of the definitions for u and v. The expression for ρ comes from solving the quadratic equation

$$\rho^2 = \xi^2 + \eta^2 + \zeta^2 = \rho(u^2 + v^2) + \zeta^2$$

With these substitutions we obtain ordinary differential equations for u and v in terms of themselves and the independent variable ζ. Solution of these gives $u(\zeta)$ and $v(\zeta)$. As stated before, u and v are constant along a dipole field line. In the real world, we expect them to be sufficiently slowly varying that very large steps can be used in the tracing. Typically 10 steps seem to be sufficient for this method, while for the direct method used in OPTRACE and HMIN, the number of steps is ~100. Note in addition that only two equations need be solved here, while in the direct approach we are solving three.

4.3.1.2 Methods of numerical integration

The equations to be solved are of the form

$$dy/dx = g(y,x)$$

The principal feature of these equations is that the right-hand side, the derivative of the solution, depends on the value of the solution itself. A second feature relevant to our particular problem is that the derivatives (right-hand sides) require the time-consuming evaluation of the magnetic field.

OPTRACE/HMIN

OPTRACE and HMIN use the open Adams 4th order numerical integration method [*Press, et. al.*, 1986; *Hildebrand*, 1956]. This method generates a solution on a sequence of uniformly spaced points. In each step the solution at a new point is generated from the value of the solution at the previous point and the first derivatives of the solution at the previous four points. Only one derivative evaluation is required per step.

The method is called "open" to distinguish it from other methods which are "closed", since they require also the derivative of the solution at the new point. However the first derivative of the solution value at any point can be obtained only if the solution value itself is known, since the right-hand sides of the equations are functions of the solution value as well as the independent variable. The closed methods are often used in what are called predictor-corrector schemes, in which an open method is used to "predict" the solution at the new point. Then the predicted solution value at the new point is used to estimate the derivative there for use in the closed formula.

The method is called 4th order to indicate that it is accurate through the 4th power in the step size, i.e., its error is proportional to the 5th power in the step size.

Since the solution must be known at 4 previous points in order to obtain it at a new point, it must be generated at the first 4 points in the sequence by another method. Actually, the solution is given to us at the first point, the boundary value. Thus we must generate from it the solution values at the next three points. In OPTRACE and HMIN this is done by the classical Runge-Kutta 4th order method [*Press, et. al.*, 1986; *Hildebrand*, 1956], which allows one to obtain the solution at a new point from just its value and derivative at the previous point. The process requires evaluations of the derivatives for two estimated solution values at the midpoint of the step, plus one evaluation for an estimated solution value at the end of the step, in addition to evaluation with the known solution value at the beginning point of the step. Thus each step requires four derivative evaluations, compared to just one per step for the open Adams method. This makes Runge-Kutta considerably slower than Adams, but it has the flexibilty of not requiring a previous multiple-point history.

The step size h is given by:

$$h = FLL/[SEGS \times f(FLL)]$$

where

FLL = estimated field line length (R_E) between 100 km intercepts

SEGS = number of steps desired when FLL = 2 R_E

f(FLL) = (-2/3)FLL + 7/3, FLL $\leq$2 R_E

= (1/18)FLL + 8/9, FLL > 2 R_E

The expression for h reflects the finding [*Radex, Inc.*, 1987] that uniform accuracy was obtained with a number of steps that minimizes for FLL = 2 and increases linearly to approximately double that amount at the shortest and longest lengths to be considered for CRRES. This shape function is reflected by the function f(FLL), while SEGS, nominally set to 100, but easily adjusted in the code, gives the desired number of steps at FLL = 2 R_E.

The procedure for estimating the field length depends on the dipole L parameter, L_d, of the initial point [*McNeil*, 1966]:

$$L_d = r/\sin^2\theta$$

where r is the radial distance and θ is the magnetic colatitude. For $L_d \geq 2\ R_E$, FLL was found empirically to fit very well the estimate

$$FLL = 2.77\ L_d - 1.86$$

For lesser values the situation is quite complicated, due to the varied effects of the non-dipole terms in the field. In this case FLL was fit to parabolic functions of L_d, with coefficients tabulated on a 7 x 13 magnetic latitude-longitude grid. FLL at any latitude and longitude is computed by bi-linear interpolation of the four nearest neighbors on the grid.

SHELLC

The third order Adams predictor-corrector method is used to obtain the solution at a new point, given the solution at the previous point and the derivatives at the previous three. The process is started as follows:

1) the solution is estimated 1/2 step forward of the starting point by linear extrapolation, using the value and derivative at the starting point;

2) The solution is then obtained one step backward from the starting point, by quadratic extrapolation using the starting point solution value and derivative, and the estimated derivative at the point 1/2 step forward;

3) The solution one step forward of the starting point is obtained by cubic extrapolation using the solution value at the starting point and the derivatives at all three previously known points. The point 1/2 step forward is now discarded, and the remaining three are available to begin the predictor-corrector process.

The step size $\Delta\zeta$ for all runs was 0.2 R_E^{-1}, the value set in the code we received. Since this probably was arrived at after extensive testing, we saw no reason to change it.

4.3.2 Step 3 - Computation of I

OPTRACE/HMIN

The interval between the starting point and its conjugate point is divided into two regions:

1. the largest subinterval beginning at the starting point which contains an even number of steps;

2. the subinterval beginning at the end of region 1 and ending at the conjugate point.

The conjugate seldom coincides with any grid point; it is found by quadratic fit of the field strength B_s through the three closest points, and solving for s such that $B_s = B$.

The integral through region 1 is performed by Simpson's Rule [*Press, et. al.*, 1986; *Hildebrand*, 1956], which is a two-step formula. The midpoint of region 2 is located by a single application of Runge-Kutta; then one application of Simpson's Rule computes the integral through this portion.

If the conjugate point lies within the first two steps a different procedure is followed. The quantity $1-B_s/B$ is fit to a parabola, from which the location and value of the minimum (B_{min}) are determined. The invariant integral is then given analytically by

$$I = (\pi/4)t(1-B_{min}/B)^{1/2}$$

where t is the arclength from the starting point to the conjugate.

SHELLC

In terms of the transformed variables the invariant integral is written:

$$I = \int (1-B_t/B)^{1/2} [(Q/\rho^2)/(d\zeta/dt)]d\zeta$$

where

$$Q = [(d\xi/dt)^2 + (d\eta/dt)^2 + (d\zeta/dt)^2]^{1/2}$$

It is shown that the field strength B_t at a point on the field line can be written as

$$B_t = \rho^3 Q$$

The step size used for the tracing is too large for the computation of I, because of the rapidly varying quantities in the integrand. To avoid having to trace at a smaller step size, which would defeat the purpose of the algorithm, Kluge defines three slowly-varying interpolation functions:

$$C = u^2 + v^2$$

$$D = Q/[1 + 3(\zeta/\rho)^2]^{1/2}$$

$$E = D(1 + \zeta^2/\rho^2)/(d\zeta/dt)$$

In a dipole field, C becomes $1/L_s$ and D and E both become equal to the dipole moment. The inverse radius ρ has previously been given in terms of the slowly-varying u, v, and the independent variable ζ. We can re-express this result here as:

$$\rho = (1/2)(C + [C^2 + 4\zeta^2]^{1/2})$$

Thus we can compute ρ analytically at any point ζ once we know C. Next, Q can be obtained analytically from D, ρ, and ζ; $d\zeta/dt$ can be computed from D, E, ρ, and ζ; and B_t can be computed from ρ and Q. Thus the entire integrand can be computed analytically at any point ζ from these interpolation functions. Four-point interpolation is used for C, three-point interpolation for D and E.

The integration is performed by the trapezoidal rule [*Press, et. al.*, 1986]. Since this method performs the integration one step at a time, the step size can be varied conveniently. It is chosen to be kρ, where k is presently set to 0.03.

The beginning and ending intervals are handled by a slight modification to account for the square root singularity in integrand - it approaches zero as the square root of the distance from the end point. If x_1 is the length of the interval, and x is the distance from the endpoint where the integrand vanishes, then the integrand is approximated by

$$G = a[x/x_1]^{1/2}$$

where a is the value of the integrand at the other end of the interval. Then the integral over this portion is

$$i = (2/3)ax_1$$

If the conjugate point is within one integration step of the starting point, I is set to zero.

4.3.3 Step 4 - Determination of L from B and I

Although an exact mathematical expression for L is not available, excellent approximations have been provided by McIlwain [1961, 1966] and Hilton [1971]. All three codes employ McIlwain's 1966 version:

$$Y = \ln(L^3B/M-1) = \Sigma_{n=0}^{9} a_n X^n$$

where

$$X = \ln(I^3B/M)$$

and the coefficients a_n are given in the table reproduced here from McIlwain [1966]. The last row in the table indicates the maximum error in Y. These numbers translate into a maximum relative error ($\Delta L/L$) of $\sim 1.6 \times 10^{-4}$.

Originally, the somewhat simpler formula given by Hilton [1971],

$$L^3B/M = 1 + a_1X^{1/3} + a_2X^{2/3} + a_3X$$

where

$$X = I^3B/M$$

$$a_1 = 1.35047$$

$$a_2 = 0.465376$$

$$a_3 = 0.0475455$$

was employed in OPTRACE and HMIN. Table 1 of Hilton's paper quotes maximum error $\Delta L/L \sim 10^{-4}$. However, comparisons with results obtained using McIlwain's formula revealed relative differences $\sim 2 \times 10^{-3}$. Thus we reverted to the tried and true McIlwain formula. Recently we have discovered that the differences may due to an error in a_2 in the computer code of Hilton's formula. Although further testing may warrant reinstatement of the Hilton formula, the saving in computation is minimal, since this step requires a very small fraction of the total effort required to compute L. Therefore we have for the time being retained McIlwain's formula.

4.3.3.1 The disappearing dipole

Historically the constancy of the Earth's magnetic dipole has been taken for granted. As in human relations, this may prove to be fatal, for the dipole moment

$$M = [(g_1^0)^2 + (g_1^1)^2 + (h_1^1)^2]^{1/2}$$

has been decreasing at the rate of approximately 0.05 % per year. The predicted 1990 value, computed from the dipole terms of the extrapolated IGRF 1985 model, is 30299 ($nT\text{-}R_e^3$), while the value used by McIlwain, in these units, is 31165.3. This latter value was imbedded into McIlwain's subroutine CARMEL, which he has over the years provided to many users. Thus this constant has become a fixture in many L computation codes, including the SHELLC package sent to us. In OPTRACE and HMIN, on the other hand, we have used the updated value for M, given above, as recommended by Hilton [1971]. Since we have only recently discovered that it was McIlwain's old M value that was used in SHELLC, many of the results of that code presented in this report were computed with this value. Consequently part of the differences between SHELLC and OPTRACE/HMIN results are undoubtedly due to this difference in the M values used. We have since modified SHELLC to use the updated dipole moment as in OPTRACE, and will present comparative results. The INTEL interpolation tables, undoubtedly, have been generated using the old dipole moment. Since we do not presently have the capability to regenerate these, the only INTEL results presented here are with the old dipole moment.

It is not totally obvious to us how to select M. We have given here the two choices that we know have been commonly used. McIlwain [1966] suggested that M be chosen to minimize the variation of L along the field lines. Although attainment of a practical algorithm for accomplishing this in the actual geomagnetic field seems unlikely, Hilton's definition, used in OPTRACE, accomplishes this in a time-varying pure dipole field: the L parameter at a point remains equal to the radial distance of the equatorial intersection of the field line through that point as the field changes.

However, what happens if we use McIlwain's fixed value, which we may call M_m, instead of the updated value, M_u? We have found previously, that for I=0,

$$L = (M/B)^{1/3}$$

Thus we find that by using McIlwain's fixed value of the dipole moment, instead of the updated value, we obtain for points at the equator (I=0) L parameter values which differ from the radial distance by the factor $(M_m/M_u)^{1/3}$. Using the values of M_u (1990) and M_m given above, we find that this factor is 1.00[illegible] Thus, in 1990, use of the fixed value M_m would result in L values nearly 1% higher at the equator than those obtained using the updated value M_u.

Now consider high latitudes, in the limit of large I and B. Here both McIlwain's and Hilton's expansions lead us to

$$L^3B/M \approx 0.04754551^3B/M$$

$$L/I \approx 0.362273$$

Thus L becomes independent of M in the high latitude limit, while it depends on M at the equator. Therefore we conclude that L is not a constant along a dipole field line unless the value of the dipole moment M employed in computation of L from B and I is the same as the value employed in computing B and I. Thus to satisfy McIlwain's criterion of minimizing the variation of L along a field line, it is obvious that for a pure dipole field we should use the same (updated) value in the final step of obtaining L from B and I as was used in computing the field. The effect of using McIlwain's subroutine CARMEL, with the fixed value M_m embedded, in conjunction with model routines that use the updated values of all coefficients to compute the field, is that this condition would not be satisfied.

In a non-dipole field, however, L is not in general constant along a field line, even if consistent values of M are employed. For the earth's internal field, however, L is approximately constant, McIlwain [1961] finding relative variations within 1% along field lines within 3 R_E (Hopefully his M value is consistent with the 1960 model he employed). However at larger distances, where the field due to external sources must be included, the variation of L along a field line can be quite substantial. For example, using the Olson-Pfitzer model for the external field and the IGRF85 for the internal field, it was found, for a field line at 2200 hours MLT with an 840 km footprint at 65^0 magnetic latitude, that L was 7.64 at the footprint and 8.88 at the equatorial crossing, for a relative variation of more than 12%. Therefore it isn't clear to us what choice of M would minimize variations of L along field lines of a realistic geomagnetic field model.

In summary, the earth's dipole moment M has changed by nearly 3% since the time of McIlwain's original definition. If we use McIlwain's original value in computing L from B and I, we get near the equator L values approximately 1% higher than those obtained when using the updated dipole moment. There are several L computation codes that use the fixed McIlwain value, and some codes that use the updated value. We should therefore be warned that the results obtained with these codes may disagree due to this disparity. It would be wise to agree in the future on a standard choice to be used by everyone.

4.3.4 Interpolation of L - Program INTEL

The L parameter is expressed in the form

$$L = d^{-1}[1+f(d,\zeta,\phi)]$$

where

$$d = \sigma^2/[\sigma^2 + \zeta^2]^{1/2}$$

$$\sigma = [(\xi-\xi_p)^2 + (\eta-\eta_p)^2]^{1/2}$$

$$\cos\phi = (\xi-\xi_p)/\sigma$$

$$\sin\phi = (\eta-\eta_p)/\sigma$$

Here $\xi_p(\zeta)$ and $\eta_p(\zeta)$ define the open field line, which goes over to the dipole limit $\xi_p = \eta_p = 0$ at $\zeta=0$. They are expressed as 4th degree polynomials (constant term = 0). This reformulation removes the polar singularity from the function which must be interpolated (i. e., the function f remains finite). The evaluation of f is by quadratic interpolation of a fourier series in ϕ on a uniform ζ-d grid. The spacing of the grid is $\Delta d = \Delta\zeta = 0.2$, with $d_{min} = 0.1$, $d_{max} = 0.9$, $\zeta_{min} = -0.9$, $\zeta_{max} = 0.9$. Not all points on this grid are actually employed, since some are below the surface. A total of 700 Fourier coefficients are tabulated, 10-30 per point, at the grid points above the surface.

5. L-SHELL COMPARISONS OF THE MODELS

The four models (Barraclough 1975, MAGSAT 1980, IGRF 1985, and Cain 1990) were compared on the basis of their L-shell evaluation as well as their B field determination (see Chapter 3). Each of these models was incorporated into software currently in use at GL. To begin with, contour plots of the differences between the models were made over a large altitude range. Then line plots of L-shell at selected longitudes were made for a wide latitude range, ±75°. To more closely examine differences between the models at latitudes pertinent to CRRES, detailed line plots were made at five altitudes for several longitudes with latitude only spanning ±20°. In the difference comparisons mentioned previously, IGRF 1985 was used as the standard. Thus, contour plots of the IGRF 1985 L-shell over the whole latitude and longitude range were done. These were made for 1980, 1985, and 1990 to look for temporal variations in L.

5.1 OVERALL MODEL DIFFERENCES

Figures 5.1a and 5.1b show the differences between the models for 1990 at 350 km and 10,000 km, respectively. IGRF 1985 was used as the reference because it is the most widely used model and was adopted as the standard by the IAGA Working Group 1. The contour plot in the lower right hand panel shows L-shell as determined by IGRF 1985. The remaining three panels show the differences between the other three models and this IGRF.

The upper left panel shows the absolute differences between Barraclough and IGRF. This model differs the most. Even so, these differences tend to be less than a percent or two from the standard. The agreement deteriorates as one approaches the poles. This is what is expected since L increases toward the poles and the models themselves are not as good nearer the poles (see Chapter 2). Whether Barraclough is higher or lower than IGRF depends upon the hemisphere. This may be due in part to the change in the position of the offset dipole. The dipole moment and the displacement of the offset dipole are known to be changing with time (see sections 4.3.3.1) [*Pinto, et. al.*, 1989]. For this comparison, the software determines the position of the offset dipole and the dipole moment from the coefficients. Thus, different offsets would be expected to lead to systematic differences in L by hemisphere. Here, Barraclough is too low in the North-East and South-West quadrants. It is too high in the North-West and South-East quadrants. Note, these differences are primarily attributable to differences between the models themselves. The differences in the offsets add to these larger differences.

The upper right panel shows differences between MAGSAT and IGRF. Here the agreement is seen to be a little better than that with Barraclough. More area is covered by the ±.001 contours and the larger contours are at higher latitudes. Still, the percent difference from the standard is about the same: generally less than one percent. Again the sign of the difference depends on the hemisphere with MAGSAT too low in the North-East and South-West quadrants and too high in the North-West and South-East quadrants (roughly).

Finally, the best agreement is seen between Cain and IGRF in the lower left panel of Figure 5.1a. For the most part the absolute differences are less than .001 with higher differences very close to the poles. This is an order of magnitude better than the two previous models discussed. The relationship between the sign of the difference and geographic position is not

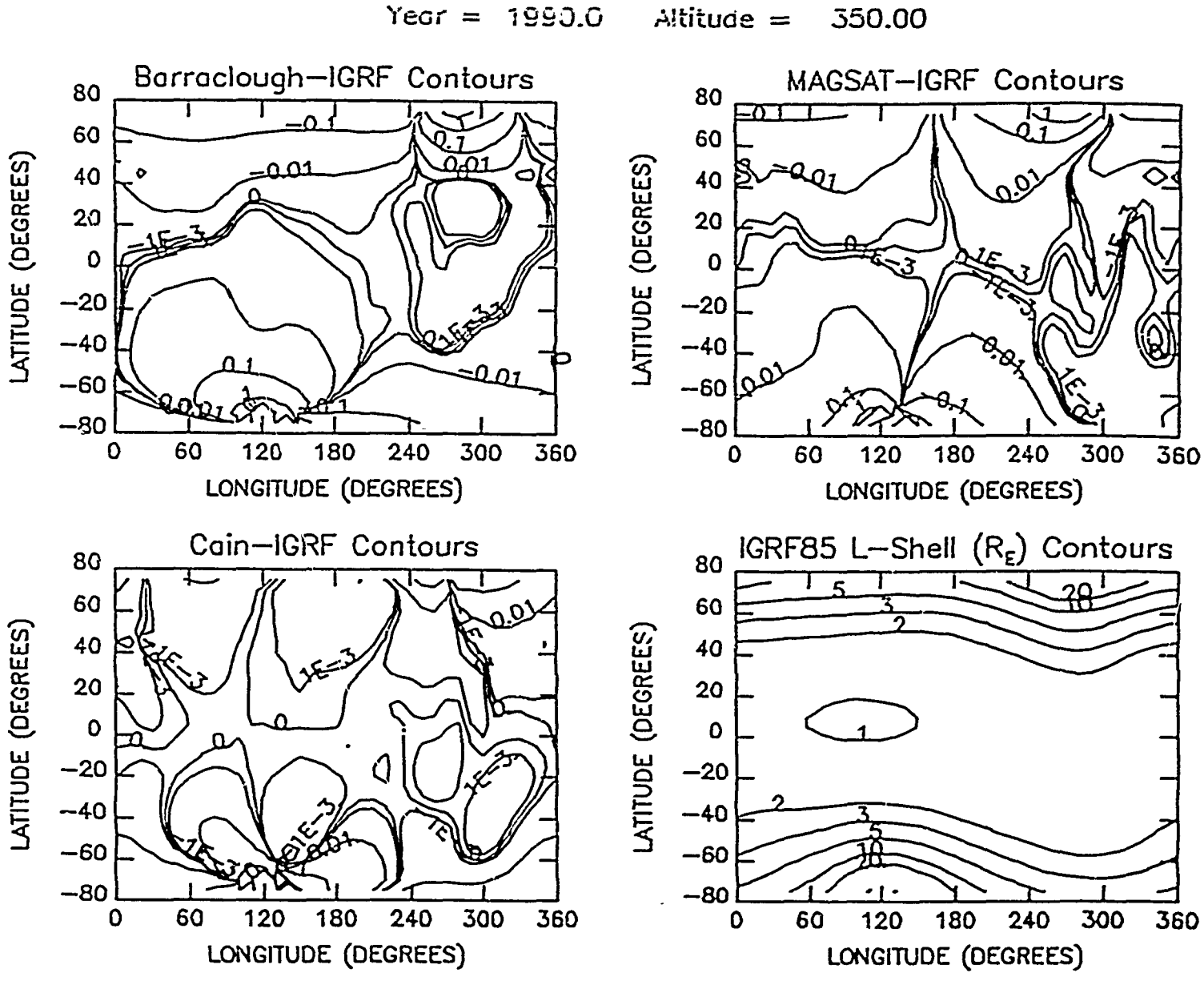

Figure 5.1a. Contour plots of model L-shell differences in Earth radii (R_E) covering the full latitude and longitude ranges. IGRF 1985 is used as a reference model. The comparisons are done for an altitude of 350 km (perigee) at 1990.0.

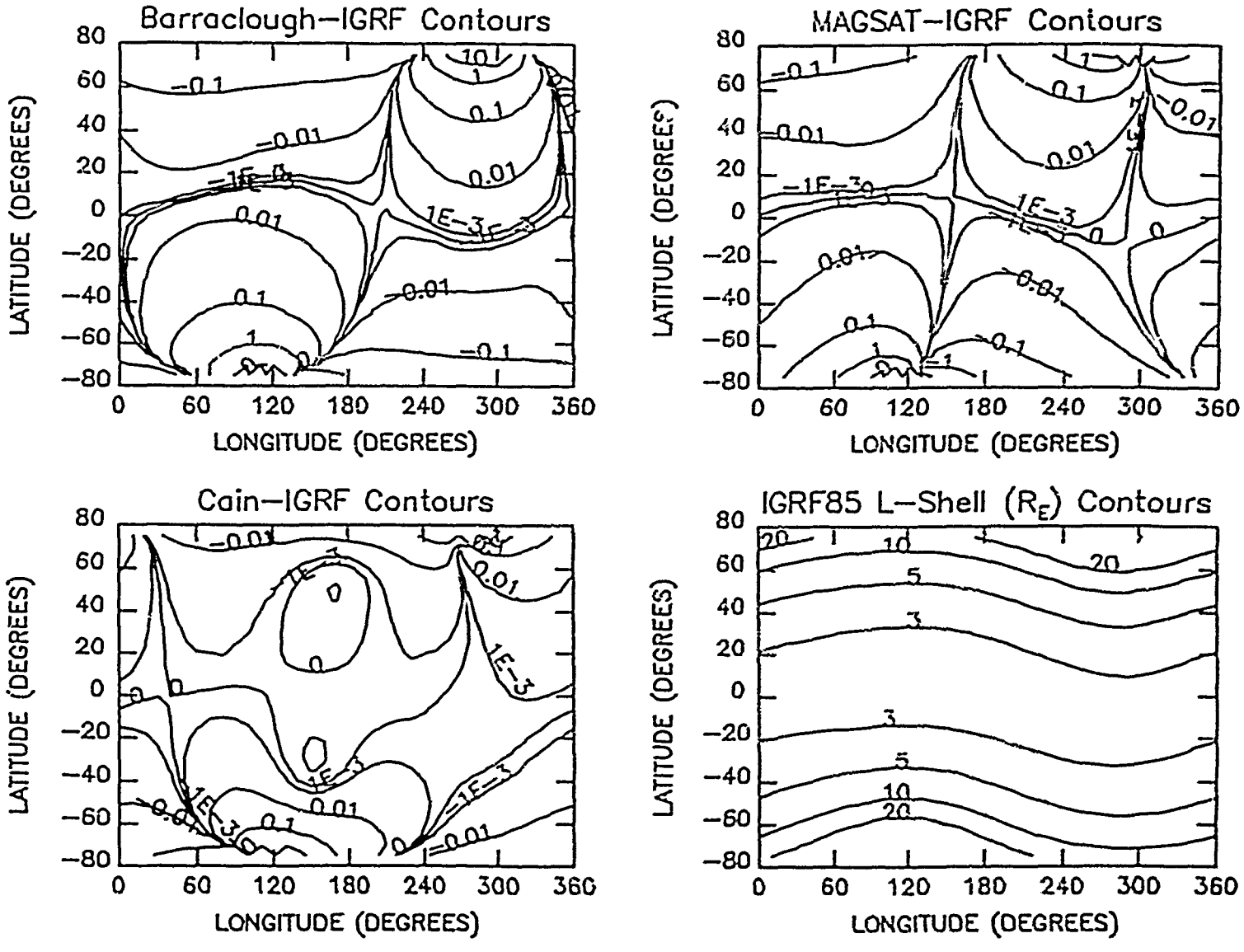

Figure 5.1b. Contour plots of model L-shell differences in Earth radii (R_E) covering the full latitude and longitude ranges. IGRF 1985 is used as a reference model. The comparisons are done for an altitude of 10,000 km at 1990.0.

so clear cut as previously. These differences are generally less than a tenth of a percent of the IGRF values. The instruments on CRRES will not be able to discern L-shell differences at this order of magnitude.

Figure 5.1b is similar to 5.1a, the difference is in the altitude at which the comparisons are made. Here, one sees the comparisons done for 10,000 km. Again, IGRF 1985 is the standard with the other three models compared to it. The L-shell contours obtained from IGRF 1985 are shown in the lower right panel. The absolute differences contoured in the other three plots are all smoother than those seen at 350 km. At higher altitudes the contributions to the internal field from the crustal components are negligible in comparison to the dipole component, thus the smaller scale detail washes out and the contours become smoother. The basic distribution of the contours has remained the same between 350 km and 10,000 km (i.e. the distribution of the positive and negative differences is still correlated with the offset dipole). However, in all three plots, the differences have increased. L increases with altitude, so even though the absolute differences have increased somewhat, the percent differences are about the same. Thus, one again sees that for CRRES, differences between Cain and IGRF will not be discernible.

5.2 COMPARISONS AT SPECIFIED LONGITUDES

Four line plots at selected longitudes were made of L-shell versus latitude (see Figure 5.2). At this scale, the agreement between the models is so close, that only one line is apparent even though all four models have been plotted on each plot. These plots were made using the high latitude data, thus, one can see longitudinal variations in L. The magnetic poles are near the two longitudes selected for the right panels. Hence, a sharp increase in L is seen in the southern hemisphere in the upper plot and in the northern hemisphere in the lower plot. The two left panels are not near the magnetic poles in longitude so only L-shells ≤ 10 are seen.

Line plots were also made at a smaller scale to look at differences between $\pm 20^{\circ}$ (see Figure 5.3a - 5.3c). Figure 5.3a shows L-shell versus latitude at 350 km and 80° east longitude for 1990 and 1980 (upper and lower panels, respectively) for all four models. In 1980 (lower panel), the agreement at this scale is so good that only one line is apparent. This agreement deteriorates somewhat by 1990 (upper panel) as is expected as one gets farther away from the epochs for which the models are derived and differences in their secular variation are manifested. Nonetheless, differences can only be seen between -20° and 4°. Here, Barraclough has the highest L values (solid line), MAGSAT is slightly lower (dotted line), and Cain and IGRF are lower still (dashed and dash-dot lines plotted on top of each other). This is what is expected with a decreasing dipole moment. A higher moment will give higher L values. Since, Barraclough is the oldest model it is expected to give the highest L values. Cain and IGRF are based on very similar data sets (see Chapter 2). Even though Cain's model incorporates a discontinuity in the secular variation after 1983, the shift in L due to this continuity is not yet apparent by 1990.

Figure 5.3b is similar to Figure 5.3a, the difference is in altitude. This shows the models at 10,000 km. Again, there is no discernible difference between the models at 1980. They all plot on top of each other. By 1990, differences again appear between -20° and 4° latitude. Barraclough gives the highest L values with MAGSAT lower and Cain and IGRF lower still. L increases with altitude, thus at 10,000 km, L is nearly 2.0 R_E higher than at 350 km. However, the differences between the models are about the same as those at the lower altitude. Cain and IGRF still overplot each other, so even at higher altitudes one cannot see

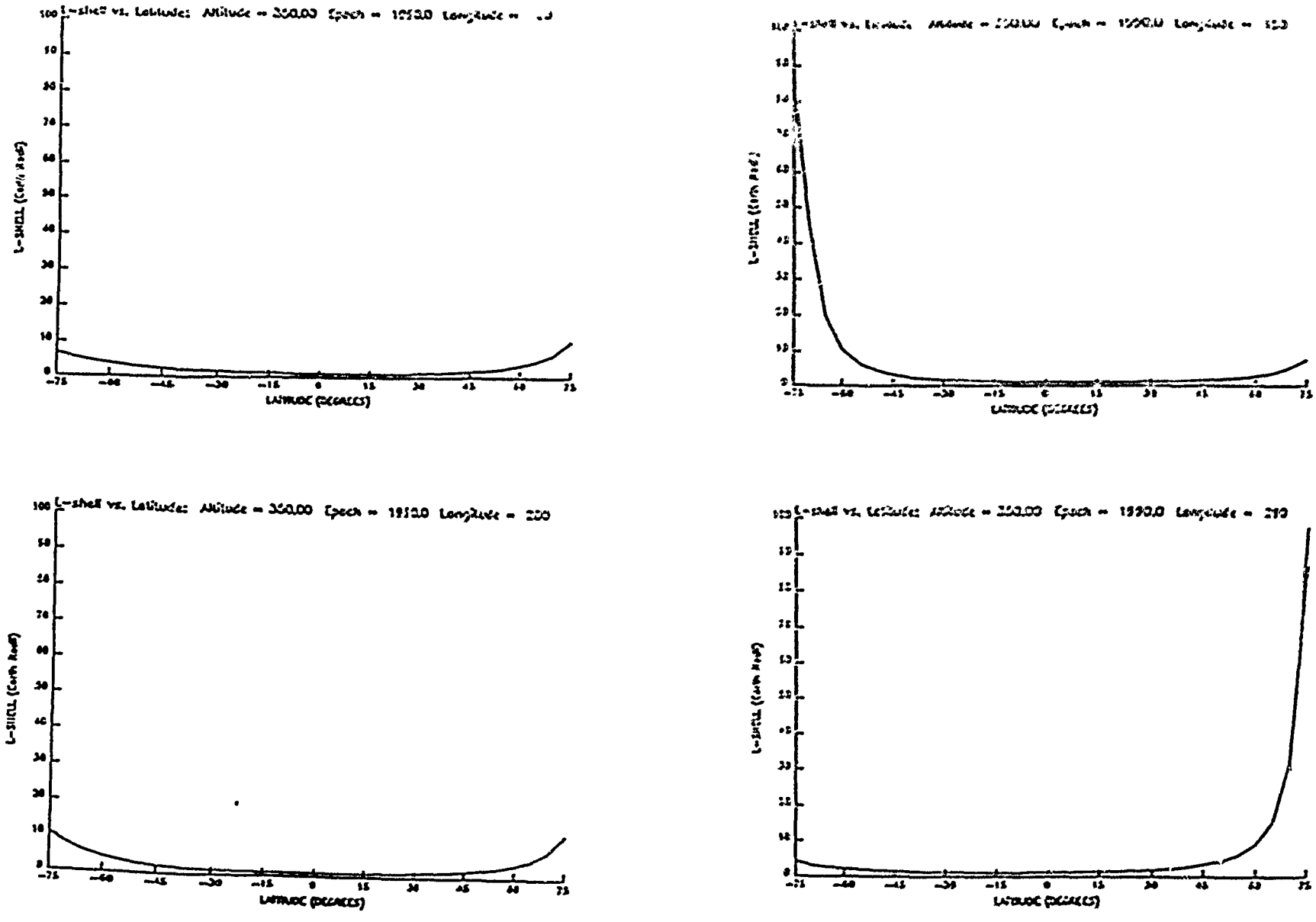

Figure 5.2. Line plots of the four models plotted together at four different longitudes over the globe for the full latitude range. The models are essentially indistinguishable at this resolution.

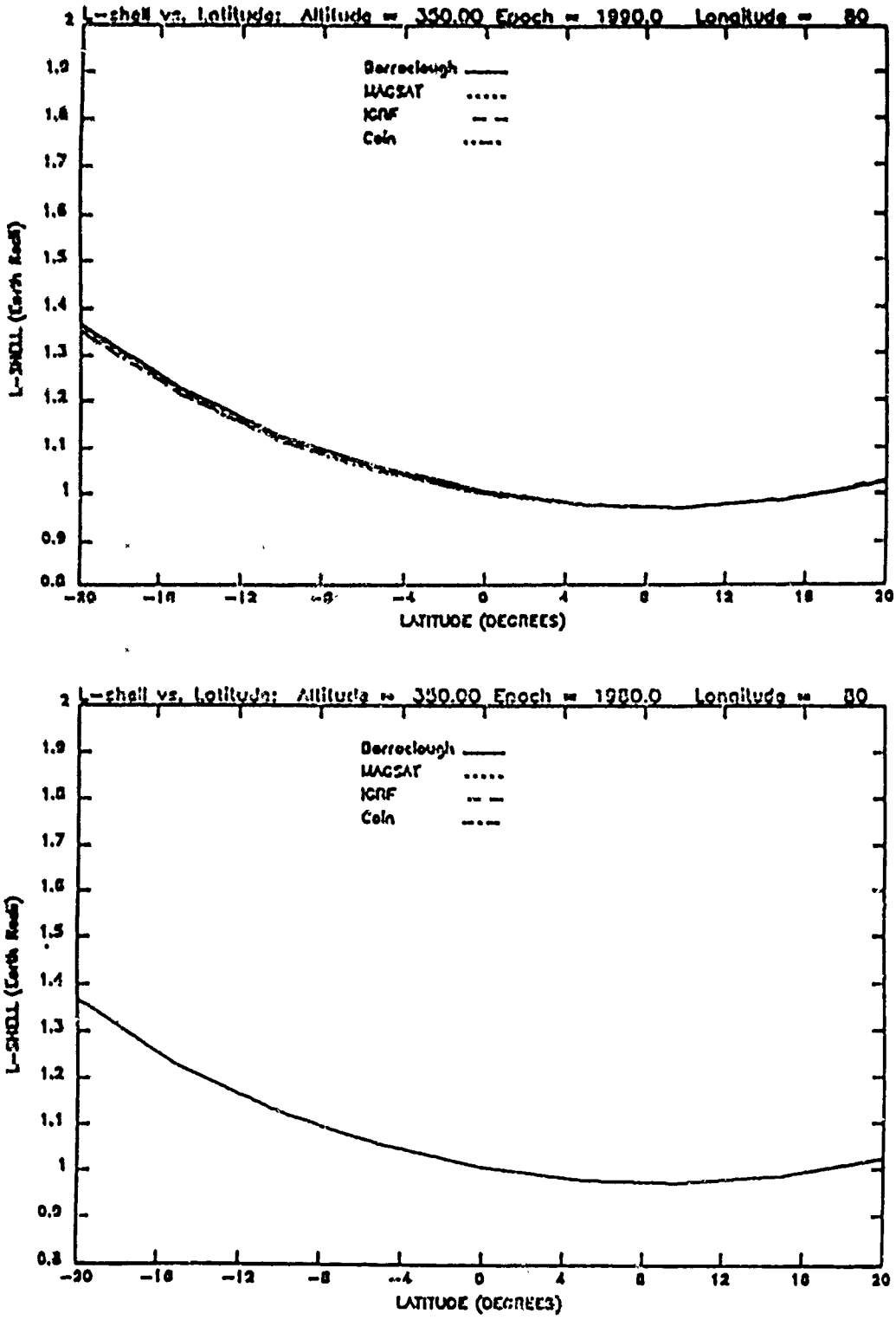

Figure 5.3a. Line plots similar to those in Figure 5.2, but over a smaller latitude range. Even at this resolution, the differences between the models are very small. The top panel shows the differences at 350 km and 80° east longitude for 1990.0. The bottom panel is the same plot done for epoch 1980.0. Discrepancies arise over time, but the differences, where distinguishable, are still quite small.

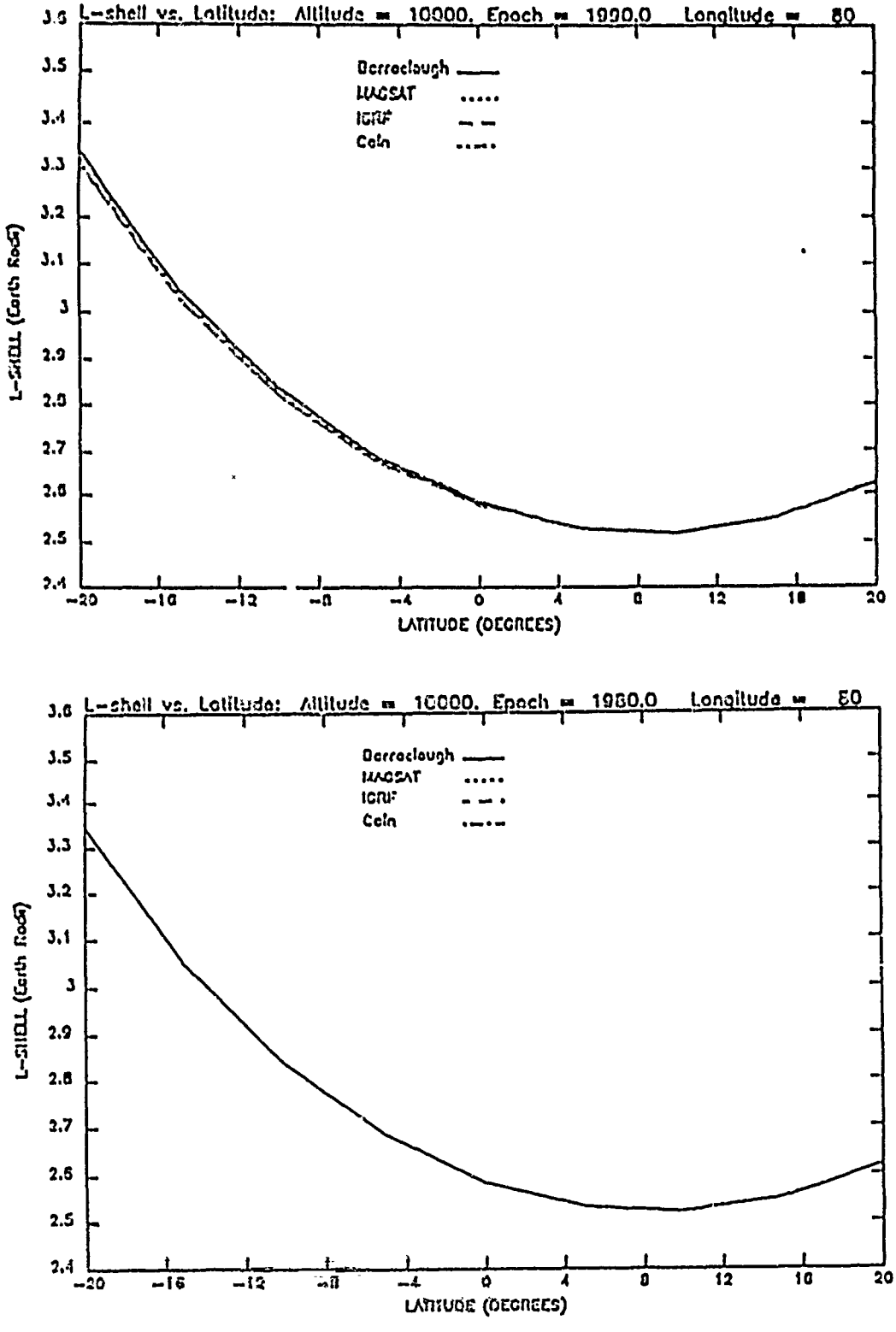

Figure 5.3b. Line plots very similar to those in Figure 5.3a, but for an altitude of 10,000 km rather than 350 km. The top panel shows the differences seen at 1990 and the bottom panel shows differences at 1980 for 80° east longitude. Again, differences increase with time, but not by much. The altitude does not seem to affect the differences much; the same relationship between the two epochs is seen for 10,000 km as for 350 km.

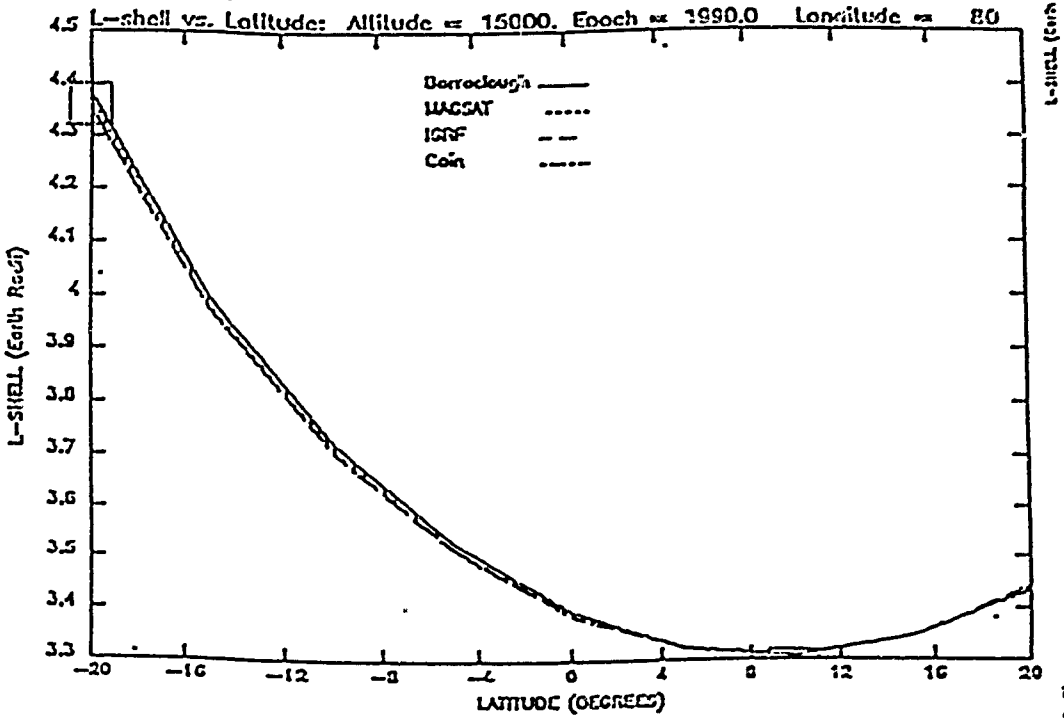

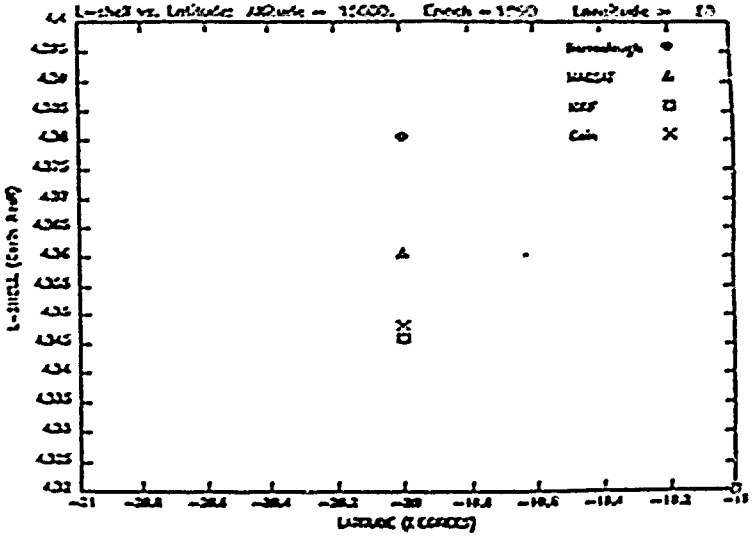

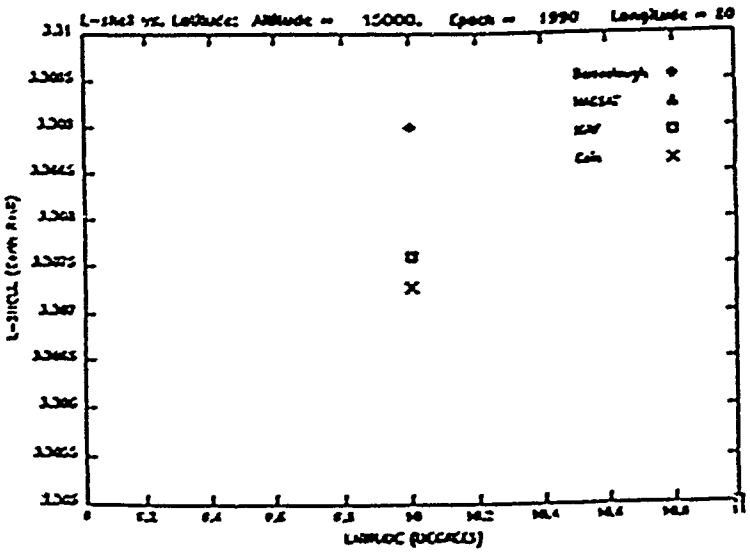

Figure 5.3c. Two details of a plot similar to Figure 5.3b (here the altitude is 15,000 km rather than 10,000 km) to better resolve the model differences. Data points were obtained at every 5° in latitude. Thus, at the resolution of the two details, only one point per model (as opposed to lines) is shown. Note, the top detail is at a larger scale than the bottom detail.

the effects of the jerk incorporated in Cain's model. At this scale (0.1 R_E), the models are difficult to resolve, thus figure 5.3c was done to show the best and worst agreement at this longitude.

Figure 5.3c is at an altitude of 15,000 km. The plot on the left is done at the same scale as figures 5.3a and 5.3b. The two boxes drawn on this plot show the scale of the two plots at the right. The upper panel has a scale 10 times larger than the lower panel. L values were only obtained at 5° increments, therefore the close-up figures only show four points rather than lines in order to see some separation between the points. In the upper plot, Barraclough is roughly .035 R_E higher than IGRF and Cain is roughly .0025 R_E higher than IGRF. This first difference is on the lower edge of detectability by CRRES instruments. However, if data is binned by 1/20 R_E as has been discussed (at least at a preliminary survey level) then even this difference is negligible. The second difference is too small to matter to CRRES at any level. Note, this upper plot is on a scale an order of magnitude larger than the lower plot, thus these differences are also of no consequence to CRRES. In fact, IGRF and Cain plot on top of each other in this lower plot.

5.3 L DETERMINED BY IGRF 1985 FOR 1990

Contour plots of L over the entire latitude and longitude range are shown in Figures 5.4a-c. Figure 5.4a shows the temporal changes in L-shell as found from IGRF 1985 evaluated at 350 km for 1990 and 1980. There is no significant change seen here. In fact, if one goes back to plots generated in 1970 by Stassinopoulos, one sees no change over 20 years. Figures 5.4b and 5.4c show L-shell contours from IGRF 1985 evaluated for 1990 for the other four primary altitudes considered in this report (850 km, 1500 km, 10,000 km, and 15,000 km). These are included as a general reference for the reader. Finally, Table 5.1 shows the maximum differences between the models for 1980 and 1990 at six altitudes (0.0 km to 10,000 km at 2000 km increments). These clearly show that Barraclough is furthest from IGRF and Cain is closest for 1990. For 1980, the differences are lower overall (as is anticipated), however, MAGSAT and Cain agree about eqally well with IGRF. Note, this is not surprising since Cain's model was based on this particular MAGSAT model then supplemented it with ground-based data (see Chapter 2).

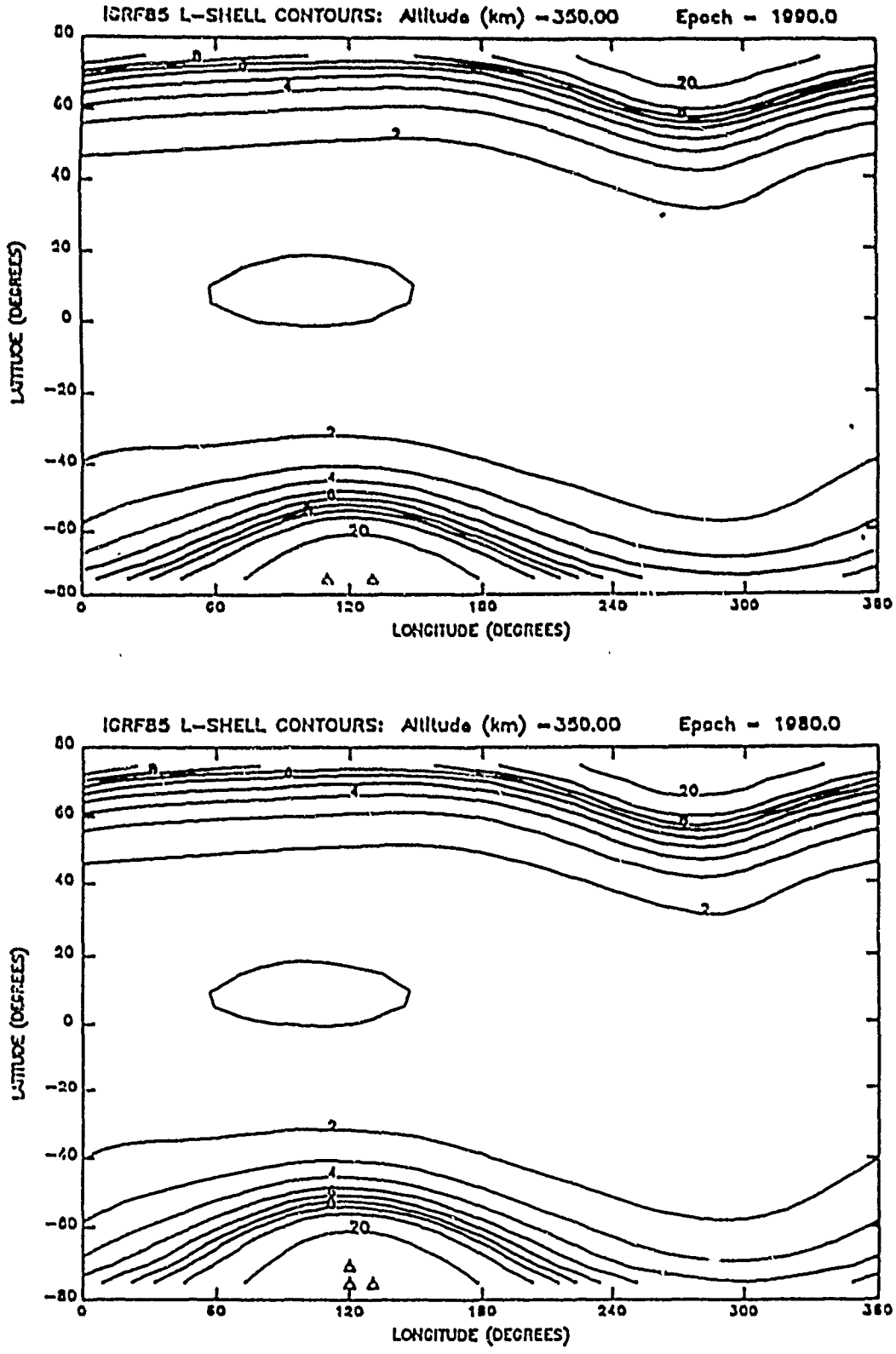

Figure 5.4a. Contours of L-shell as determined by IGRF 1985 over the full range of latitudes and longitudes at 350 km for 1990 (top) and 1980 (bottom). There is no visible difference between these epochs.

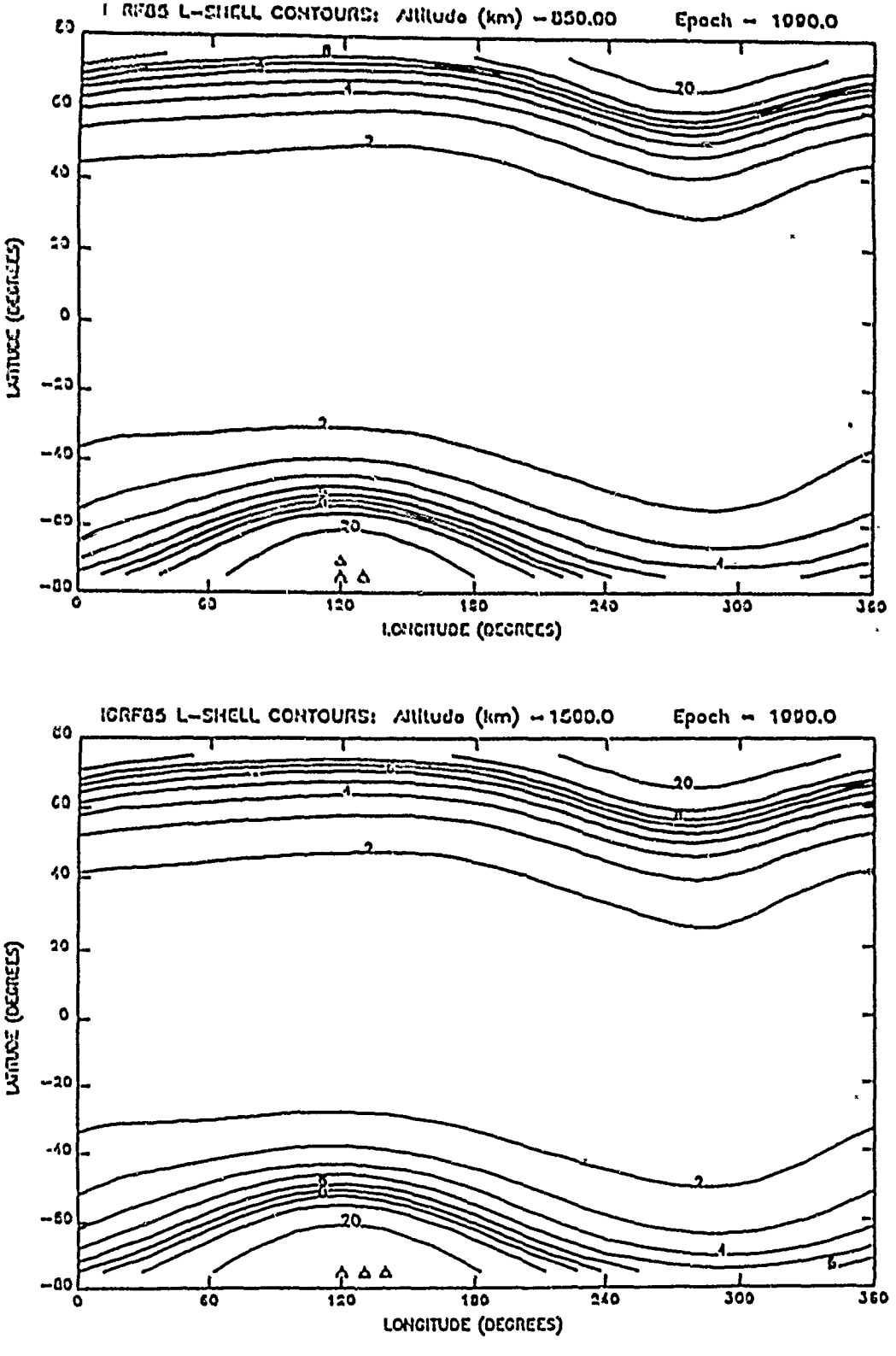

Figure 5.4b. Contours of L-shell as determined by IGRF 1985 for 1990 over the full range of latitudes and longitudes at 850 km (top) and 1500 km (bottom).

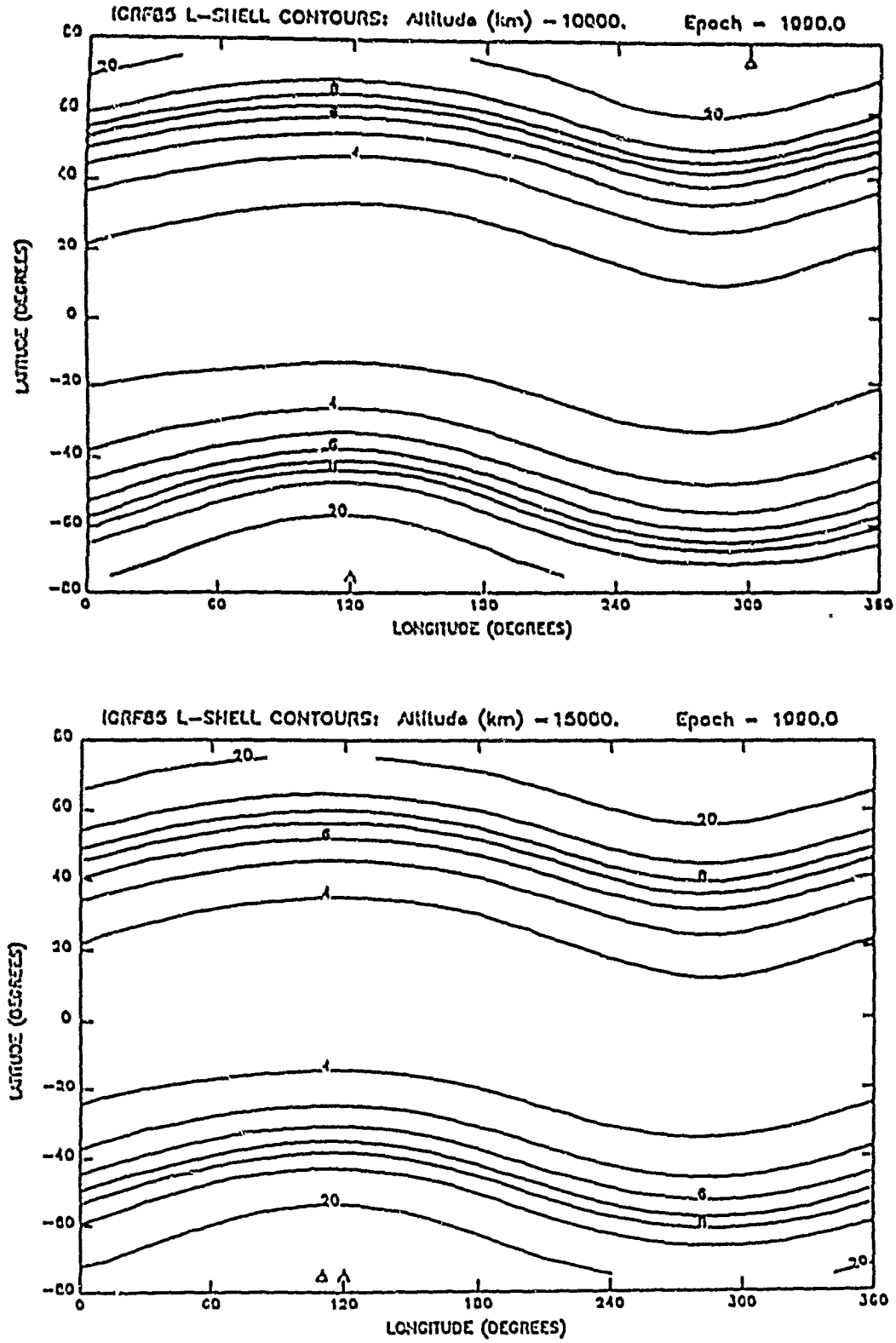

Figure 5.4c. Contours of L-shell as determined by IGRF 1985 for 1990 over the full range of latitudes and longitudes at 10,000 km (top) and 15,000 km (bottom).

Table 5.1. MAXIMUM L-SHELL DIFFERENCES BETWEEN ±20° LATITUDE
All models Compared to IGRF 1985 (Model-IGRF)

Year	Alt. ($x10^3$ km)	Barr ($x10^{-3}$)	Magsat ($x10^{-3}$)	Cain ($x10^{-3}$)
1980	0.0	4.10	1.32	2.86
	2.0	4.13	1.08	1.98
	4.0	4.42	1.13	1.61
	6.0	5.13	1.03	-0.57
	8.0	4.98	1.28	1.04
	10.0	4.73	1.06	-0.54
1990	0.0	19.89	11.19	3.26
	2.0	20.31	10.57	2.10
	4.0	22.50	10.40	2.45
	6.0	24.59	11.27	2.44
	8.0	25.99	11.59	2.64
	10.0	28.77	12.30	3.51

6. COMPARISONS OF THE SOFTWARE

Another aspect of the analysis of these models is that of the software which uses them. A package already exists for CRRES which incorporates the IGRF 1985 model. This package (OPTRACE) was modified to include the other three models: Barraclough 1975, MAGSAT 1980, and Cain 1990. The MAGSAT model contains 50 coefficients to allow for more detailed modelling of the field. However, evaluation of this many terms requires an exorbitant amount of computer time. Thus, a truncated version of this model was used in this analysis. OPTRACE was further modified to exclude external field contributions. This routine requires more CPU time than another code also in use at GL, HMIN. This second code was modified to give the same results as those initially obtained from OPTRACE (see Chapter 4). It was this code which was used to do the B field and L-shell comparisons in Chapters 3 and 5, respectively.

Software was received from Dr. J. C. Cain to calculate L-shell using both integration of the spherical harmonic coefficients and using interpolation tables. Both of these codes from Cain were originally developed in the early 1970s by Kluge (see Chapter 4). In order to avoid confusion, the integration code will be referred to as Kluge/Cain and the interpolation code will be referred to as Interpolation. The advantage of using the interpolation tables is one of greatly reduced CPU time in the processing. However, the question arises as to whether or not the increased speed sacrifices accuracy. In comparisons between interpolated L values and those obtained by integration, it is found that the interpolated values are sufficiently accurate for most applications. However, a problem was found with these codes. Cain coded a value for the dipole moment into the integration code rather than calculating it from the coefficients (see Chapter 4). The value he selected dates back to the mid-1960s and is now out of date. The dipole moment and the position of the offset dipole are changing rapidly enough that a noticeable difference is seen over 20 years (see Section 4.3.3.1). Thus, the interpolated values are not as accurate as they could be since the tables were based on the results from Kluge/Cain. Using results from a model which incorporates the current dipole moment, a more accurate set of tables could be obtained.

A similar approach to that used with the magnetic field and L-shell comparisons was taken. To begin with, contour plots of the differences between the codes were generated. Then line plots to high latitude at selected longitudes were made. More detailed lineplots within the CRRES latitude range were then considered. After reviewing the discrepancies between the codes, their efficiency was also evaluated.

6.1 OVERALL COMPARISONS OF THE CODES

Contour plots over the entire latitude and longitude ranges of the differences between Interpolated-OPTRACE/Cain, Interpolated-OPTRACE/IGRF, Interpolated-Kluge/Cain, and Kluge/Cain-OPTRACE/Cain are shown in Figures 6.1 and 6.2. Figure 6.1a shows the L-shell differences for these four cases for 1990 and 350 km altitude. Three of the plots are to be used in evaluating the accuracy of the Interpolation code. The fourth plot (lower right panel) shows the agreement between Kluge/Cain and OPTRACE using the same model. Kluge/Cain uses a transformation to inverse coordinates to simplify the integration (i.e., the integration is performed over a straight line rather than a curve as is done in OPTRACE). However, one expects the agreement here to be quite close. The agreement is seen to be very good in all four plots. Recall that in the model comparisons, the differences between Cain and IGRF were very small and for the most part negligibly small. This is apparent

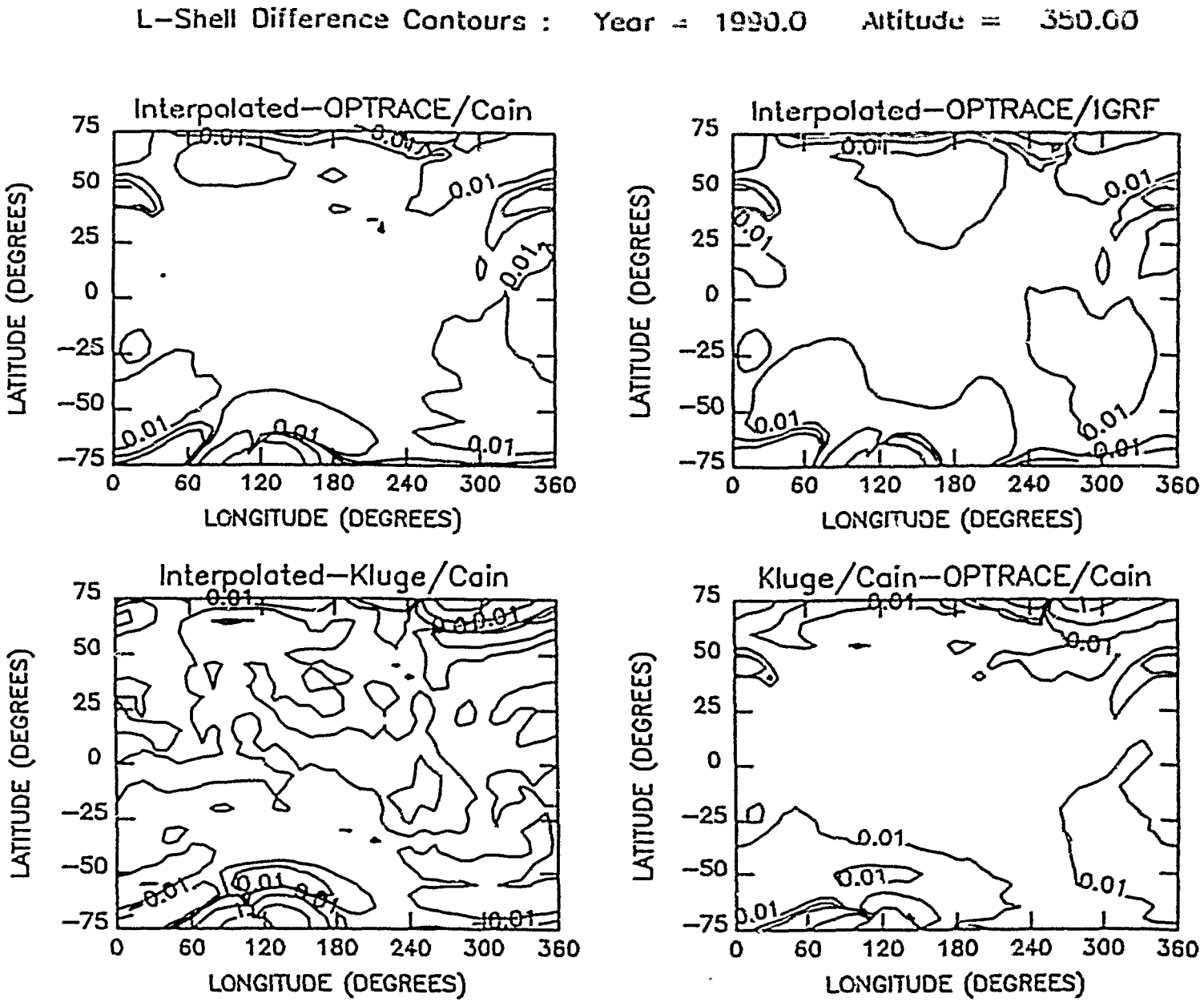

Figure 6.1a. Contour plots of L-shell differences in Earth radii (R_E) covering the full latitude and longitude ranges as determined form the various software packages: Interpolated, Kluge/Cain, OPTRACE/Cain, and OPTRACE/IGRF. The comparisons are done for an altitude of 350 km (perigee) at 1990.0.

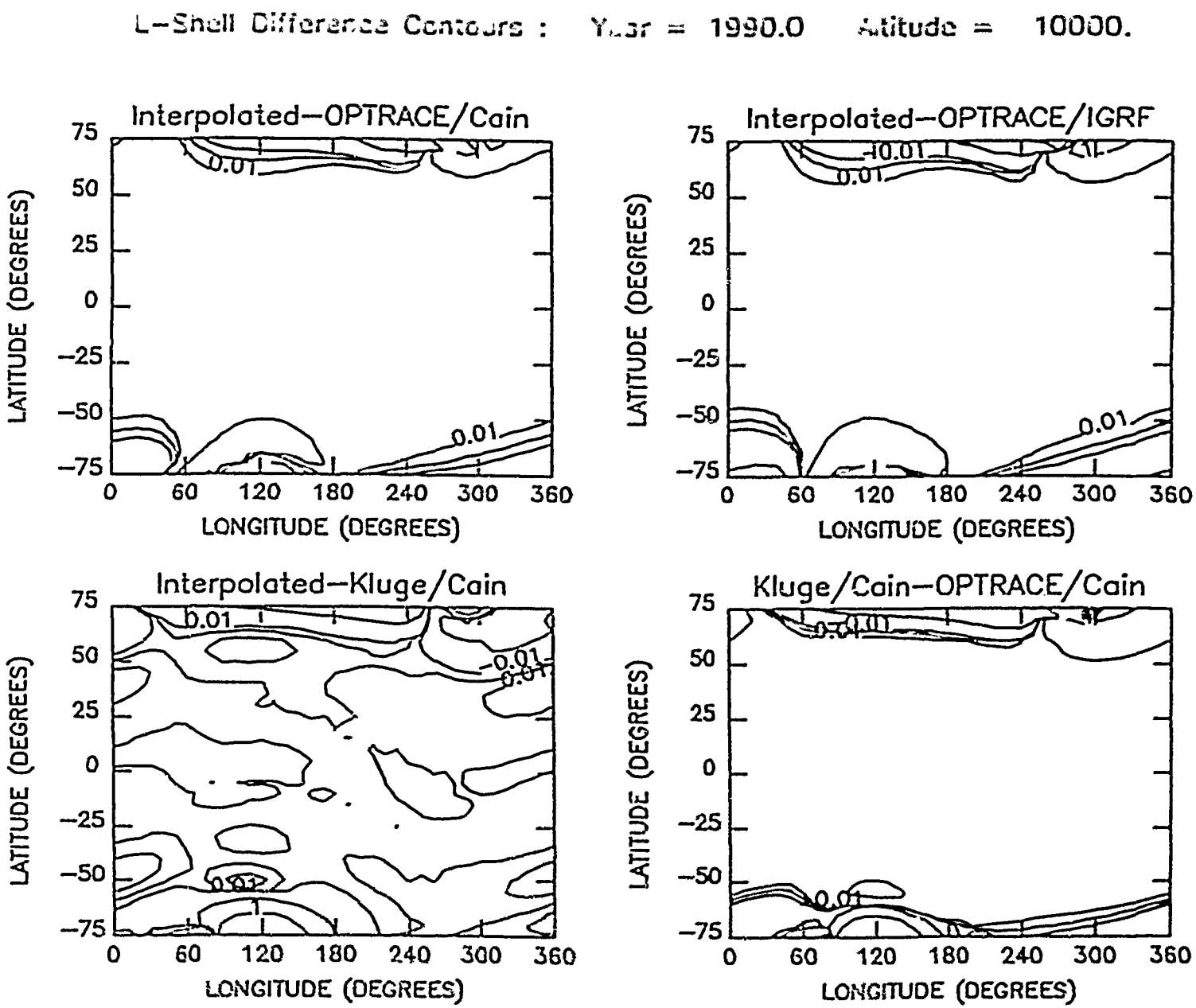

Figure 6.1b. Contour plots of model L-shell differences in Earth radii (R_E) covering the full latitude and longitude ranges as determined form the various software packages: Interpolated, Kluge/Cain, OPTRACE/Cain, and OPTRACE/IGRF. The comparisons are done for an altitude of 10,000 km at 1990.0.

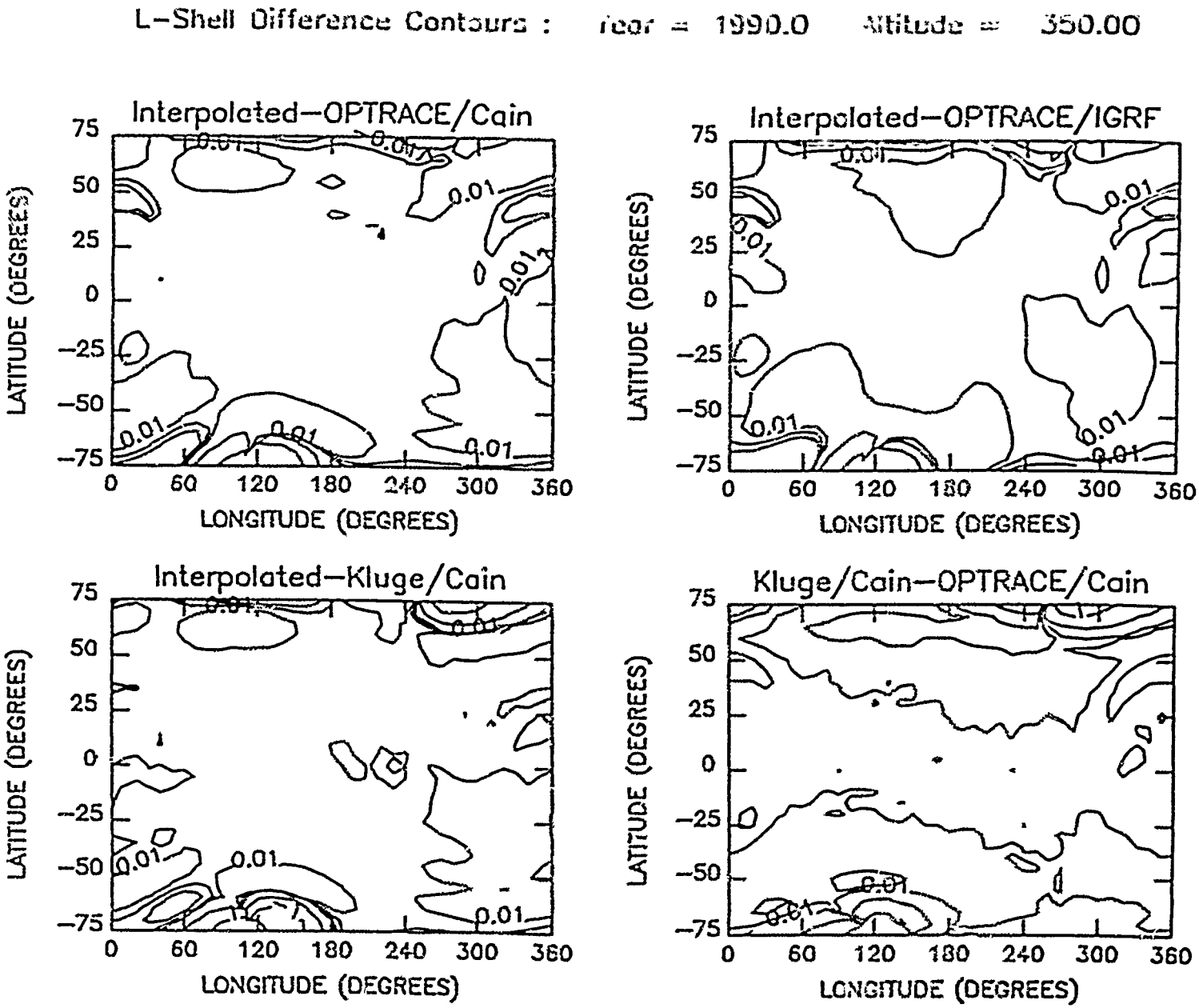

Figure 6.2a. Contour plots of L-shell differences in Earth radii (R_E) covering the full latitude and longitude ranges as determined form the various software packages: Interpolated, Kluge/Cain, OPTRACE/Cain, and OPTRACE/IGRF. The comparisons are done for an altitude of 350 km (perigee) at 1990.0 using an updated value for the dipole moment.

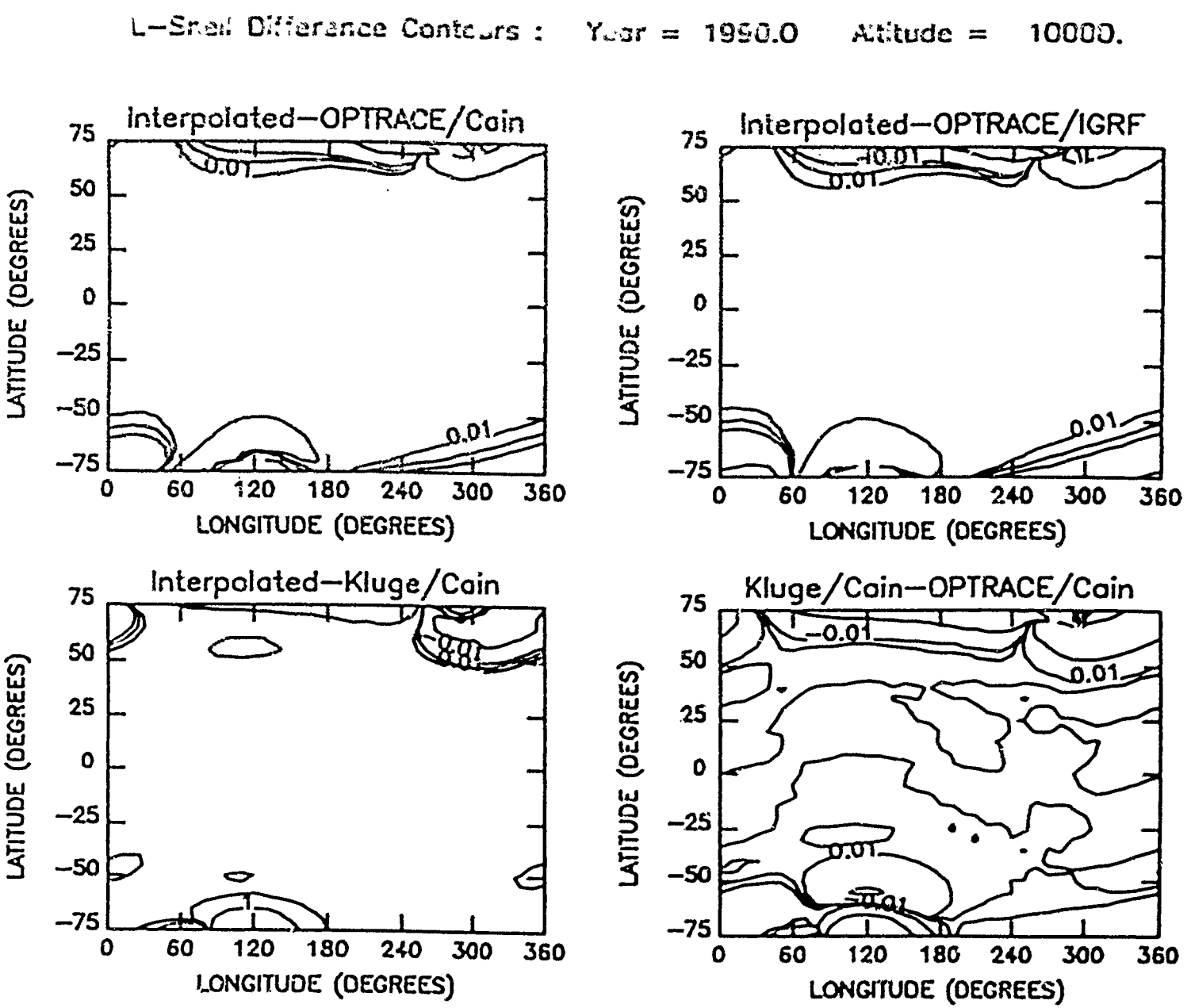

Figure 6.2b. Contour plots of model L-shell differences in Earth radii (R_E) covering the full latitude and longitude ranges as determined form the various software packages. Interpolated, Kluge/Cain, OPTRACE/Cain, and OPTRACE/IGRF. The comparisons are done for an altitude of 10,000 km at 1990.0 using an updated value for the dipole moment.

here as the top two panels which show the differences between Interpolated and Optrace/Cain and OPTRACE/IGRF, respectively, show very similar difference contours. The differences between Interpolated and Kluge/Cain are very small (most of the contours are 0. level contours). This is expected since the Interpolation tables were derived from the results of Kluge/Cain. Thus, the differences between Kluge/Cain and OPTRACE/Cain (lower right panel) are nearly the same as those seen for Interpolated and OPTRACE/Cain (upper left panel).

These same properties are seen in Figure 6.1b as well. Here, comparisons are made at an altitude of 10,000 km. The differences are a bit smaller than at 350 km. Again, the top two plots and the lower right plot look very similar due to the close agreement between the Cain and IGRF models and the close agreement between Interpolated and Kluge/Cain. Again, the smallest differences are found between Interpolated and Kluge/Cain (lower left plot). However, when the discrepancy between the dipole moments arose, these results changed a little bit. Re-evaluating Kluge/Cain with the updated moment led to better agreement between Kluge/Cain and OPTRACE/Cain than is seen for Interpolated and Kluge/Cain. Note, one is not able to similarly update the interpolation tables, they must be regenerated from results which were obtained with the current moment. Thus, in Figures 6.2a and 6.2b (350 km and 10,0000 km, respectively), the picture has changed somewhat from Figures 6.1a and 6.1b. One now sees the best agreement between Kluge/Cain and OPTRACE/Cain (lower right panel) and the other three plots have very similar difference contour distributions. Note, the differences have not increased.

6.2 COMPARISONS AT SPECIFIED LONGITUDES

The high latitude line plots taken at four longitudes over the globe (20°, 150°, 200°, and 290° east longitude) show the results from Interpolated, Kluge/Cain, OPTRACE/Cain, OPTRACE/IGRF (Figure 6.3). At this resolution, no difference between the four routines can be seen.

A plot done over the ±20° latitude range shows the offset of the Interpolated results from the those of the other three (note the current moment was used in Kluge/Cain here) in Figure 6.4. The Interpolated results are represented by the solid line at higher L values than the other three (which appear to be one line, the dashed, dotted, and dot-dash lines all plot over each other). When this was first done with the old moment, Interpolated and Kluge/Cain plotted over each other and were offset from the OPTRACE results to higher values of L. This is what is expected since a higher dipole moment leads to higher values of L.

To separate the models a little better, a plot with details on a much smaller scale was done, Figure 6.5. Here a line plot like that shown in figure 6.4 was done at 80° east longitude and 15,000 km altitude for 1990. Two boxes are drawn on the plot on the left to show the regions which are detailed on the right. Figure 6.5 was produced using the old dipole moment. Thus, in both details, Interpolated and Kluge/Cain are very near each other and are shifted to a higher L than the OPTRACE results which are also near each other. Note, the upper panel has a scale which is twice as large as that of the lower plot. The differences are small, but not negligible. In the upper plot, Interpolated and Kluge/Cain are about .04 R_E different. In the lower plot, the difference is roughly .025 for Interpolated and .03 for Kluge/Cain.

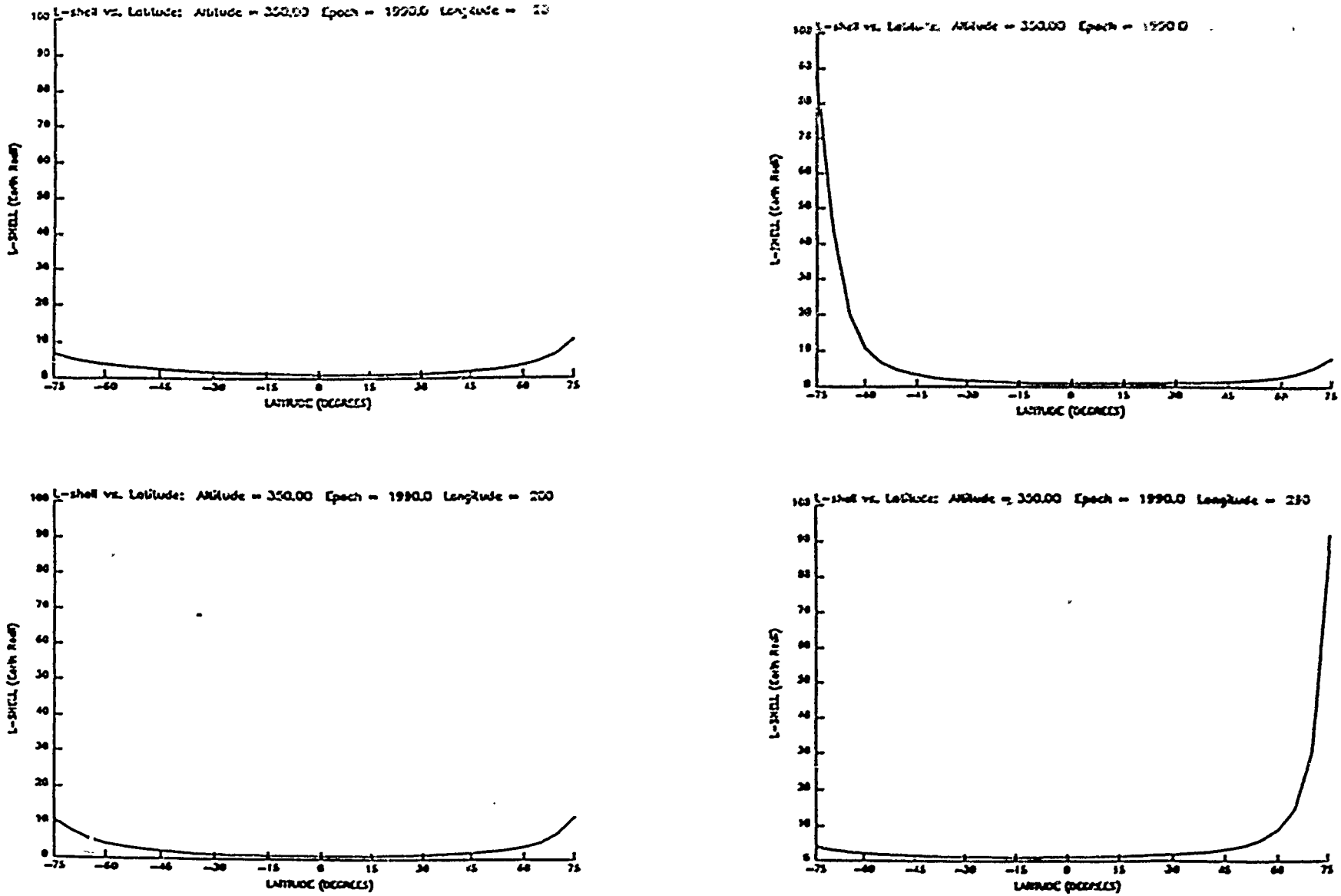

Figure 6.3. Line plots of L-shell as determined by each of the packages (Interpolated, Kluge/Cain, OPTRACE/Cain, and OPTRACE/IGRF) plotted together at four different longitudes over the globe for the full latitude range. The results are indistinguishable at this resolution.

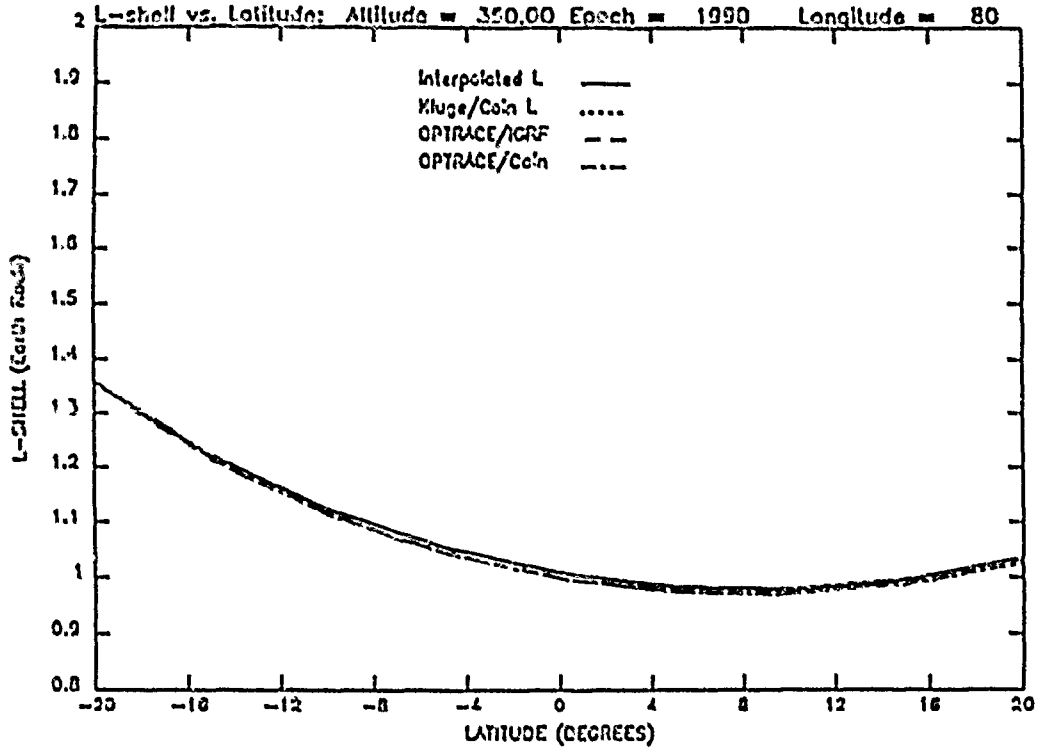

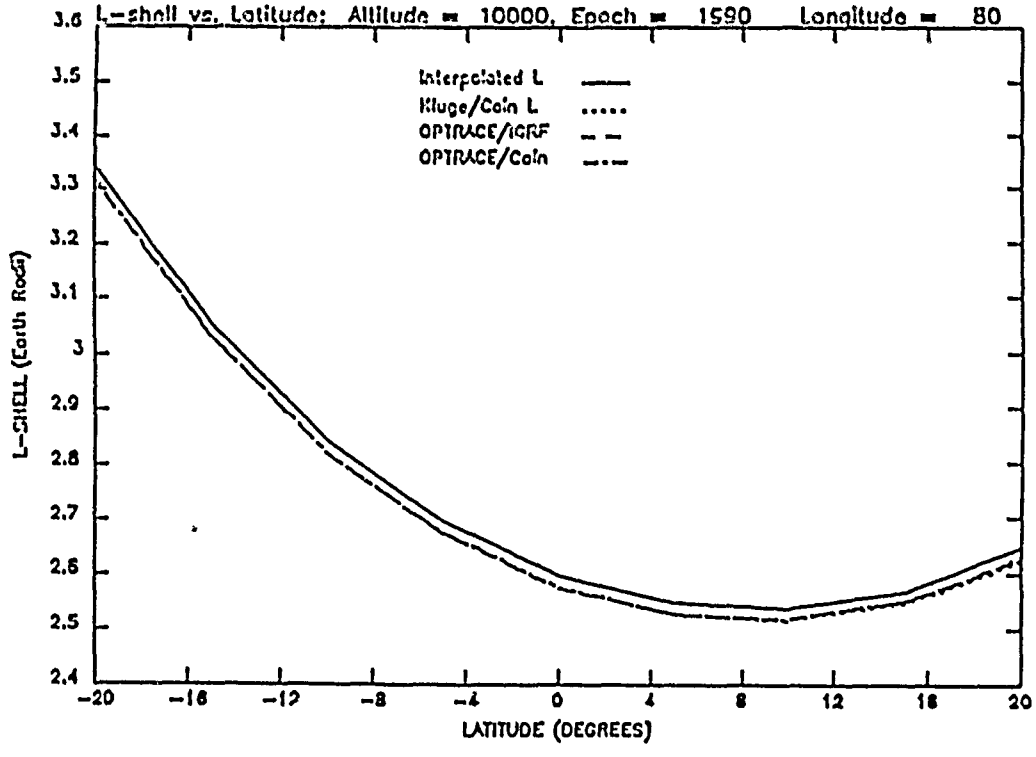

Figure 6.4. Line plots similar to those in Figure 6.3, but over a smaller latitude range. Even at this resolution, the differences between the models are very small. Here, the current value for the dipole moment has been used, thus, only Interpolated results are offset from the other three routines. The top panel shows the differences at 350 km and 80° east longitude for 1990.0. The bottom panel is the same plot done for epoch 10,000 km. The offset is larger for the higher altitude, but Kluge/Cain, OPTRACE/Cain, and OPTRACE/IGRF still agree very well.

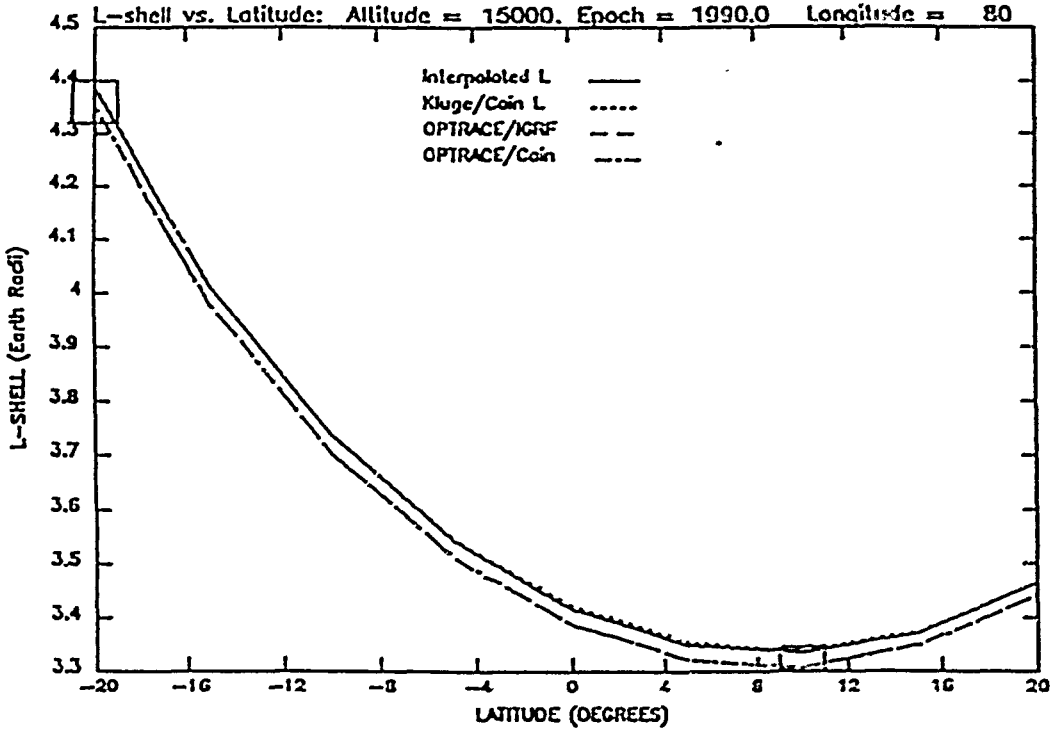

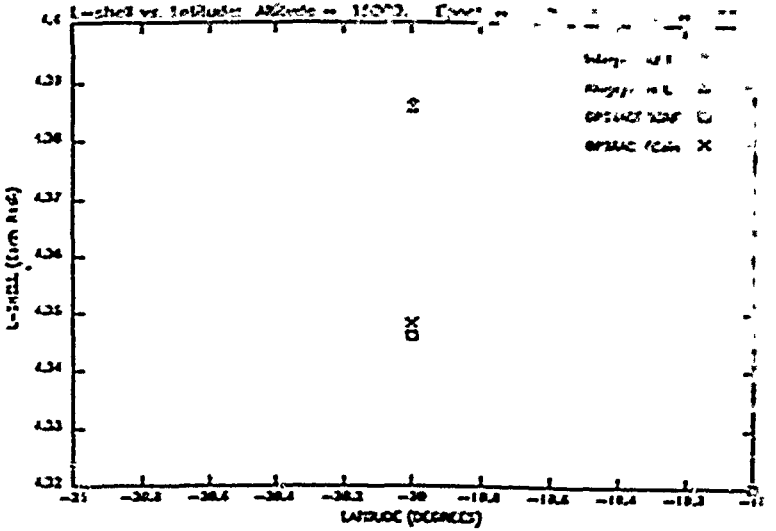

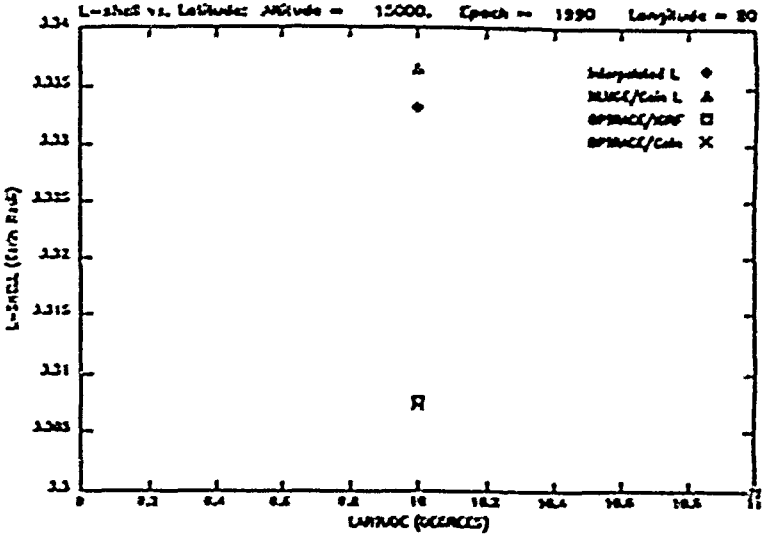

Figure 6.5. Two details of a plot similar to Figure 6.4 (here the altitude is 15,000 km) to better resolve the differences between the packages. Data points were obtained at every 5° in latitude. Thus, at the resolution of the two details, only one point per model (as opposed to lines) is shown. Note, the top detail has a scale twice the size of the bottom detail. These results were found using the old dipole moment. Note, how well Interpolated and Kluge/Cain agree and how far they are offset from OPTRACE/Cain and OPTRACE/IGRF.

Using the current dipole moment in Kluge/Cain brings it into closer agreement with the OPTRACE results as seen in Figure 6.6. In the left panel of figure 6.6, Kluge/Cain now coincides with the OPTRACE results. The upper detail shows a shift of about .03 R_E closer to the OPTRACE points. The lower detail has a slightly larger shift than that, placing Kluge/Cain a little bit lower than the OPTRACE points. Clearly, the different dipole moment makes a significant difference in the L-shell results (see Table 6.1)

6.3 TIMING COMPARISONS

6.3.1 Optimizing the Code

At the start of this project, OPTRACE was modified to perform internal field calculations only without any external contributions. It was further modified to include the other three models (Barraclough, MAGSAT, and Cain). The MAGSAT model was comprised of n=50 terms, which were very time consuming to evaluate. Thus, MAGSAT was used in three different subroutines for the modified OPTRACE which allowed the user to select interactively whether to use the full blown n=50 set or one of the two smaller sets, one truncated at n=15 and the other at n=20. Throughout all of the modifications, tests were run to check for accuracy and efficiency. Up until the full field comparisons were run for each of the models (using the n=15 MAGSAT version), short tests were run on a selected few points which spanned the latitude, longitude and altitude range. It was found that the differences were small between MAGSAT n=15 and n=50. Even though the detail of the higher order model was lost, the time saved justified it (Table 6.2).

Another factor of interest when discussing efficiency is that of the number of segments (or steps) used in integrating over the field line. The more segments used, the better the accuracy will be. However, this can also become time consuming, so one needs to sacrifice some of the accuracy for the sake of efficiency without compromising the integrity of the results. For the purpose of this report, 50 segments were found to be sufficient (Table 6.3).

6.3.2 Comparisons with Cain's Routines

Having resolved these questions, the full field comparisons were done using OPTRACE with 50 segments (Table 4). Clearly, these were time consuming computations. In comparing the efficiency of OPTRACE with the two codes sent by Cain, it became necessary to remove all of the extraneous calculations done in OPTRACE so that only L was being determined. This would have proved to be an intricate task, so to save a good bit of effort, HMIN was modified for the purpose of simply finding L. HMIN uses essentially the same routines as OPTRACE and by replacing two subroutines, it was made into the same algorithm as that in OPTRACE for consistency sake. There is a difference regarding the length along the field line each of these routines traces. OPTRACE traces to the 100 km intercept whereas HMIN goes only to the conjugate point (see Chapter 4). Thus, HMIN is the faster of the two routines.

For the full fields obtained for 1985, the modified Hmin routine was used to obtain L. The CP time required to do so was then compared to the Kluge/Cain integration method and to th Interpolation tables (Table 6.5). For internal fields only, the interpolation is the most efficient. However, to really take advantage of this, one needs to update the tables with the current dipole moment. The integration sent by Cain is also significantly faster than the

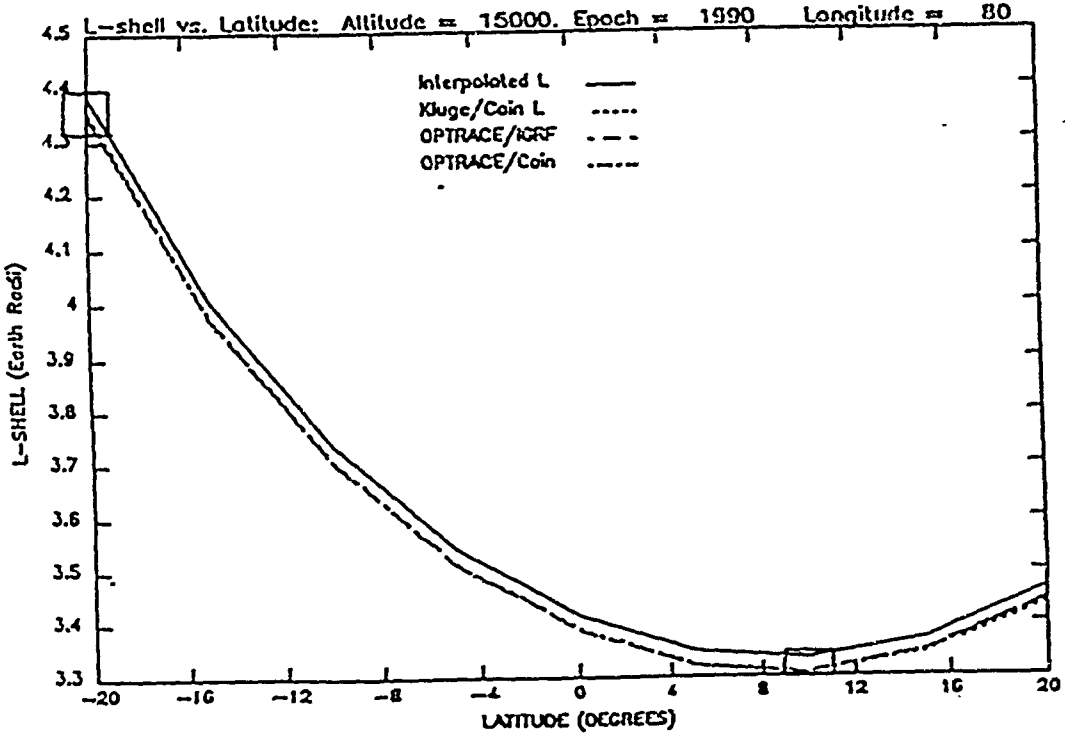

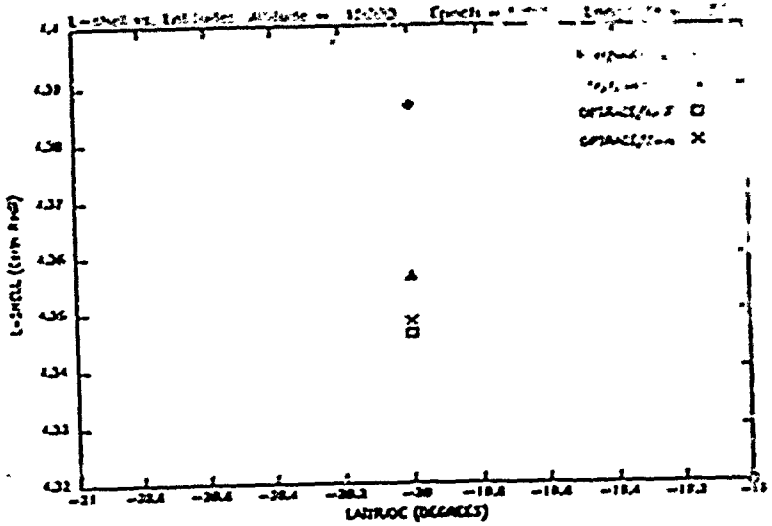

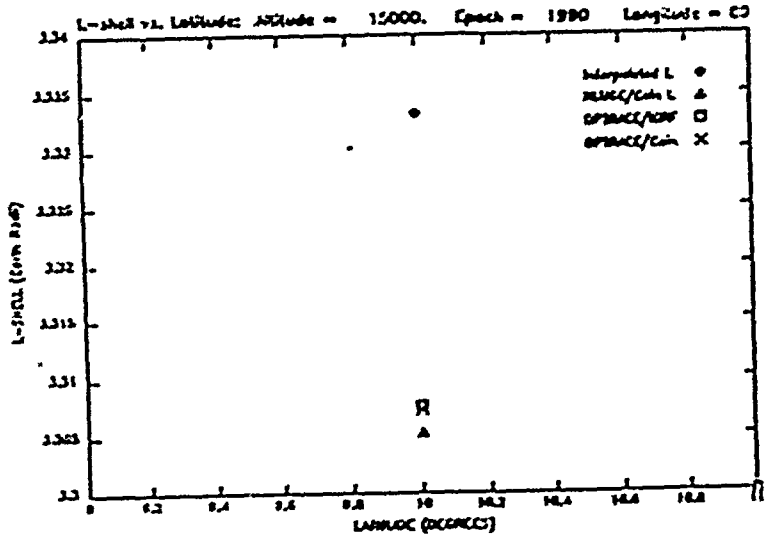

Figure 6.6. Two details of a plot similar to Figure 6.4 (here the altitude is 15,000 km) to better resolve the differences between the packages. Data points were obtained at every 5° in latitude. Thus, at the resolution of the two details, only one point per model (as opposed to lines) is shown. Note, the top detail has a scale twice the size of the bottom detail. These results were found using the current dipole moment. Note, the shift in the values for Kluge/Cain. It now agrees much better with the OPTRACE results. The Interpolation results are not so easily altered, thus, it is still offset.

Table 6.1. Changes in the Dipole Moment and Position as Calculated by Barraclough 1975, MAGSAT 1980, IGRF 1985, and Cain 1990 Extrapolated to 1990.5, 1975.5, and 1965.5.

Dipole Attributes	*Year*	*Barraclough*	*Magsat*	*IGRF1985*	*Cain*
Moment	1990.5	0.30255	0.30270	0.30285	0.30299
	1975.5	0.30687	0.30699	0.30703	0.30706
	1965.5	0.30975	0.30987	0.30983	0.30980
Offset from Center (in R_E)	1990.5	0.08006	0.08114	0.08100	0.08135
	1975.5	0.07460	0.07486	0.07504	0.07425
	1965.5	0.07118	0.07075	0.07114	0.06962
Latitude	1990.5	23.6	21.8	21.3	21.2
	1975.5	19.9	19.8	20.0	20.1
	1965.5	17.2	18.3	19.1	19.3
Longitude	1990.5	147.2	146.3	146.1	146.0
	1975.5	147.9	147.7	147.7	148.0
	1965.5	148.5	148.7	148.9	149.4

Table 6.2. Differences in L values due to using more coefficients in the Magsat model. More coefficients lead to more detail, particularly at low altitudes. However, based on the comparisons below, the improvement did not justify the additional computation time required by the greater number of coefficients (9.40 times longer).

GLAT	*GLON*	*ALT*	*L-SHEL(15)*	*L-SHEL(50)*	*ΔL(15-50)*
85.	36.	0.	28.13959	28.14000	-.00041
70.	72.	0.	5.40458	5.40438	.00020
50.	108.	0.	1.84936	1.84930	.00006
30.	144.	0.	1.10648	1.10647	.00001
10.	180.	0.	.98319	.98320	-.00001
0.	216.	0.	.98005	.97992	.00013
-20.	252.	0.	1.05520	1.05523	-.00003
-40.	288.	0.	1.27467	1.27473	-.00006
-60.	324.	0.	2.21630	2.21627	.00003
-80.	360.	0.	6.56247	6.70409	-.14162
85.	36.	500.	29.32115	29.32111	.00004
70.	72.	500.	5.64683	5.64677	.00005
50.	108.	500.	1.96966	1.96965	.00001
30.	144.	500.	1.19406	1.19406	---
10.	180.	500.	1.05940	1.05940	---
0.	216.	500.	1.05868	1.05867	.00001
-20.	252.	500.	1.13369	1.13370	-.00001
-40.	288.	500.	1.37512	1.37512	---
-60.	324.	500.	2.41738	2.41739	-.00001
-80.	360.	500.	7.43303	7.43300	.00003
85.	36.	1000.	30.53374	30.53370	.00004
70.	72.	1000.	5.90096	5.90094	.00002
50.	108.	1000.	2.09167	2.09166	.00001
30.	144.	1000.	1.28178	1.28178	---
10.	180.	1000.	1.13587	1.13587	---
0.	216.	1000.	1.13705	1.13705	---
-20.	252.	1000.	1.21287	1.21287	---
-40.	288.	1000.	1.47585	1.47585	---
-60.	324.	1000.	2.61466	2.61466	---
-80.	360.	1000.	8.31703	8.31702	.00001
85.	36.	5000.	41.04362	41.04362	---
70.	72.	5000.	8.19541	8.19541	---
50.	108.	5000.	3.09190	3.09190	---
30.	144.	5000.	1.98775	1.98775	---
10.	180.	5000.	1.75498	1.75498	---
0.	216.	5000.	1.76321	1.76321	---
-20.	252.	5000.	1.85660	1.85660	---
-40.	288.	5000.	2.28891	2.28891	---
-60.	324.	5000.	4.16962	4.16962	---
-80.	360.	5000.	15.46061	15.46061	---
85.	36.	10000.	54.94462	54.94462	---
70.	72.	10000.	11.28205	11.28205	---
50.	108.	10000.	4.36666	4.36666	---
30.	144.	10000.	2.87586	2.87586	---
10.	180.	10000.	2.53910	2.53910	---
0.	216.	10000.	2.54807	2.54807	---
-20.	252.	10000.	2.66963	2.66963	---
-40.	288.	10000.	3.30894	3.30894	---
-60.	324.	10000.	6.09631	6.09631	---
-80.	360.	10000.	24.41243	24.41243	---
85.	36.	15000.	69.10153	69.10153	---
70.	72.	15000.	14.43114	14.43114	---
50.	108.	15000.	5.65149	5.65149	---
30.	144.	15000.	3.76838	3.76838	---
10.	180.	15000.	3.32745	3.32745	---
0.	216.	15000.	3.33417	3.33417	---
-20.	252.	15000.	3.48378	3.48378	---
-40.	288.	15000.	4.32936	4.32936	---
-60.	324.	15000.	8.02087	8.02087	---
-80.	360.	15000.	33.35608	33.35608	---

Table 6.3. Differences in L values due to using more segments in the integration of the field line. More segments leads to greater accuracy, however much more CPU time is then required to do the evaluation (1.77 times longer). The improvement of 100 segments over 50 segments was not deemed sufficient to warrant the additional time required for the full field comparisons for this report.

GLAT	*GLON*	*ALT*	*IGRF(SEGS=50)*	*IGRF(SEGS=100)*	*DIFFERENCE*
85.	36.	0.	28.02248	28.05233	-.02985
70.	72.	0.	5.39173	5.39588	-.00415
50.	108.	0.	1.84718	1.84766	-.00048
30.	144.	0.	1.10581	1.10583	-.00002
10.	180.	0.	.98299	.98300	-.00001
0.	216.	0.	.98014	.98014	.00000
-20.	252.	0.	1.05618	1.05619	-.00001
-40.	288.	0.	1.27461	1.27470	-.00009
-60.	324.	0.	2.21627	2.21781	-.00154
-80.	360.	0.	6.55010	6.56058	-.01048
85.	36.	500.	29.19832	29.22007	-.02175
70.	72.	500.	5.63183	5.63594	-.00411
50.	108.	500.	1.96743	1.96838	-.00095
30.	144.	500.	1.19340	1.19346	-.00006
10.	180.	500.	1.05930	1.05931	-.00001
0.	216.	500.	1.05877	1.05878	-.00001
-20.	252.	500.	1.13447	1.13450	-.00003
-40.	288.	500.	1.37503	1.37518	-.00015
-60.	324.	500.	2.41701	2.41791	-.00090
-80.	360.	500.	7.42500	7.43425	-.00925
85.	36.	1000.	30.41567	30.42866	-.01299
70.	72.	1000.	5.88853	5.89085	-.00232
50.	108.	1000.	2.08936	2.09028	-.00092
30.	144.	1000.	1.28112	1.28121	-.00009
10.	180.	1000.	1.13582	1.13584	-.00002
0.	216.	1000.	1.13716	1.13718	-.00002
-20.	252.	1000.	1.21351	1.21355	-.00004
-40.	288.	1000.	1.47574	1.47620	-.00046
-60.	324.	1000.	2.61405	2.61580	-.00175
-80.	360.	1000.	8.30901	8.31489	-.00588
85.	36.	5000.	40.87692	40.88698	-.01006
70.	72.	5000.	8.18040	8.18469	-.00429
50.	108.	5000.	3.08894	3.08986	-.00092
30.	144.	5000.	1.98704	1.98756	-.00052
10	180.	5000.	1.75502	1.75535	-.00033
0.	216.	5000.	1.76341	1.76358	-.00017
-20.	252.	5000.	1.85671	1.85728	-.00057
-40.	288.	5000.	2.28854	2.28959	-.00105
-60.	324.	5000.	4.16793	4.16926	-.00133
-80.	360.	5000.	15.44047	15.44737	-.00690
85.	36.	10000.	54.72477	54.73180	-.00703
70.	72.	10000.	11.26230	11.26473	-.00243
50.	108.	10000.	4.36294	4.36490	-.00196
30.	144.	10000.	2.87506	2.87641	-.00135
10.	180.	10000.	2.53915	2.53952	-.00037
0.	216.	10000.	2.54827	2.54857	-.00030
-20.	252.	10000.	2.66947	2.67000	-.00053
-40.	288.	10000.	3.30815	3.30901	-.00086
-60.	324.	10000.	6.09358	6.09528	-.00170
-80.	360.	10000.	24.38652	24.39253	-.00601
85.	36.	15000.	68.82715	68.83137	-.00422
70.	72.	15000.	14.40627	14.40871	-.00244
50.	108.	15000.	5.64692	5.64828	-.00136
30.	144.	15000.	3.76747	3.76839	-.00092
10.	180.	15000.	3.32752	3.32827	-.00075
0.	216.	15000.	3.33439	3.33473	-.00034
-20.	252.	15000.	3.48343	3.48408	-.00065
-40.	288.	15000.	4.32814	4.32982	-.00168
-60.	324.	15000.	8.01708	8.01898	-.00190
-80.	360.	15000.	33.31976	33.32451	-.00475

Table 6.4. Ratios of the required CPU time for the full field L-shell evaluations using the four models in OPTRACE. L determined for every 5° in latitude over ±75° and for every 10° in longitude. Various altitudes were grouped together for the computations as indicated. The average computation time for altitudes between 0 km and 10,000 km using IGRF 1985 extrapolated to 1988 was used as the unit time.

ALTS	*YEAR*	*Barraclough*	*Magsat*	*IGRF 1985*	*Cain*
500km-1000km	1980	1.279	1.874	0.951	1.865
(step=500km)	1984	1.290	1.871	0.960	1.878
	1988	1.289	1.857	0.949	1.854
0km-10,000km	1980	1.380	2.011	-----	2.014
(step=2000km)	1982	1.379	2.001	1.020	2.013
	1984	1.383	2.002	1.024	2.010
	1986	1.376	2.016	1.024	2.014
	1988	1.378	2.009	1.017	2.003
	1990	1.373	2.014	1.018	2.004
15,000km-40,000km	1980	2.204	3.220	1.641	3.219
(step=5000km)	1984	2.211	3.229	1.648	3.239
	1988	2.210	3.227	1.645	3.227

Table 6.5. Ratios of the CPU time required by HMIN, Kluge/Cain Integration, and Interpolation. These are full field evaluations of L taken every 5° over ±75° in latitude and over every 10° in longitude. The computations were done for various altitudes, grouped as indicated. All evaluations were for 1985. The average computation time for altitudes between 0km and 10,000km using IGRF 1985 extrapolated to 1988 was used as the unit time.

ALTS	*500km–1000km (step=500)*	*2000km–8000km (step=2000)*	*10,000km–40,000km (step=5000)*
Interpolated	0.003	0.003	0.003
Integrated	0.052	0.042	0.044
HMIN(Cain-50)	0.812	0.817	1.443
HMIN(IGRF-50)	0.411	0.411	0.733
HMIN(Cain-100)	1.305	1.268	2.297
HMIN(IGRF-100)	0.663	0.637	1.138

technique used in OPTRACE or HMIN. This is due to the use of inverse coordinates centered on the dipole so that one integrates over a straight line rather than a curve as in OPTRACE.

REFERENCES

Backus, G., "Poloidal and Toroidal Fields in Geomagnetic Field Modelling", Rev. of Geophys., Vol. 24, Pp. 75-109, 1986.

Barraclough, D. R., "International Geomagnetic Reference Field: the Fourth Generation", Phys. Earth Planet. Inter., Vol. 48, Pp. 279-292, 1987.

Barraclough, D. R., Harwood, J. M., Leaton, B. R., and Malin, S. R. C., "A Model of the Geomagnetic Field at Epoch 1975", Geophys. J. R. Astr. Soc., Vol. 43, Pp. 645-659, 1975.

Barraclough, D. R., and Kerridge, D. J., "BGS Candidate Models for the 1985 Revision of the International Geomagnetic Reference Field", Phys. Earth Planet. Inter., Vol. 48, Pp 306-312, 1987.

Cain, J. C., Private Communication, November 1987.

Cain, J. C., Frayser, J., Muth, L., Schmitz, D., "The Use of Magsat Data to Determine Secular Variation", J. Geophys. Res., Vol. 88, Pp. 5903-5910, 1983.

Cain, J. C., Hendricks, S. J., Langel, R. A., and Hudson, W. V., "A Proposed Model for the International Geomagnetic Reference Field - 1965", J. Geomagn. Geoelect., Kyoto, Vol. 19, Pp. 335-355, 1967.

Cain, J. C., and Kluth, C., "Evaluation of the 1985-1990 IGRF Secular Variation Candidates", Phys. Earth Planet. Inter., Vol. 48, Pp. 362-378, 1987.

Cain, J. C., Wang, Z., Kluth, C., and Schmitz, D. R., "Derivation of a Geomagnetic Model to n=63", Geophys. J., Vol. 97, Pp. 431-441, 1989a.

Cain, J. C., Wang, Z., Schmitz, D. R., and Meyer, J., "The Geomagnetic Spectrum for 1980 and Core-Crustal Separation", Preprint, Geophys. J., Vol. 97, Pp. 443-447, 1989b.

Gauss, C. F., "Allgemeine Theorie des Erdmagnetismus. Resultate aus den Beobachtugen des Magnetishen Vereins im Jahre 1838", Leipzig, 1839. (Reprinted in "Werke", Vol. 5, Pp. 119-193, Konigliche Gesellschaft der Wissenschalten, Gottingen, 1877.)

Golovkov, V. P., and Kolomiitseva, G. I., "Models of Secular Geomagnetic Variation 1980-1990", Phys. Earth Planet. Inter., Vol. 48, Pp. 320-323, 1987.

Hildebrand, F. B., Introduction to Numerical Analysis, McGraw-Hill Book Company, Inc., New York/Toronto/London, 1956.

Hilton, H. H., "L Parameter, a New Approximation", J. Geophys. Res., Vol. 76, Pp. 6952-6954, 1971.

IAGA Division I, Working Group 1, "International Geomagnetic Reference Field Revision 1985," Eos, Vol.67, no. 24, 1986.

Iijima, T., and Potemra, T. A., "Field-aligned Currents in the Dayside Cusp Observed by Triad", J. Geophys. Res., Vol. 81, Pp. 5971-5979, 1976.

References (cont'd)

Kluge, G., "Calculation of Field Lines and the Shell Parameter L from Multipole Expansions of the Geomagnetic Field", European Space Operations Center (ESOC), International Note No 66, 1970.

Kluge, G., "Direct Computation of the Magnetic Shell Parameter", Comp. Phys. Comm. Vol. 3, Pp. 31-35, 1972.

Kluge, G., and Lenhart, K. G., "Numerical Fits for the Geomagnetic Shell Parameter", Comp. Phys. Comm. Vol. 3, Pp. 36-41, 1972.

Langel, R. A., and Estes, R. H., "The Near-Earth Magnetic Field at 1980 Determined from Magsat Data", J. Geophys. Res., Vol. 90, Pp. 2495-2509, 1985.

Maeda, H., Kamei, T., Iyemori, T., and Araki, T., "Geomagnetic Perturbations at Low Latitudes Observed by Magsat", J. Geophys. Res., Vol. 90, Pp. 2481-2486, 1985.

Malin, S. R. C., "Geomagnetic Secular Variation and Its Changes, 1942.5 to 1962.5", Geophys. J. R. Astr. Soc., Vol. 17, Pp. 415-441, 1969.

Malin, S. R. C., and Clark, A. D., "Geomagnetic Secular Variation 1962.5 to 1967.5", Geophys. J. R. Astr. Soc., Vol. 36, Pp. 11-20, 1974.

McIlwain, C. E., "Coordinates for Mapping the Distribution of Magnetically Trapped Particles", J. Geophys. Res., Vol. 66, Pp. 3681-3691, 1961.

McIlwain, C. E., "Magnetic Coordinates", Pp. 45-61 in Radiation Trapped in the Earth's Magnetic Field, B. McCormac, editor, D. Reidel, Dordrecht, Netherlands, 1966 (also Space Sci. Rev., Vol. 5, Pp. 585-598, 1966).

McNeil, W. J., Private Communication, July 1986.

Olson, W. P., and Pfitzer, K. A., "Magnetospheric Magnetic Field Modeling", Annual Scientific Report, McDonnel Douglas Astrodynamiesa Company-West, Huntington Beach, CA, 1977.

Peddie, N. W., and Zunde, A. K., "A Model of Geomagnetic Secular Variation for 1980-1983", Phys. Earth Planet. Inter., Vol. 48, Pp. 324-329, 1987a.

Peddie, N. W., and Zunde, A. K., "Assessment of Models Proposed for the 1985 Revision of the International Geomagnetic Reference Field", Phys. Earth Planet. Inter., Vol. 48, Pp. 330-337, 1987b.

Pinto, O., Jr., and Gonzalez, W. D., "SAMA: For How Long?", EOS, Vol. 70, p. 17, 1989.

Press, W. H., Flannery, B. P., Teukolsky, S. A., and Vetterling, W T., Numerical Recipes The Art of Scientific Computing, Cambridge University Press, Cambridge/New York/New Rochelle/Melbourne/Sydney, 1986.

References (cont'd)

Quinn, J. M., Kerridge, D. J., and Barraclough, D. R., "IGRF candidates for 1980 and 1985", Phys. Earth Planet. Inter., Vol, 48, Pp. 313-319, 1987.

Radex, Inc., "CRRES Data Processing Ephemeris File Generating System Product Development Specification", Radex, Inc., Bedford, MA 01730, RXR87041, 1987.

Schmitz, D. R., Meyer, J., and Cain, J. C., "Modelling the Earth's Geomagnetic Field to High Degree and Order", Geophys. J., Vol. 97, Pp. 421-430, 1989.

Stern, D. P., "Representation of Magnetic Fields in Space", Rev. of Geophys. and Space Phys., Vol. 14, Pp. 199-214, 1976.